

Dye-sensitized CdSe quantum dot hybrid materials: A new approach for optical patterning

Dissertation

der Mathematisch-Naturwissenschaftlichen Fakultät
der Eberhard Karls Universität Tübingen
zur Erlangung des Grades eines
Doktors der Naturwissenschaften
(Dr. rer. nat.)

vorgelegt von
Dipl.-Chem. Björn Märker
aus Pirna

Tübingen
2020

Gedruckt mit Genehmigung der Mathematisch-Naturwissenschaftlichen Fakultät der Eberhard Karls Universität Tübingen.

Tag der mündlichen Qualifikation:	22.02.2021
Stellvertretender Dekan:	Prof. Dr. József Fortágh
1. Berichterstatter:	Prof. Dr. Marcus Scheele
2. Berichterstatter:	PD Ph.D. Dai Zhang

List of Contents

Acronyms.....	6
Symbols	8
1. Summary	9
1.1 Summary in English	9
1.2 Zusammenfassung in Deutsch.....	9
2 Introduction.....	11
3 Theoretical Background	13
3.1 Quantization of physical properties in semiconductor nanoparticles	13
3.1.1 Particle in a box model.....	13
3.1.2 Semiconductor nanoparticles	15
3.1.3 Defects and their influence on the optical properties.....	18
3.2 The Role of QD surface and surface ligands in optical properties	20
3.3 CdSe based hybrid materials	23
3.4 Properties of organic semiconductors on the example of Phthalocyanines	25
3.4.1 Optical properties.....	26
3.4.2 Dielectric properties.....	28
3.4.3 Catalytic properties	29
3.5 Optical patterning using semiconductor materials.....	30
3.6 Confocal microscopy.....	33
4 Experimental	36
4.1 Methods and Instruments	36
4.1.1 UV-vis Absorption spectroscopy	36

Size evaluation using absorption spectroscopy	36
4.1.2 Confocal fluorescence microscopy.....	37
4.1.3 Atomic force microscopy imaging.....	39
4.1.4 Scanning/Transmission electron microscopy imaging.....	39
4.1.5 Raman spectroscopy	39
4.2 Synthesis.....	40
4.3 Synthesis of phthalocyanine linker molecules	40
4.4 CdSe Synthesis	41
4.4.1 Hot Injection Synthesis of CdSe with TOPO Ligands	41
Characterization	42
4.4.2 Hot Injection Synthesis of CdSe with mixed Ligands	43
Characterization	43
4.4.3 Heat Up Synthesis of CdSe with OA and MA Ligands.....	44
Characterization	45
4.5 Phase transfer of QDs using Ammonium Iodide and hybrid ligand shell with n-butylamine	46
NMR spectra.....	46
4.6 Sample preparation	47
4.6.1 Hybrid nanocomposite film preparation using dip coating	48
4.6.2 Hybrid nanocomposite film preparation using drop casting	49
5 Results	50
5.1 Synthesis of CdSe based hybrid materials.....	50
5.1.1 Structural analysis using SEM images and AFM.....	51
5.1.2 UV-vis absorption	55
5.1.3 Raman spectroscopy	56
5.1.4 Summary	59

5.2	Optical patterning.....	60
5.2.1	Positive fluorescence contrast patterning	61
5.2.2	Negative fluorescence contrast	64
5.2.3	Summary	65
6	Discussion.....	66
7	Conclusion	72
8	Outlook.....	73
9	Acknowledgements.....	75
10	List of figures	77
11	References.....	84

Acronyms

4APc	<i>4,4',4'',4'''-tetranitro phthalocyanine</i>
AFM	Atomic force microscopy
APD	Avalanche Photo Diode
BA	n-butylamine
BS	Beam splitter
CBE	Conductance band edge
CCD	Charge-coupled device
CdO	Cadmium oxide
CdSe	Cadmium selenide
Cu4APc	Copper <i>4,4',4'',4'''-tetranitro phthalocyanine</i>
CW	Continuous wave
DCM	Dichloromethane
DMF	Dimethylformamide
DMSO	Dimethyl sulfoxide
DOS	Density of states
Fe4APc	Iron <i>4,4',4'',4'''-tetranitro phthalocyanine</i>
H ₂ APc	<i>4,4',4'',4'''-tetranitro phthalocyanine</i>
HAD	hexadecylamine
HOMO	Highest occupied molecule orbital
LUMO	Lowest unoccupied molecule orbital
MA	Myristic acid
MO	Microscope objective
MPTMS	(3-Mercaptopropyl) trimethoxy silane
NA	Numerical aperture
Ni4APc	nickel <i>4,4',4'',4'''-tetranitro phthalocyanine</i>
NMF	N-methylformamide
OA	Oleic acid
ODE	1-octadecene
ODPA	Octadecylphosphonic acid

Pc	Phthalocyanine
PH	Pinhole
PSF	Point spread function
QD	Quantum dot
RMS	Root mean square
ROS	Reactive oxygen species
SEM	Scanning electron microscopy
TEM	Tunneling electron microscopy
THF	Tetrahydrofuran
TOP	Trioctylphosphine
TOPO	Trioctylphosphine oxide
TOPSe	Trioctylphosphine selenium
UV-Vis	Ultraviolet-visible
VBE	Valence band edge
Zn4APc	Zinc 4,4',4'',4'''-tetrinitro phthalocyanine

Symbols

Symbols

Symbol	Description	Unit
h	plank constant	Js
\hbar	reduced plank constant	Js
m	mass	kg
m_{eh}	reduced electron hole mass	kg
L	length	m
$E_{g,NC}$	Bandgap energy of the nanocrystal	eV
$E_{g,Bulk}$	Bandgap energy of bulk material	eV
E_{qc}	Energy of quantum confinement	eV
E_C	Energy of coulomb interaction	eV
π	pi	
r	Radius of a quantum dot	m
e	Elemental charge	C
ϵ_{∞}	Relative electric permittivity at high frequencies	
ϵ	Relative electric permittivity	
Δx	distance of two separate objects	m
λ	wavelength	m
n	Refractive index	
NA	Numerical aperture	
ϵ	Extinction coefficient	$M^{-1}cm^{-1}$
D	Diameter of quantum dot	m
A	Absorption intensity	

1. Summary

1.1 Summary in English

In this work, CdSe based quantum dots (QD) are functionalized with β -tetraaminophthalocyanine dye molecules to create a functional organic-inorganic semiconductor hybrid material. This process is optimized to achieve a solution-processable material, allowing for the controlled preparation of highly homogenous QD films. The dual nature of the material leads to two individually addressable optical resonances, which are exploited in an optical read/ optical write process, creating complex optical patterns. During this process, a positive and negative fluorescence contrast are created depending on the employed excitation wavelength. This is enabled by a fluorescence enhancement of the quantum dot under excitation, in conjunction with a fluorescence bleaching of the organic dye under ambient excitation conditions. The result of the patterning process is strongly dependent on the excitation wavelength used during writing and read out of the pattern, allowing for the use of both positive and negative fluorescence contrast simultaneously depending on the wavelength. Further investigations reveal that the presence of the organic dye not only enables negative optical patterning, but also enhances the contrast during positive patterning. We show a new approach to functionalize inorganic semiconductor QDs with functional organic molecules and highlight the possibilities arising from this combination.

1.2 Zusammenfassung in Deutsch

In dieser Dissertation werden CdSe Quanten Dots (QD) mit β -tetraaminophthalocyanin Farbstoff Molekülen funktionalisiert, um anorganische-organische hybrid Halbleiter Materialien zu synthetisieren. Diese Synthese wird optimiert, um ein flüssig verarbeitbares Material zu erzeugen, welches für die Präparation von möglichst homogenen QD Hybrid Filmen verwendet werden kann. Die Dualität dieses Materials führt dazu, dass es zwei individuell adressierbare optische Resonanzen aufweist, welche in einem optischen Lese/Schreibprozess ausgenutzt werden, um komplexe optische Muster zu erzeugen. In diesem Prozess werden sowohl ein positiver als auch ein negativer Fluoreszenzkontrast erzeugt, welche abhängig sind von der benutzten Anregungswellenlänge. Das wird ermöglicht durch die Fluoreszenzverstärkung der QDs unter Anregung, in Verbindung mit der Photobleichung des organischen Farbmoleküls unter Anregung in atmosphärischen Bedingungen. Das Ergebnis des optischen Strukturierungsprozesses hängt stark von der

Summary

Anregungswellenlänge ab, welche für den optischen Schreibprozess und den anschließenden Ausleseprozess verwendet wird. Dies sorgt dafür, dass gleichzeitig ein positiver und negativer Fluoreszenzkontrast abgebildet werden können, abhängig von der verwendeten Wellenlänge. Weitere Untersuchungen zeigen, dass das Vorhandensein des organischen Farbmoleküls nicht nur die Erzeugung eines negativen Fluoreszenzkontrastes ermöglicht, sondern ebenfalls zu einer Verstärkung des positiven Kontrastes beiträgt. Wir zeigen einen neuen Ansatz für die Funktionalisierung von anorganischen Halbleiter QD mit funktionellen organischen Molekülen und heben die neuen Verwendungsmöglichkeiten hervor, die sich aus dieser Kombination ergeben.

2 Introduction

The first CdSe based quantum dots (QD) were already used in the early 20th century incidentally, through incorporation into silicate glasses giving them a yellow-reddish coloration.¹ The first syntheses of well-defined colloidal CdSe semiconductor QDs were published at the beginning of the 1990s and have since been of great scientific interest, due to their excellent properties as fluorescence emitters.^{2,3} Through constant development, CdSe QDs today are some of the most well-researched and known representatives of semiconductor nanoparticles available.

Today there are a wide variety of established synthetic approaches, using different precursors, solvents and stabilizing agents to obtain CdSe QDs with clearly defined shape and size distributions.⁴⁻⁶ This allows for specific control of the optical absorption and emission properties of the QDs, which are directly linked to their physical properties.⁷ Great efforts have been undertaken to further elucidate the changes in the electronic structure and resulting optical properties of the QDs in comparison to the bulk material. The understanding of the change in optical properties, due to the size and shape of the CdSe Quantum emitter, allowed for the engineering of the optical properties without changing the chemical composition of the material.⁸

This tunability lead to their implementation in a range of optical and electric applications, for example as solar cell material or as highly stable fluorescence markers for medical purposes.^{9,10} To further tailor the optical and electric properties of these CdSe QD based materials, they can be functionalized using organic molecules as surface Ligands replacing the native ligand shell. One example for such a modification is the introduction of organic dye molecules such as phthalocyanines as optical sensitizing agents. Here, the organic dye functions as an optical antenna, extending the optical absorption of the combined material to the near Infra-red region of the optical spectrum and increasing the overall conversion rate.¹¹

More recently, semiconductor QDs have received increasing attention for application as absorber materials in optical patterning processes.^{12,13} This patterning process exploits the fact that CdSe QDs show an increase in fluorescence quantum yield under above-bandgap excitation, in ambient conditions. Using this, the optical pattern is written into the material using optical excitation of the QDs, generating a positive fluorescence contrast. The pattern can then be depicted through imaging of the spatial fluorescence distribution.

Introduction

Contrary to this, a negative fluorescence contrast has been difficult to achieve and has shown low pattern stability, due to destruction of the CdSe QDs. To address this limitation, we introduce a hybrid material of β -tetraaminophthalocyanine functionalized CdSe QDs.

In this work, we present synthetic approaches to remove the native ligand shell of the synthesized CdSe QDs and replace them with β -tetraaminophthalocyanine molecules forming an organic inorganic semiconductor hybrid material. We aim to establish the optical properties of this new QD based hybrid material through absorption and emission spectroscopy and further process it into highly ordered QD films. After establishing the structural properties, these films are used to create complex optical patterns under laser excitation, employing a confocal fluorescence microscopy setup. The changes in optical properties due to the patterning process are investigated by fluorescence spectroscopy.

3 Theoretical Background

3.1 Quantization of physical properties in semiconductor nanoparticles

The main interest in nanoparticle-based materials results from the physical properties that can be exhibited by materials reaching the nanometer size domain compared to their bulk material counterparts and can no longer just be explained using classical physics. Due to the small size of particles used in this work, which are below 5 nm, the material, electronic and optical properties show clear quantization effects which can be explained using quantum mechanics. In the following, a summary of the quantum mechanical basis governing the physical properties of nanoparticles will be undertaken. This by no means is meant as an overarching approach to quantum mechanics as a whole or a full understanding of nanoparticle specific properties, as this would be outside the scope of this work. This work will focus on the explanation of a “particle in a box” model and how it relates to the physical properties of nanoparticles as an explanation for band like structures in crystalline nanoparticles and the resulting optical and electronic properties. For a comprehensive understanding of the basics of quantum mechanics the reader is encouraged to further study the sources cited in this chapter and the following books that provided the basis for this work.^{14–16}

- G. Wedler, H. J. Freund, *Lehrbuch der physikalischen Chemie 6. Auflage*, Wiley-VCH, Weinheim, **2012**.
- P. Atkins, J. Paula, *Physikalische Chemie 5. Auflage*, Wiley-VCH, Weinheim, **2013**.
- W. Göpel, C Ziegler, *Einführung in die Materialwissenschaften: Physikalisch-chemische Grundlagen und Anwendungen*, Vieweg+Teubner Verlag, **1996**.

3.1.1 Particle in a box model

The particle in a box model lends itself as an explanation on a quantum mechanical basis for the quantum confinement observable in the nanoparticles used in this work. The basis for this model is the Schrödinger equation for a free moving particle defined as:

$$\hat{H}\psi = E\psi \text{ with } \hat{H} = \frac{\hbar^2}{2m} \frac{d^2}{dx^2} \quad 1$$

If we solve this for the Energy E we obtain the following general solution:

Theoretical Background

$$E_k = \frac{k^2 \hbar^2}{2m} \quad 2$$

For a freely moving particle, **equation 2** can be solved for all possible values of k , meaning there is no quantization of the movement energy in a free moving particle.

The result of this is the specialized case of the particle in a box, when we start to restrict the free movement of the particle as shown in **Figure 1** (left) in a one-dimensional system in which the particle is enclosed in two potential walls at $x = 0$ and $x = L$. This means that inside the box between 0 and L , there is no potential ($V=0$), which instantaneously increases to infinity ($V=\infty$) below 0 or above L . Inside the potential walls, the solution for the Schrödinger equation is identical to a freely moving particle and we can use the general solution from **Equation 2** describing the particle as a wave function inside the walls of the box. Due to the restrictions of the box model, the wave function must have a value of zero at the potential walls $x=0$ and $x=L$, only allowing for integer values of k resulting in this more specialized form of the Schrödinger equation:

$$E_n = \frac{h^2}{8mL^2} n^2 \quad 3$$

with the Planck constant $h = 2\pi\hbar$ and the quantum number $n= 1,2, 3, \dots$, the length of the box L and the particles mass m . As n can only take integer values, the energy of a particle in this system is clearly quantized. The Equation also shows us that the distance between energy levels increases with higher quantum numbers due to the quadratic nature of the equation as shown in **Figure 1** (right).

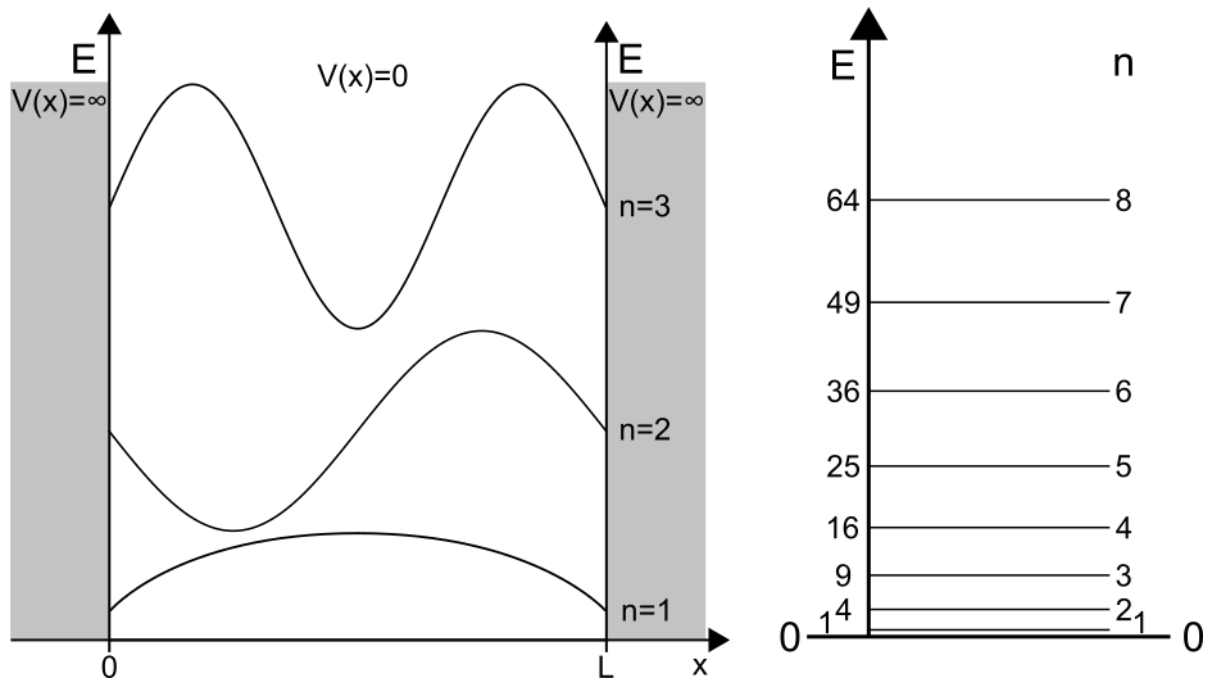


Figure 1: Left-Schematic visualization of the “particle in a box” concept for the first three quantum numbers n as wavefunctions. The Potential barriers $V(x)$ for $x < 0$ and $x > L$ are assumed to be infinitely high. Right-Schematic visualization of the resulting Energy levels of excited particles in a box for the first eight quantum numbers, showing the increasing distance between energy levels with higher quantum numbers.

The particle in a box model can be used as an explanation for the quantization effect observed in semiconductor quantum dots (QD). To do this, we want to take a closer look on the electronic structure of semiconductors.

3.1.2 Semiconductor nanoparticles

As shown in the particle in a box model, an electron in a solid material can only occupy certain electronic states that are limited by the material properties or, as in our model, the spatial limitations that are forced upon them. Contrary to the model of an isolated particle, in a three-dimensional material the electronic properties emerge from the interaction of multiple atoms, which leads to an overlap of electronic states forming energy bands. The bands can be described by the density of states (DOS), which specifies how many available states can be occupied by electrons with a given energy as shown in **Figure 2**. In solid state physics the occupation of these energy bands with electrons in a material is indicated by the Fermi energy E_F , which is defined as the energy between the highest occupied electronic state and the lowest unoccupied electronic state of a material, in its ground state at a temperature of 0 K. Looking at a semiconductor crystal, the valence band lies below E_F and is therefore filled with electrons. Contrary to that, the energetically higher lying conductance band is deprived of

Theoretical Background

electrons. Both bands are separated through the bandgap, a region in which no allowed electronic states exist that can be occupied by electrons. This bandgap varies depending on the semiconductor material that is observed and is responsible for the optical electronic properties of the semiconductor.

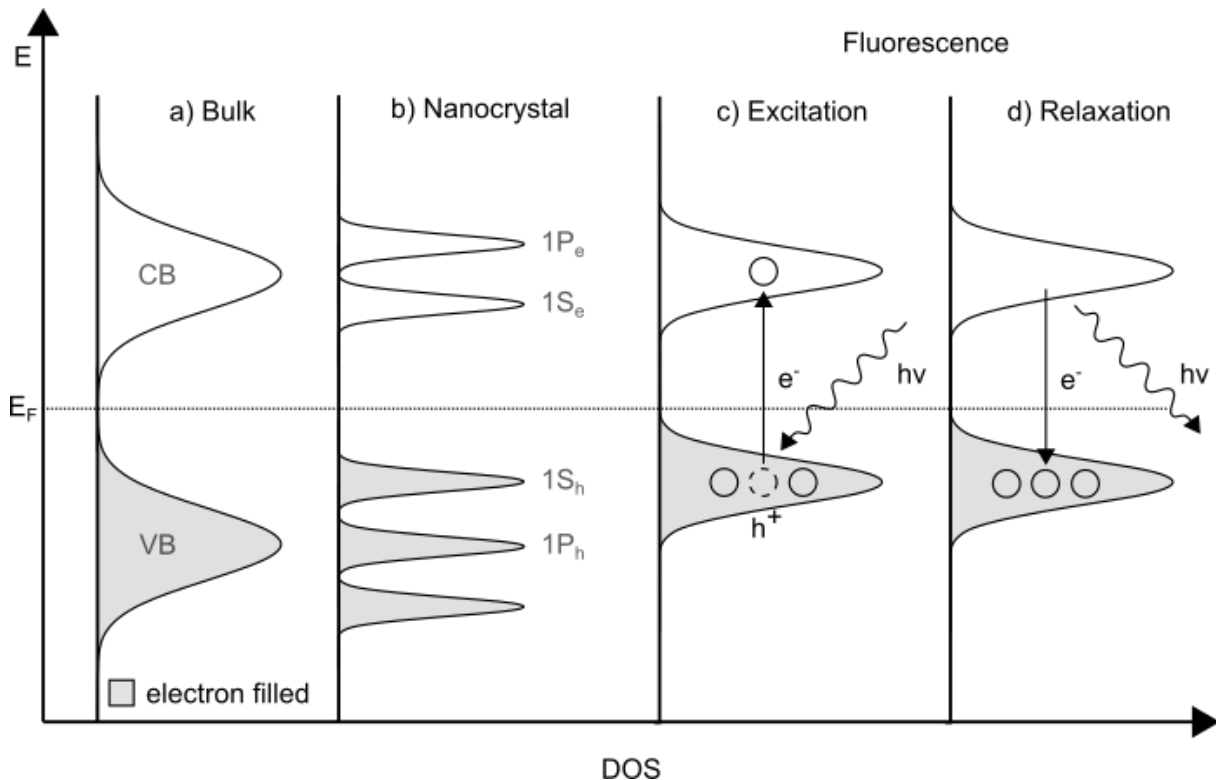


Figure 2: Schematic visualization of the semiconductor density of states (DOS) correlated to the energy E . The density of states below the Fermi Energy level E_F are filled with electrons, while the energy levels above are unoccupied and can be populated by exciting electrons. a) DOS of bulk semiconductor material with electron filled valence band (VB) and unoccupied conduction band (CB). b) Splitting of CB and VB into a molecule orbital-like DOS inside semiconductor nanocrystals. c) Excitation of electrons by light from the VB in the CB. d) Relaxation of electrons under light emission from the CB to the VB.

Upon shrinking the size of a semiconductor crystal, a point is reached where the properties change from the above described bulk semiconductor to those of a nanoparticle semiconductor (**Figure 2 a,b**).^{17–19} This happens when the spatial dimensions of the crystal become smaller than the exciton Bohr radius of the material. In this case, the electric wave function of the particle is spatially confined compared to the bulk material. This spatial confinement leads to a change of the continuous energy bands of the bulk material into more discrete energy levels, similar to a “particle in a box model” shown in **Figure 2b**, which influences the effective bandgap of a semiconductor nanocrystal compared to the bulk semiconductor.

As shown in **Figure 2** (c. d), through optical or thermal excitation electrons from the valence band can be transferred into the conductance band bridging the bandgap of the material, which can then be available as free charge carriers in the material. During this process, a hole is created in the valence band, together with the excited electron it forms an exciton, a so-called quasi particle. Through relaxation of the excited electron under emission of radiation or heat, the electron and hole can recombine back to their initial state. If the excitation and subsequent relaxation of the system is achieved through the absorption and emission of light, the process is either called fluorescence or phosphorescence depending on the timescale of the relaxation. Fluorescence is a major characteristic of semiconductor QDs.

The bandgap energy of a nanocrystal $E_{g,NC}$ is calculated as the sum of the bandgap energy of the bulk material $E_{g,Bulk}$ and the energy of the quantum confinement E_{qc} and the energy from the Coulomb interactions between electrons and holes in the nanocrystal E_C :

$$E_{g,NC} = E_{g,Bulk} + E_{qc} - E_C = E_{g,Bulk} + \frac{\hbar^2\pi}{2m_{eh}r^2} - \frac{1,765e^2}{\epsilon_{\infty}r} \quad 4$$

with m_{eh} as the reduced electron hole mass, e as the elemental charge, ϵ_{∞} as the dielectric constant at infinite frequencies and the crystal radius r . As shown in **Equation 4** E_{qc} is correlated to the size of the nanocrystal with $1/r^2$, resulting in a smaller nanocrystal having an increasingly larger bandgap energy. For CdSe-nanoparticles, we would expect a bandgap with an energy larger than ~ 1.7 eV that has been observed for the bulk material.^{20–22} CdSe nanocrystals show a band gap somewhere in the range of 1.8–4.0 eV for a particle size between 5 and 2 nm, with slight variations depending on synthetic approach and the technique used to determine the bandgap.^{23–25} In **Figure 3**, a theoretical calculation of the DOS of a CdSe nanocrystal can be seen. The calculation confirms a change of the general band structure compared to the bulk material, albeit with an expectedly larger bandgap.²⁶

The calculations confirm the broadening of the bandgap from bulk CdSe to a nanoparticle with a radius of 1 nm. Looking at the difference in the energies of the valence band edge (VBE) and conduction band edge (CBE), the bandgap is calculated. For the bulk material, this results in a bandgap of 1.72 eV (CBE -3.52 eV, VBE -5.24 eV) and a much larger bandgap of 4.1 eV (CBM - 2.17 eV, VBM -6.27 eV) for the nanoparticle.

Theoretical Background

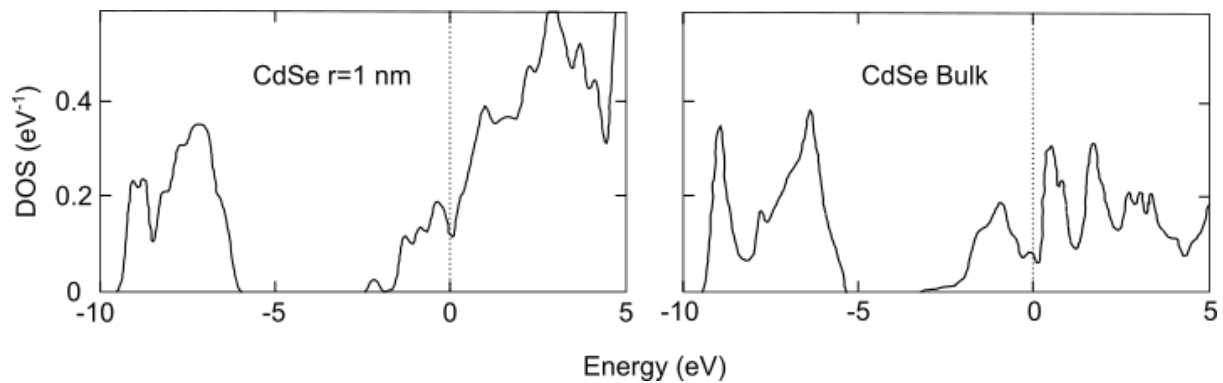


Figure 3: Theoretically calculated density of states in CdSe bulk material and a 1 nm radius nanocrystal of CdSe. The Zero is the vacuum Energy. The theoretical calculations show a clear change in the band structure of the QD compared to the bulk material. The CBE of the nanoparticle at -2.17 eV and the VBE of -6.27 result in a calculated bandgap of 4.1 eV compared to the smaller calculated bandgap of the bulk material of 1.72 eV (CBE -3.52 eV, VBE -5.24 eV). This figure has been taken from the work of L.W. Wang and A. Zunger as an abridged version.²⁶ Copyright 1996 The American Physical Society.

Although a CdSe nanoparticle shows similar behavior as described by the particle in a box model, the potential barrier is not infinitely high like in the theoretical model but is dictated by the structure of the particle surface and the chemical environment. These finite potential walls are unable to contain the wavefunction fully inside the range of the particles and allow for it to tunnel through the potential barriers. This allows for the wavefunction of nanoparticles to potentially overlap with another nanoparticle or with electrons in molecule orbitals that are spatially close. Hence, we also have to consider the environment of the nanoparticle and consider its influence on the optical and electric properties of the nanoparticle (**chapter 3.2**).

3.1.3 Defects and their influence on the optical properties

All discussed electronic and optical features of nanoparticles have assumed a structurally perfect nanocrystal, but defects in the crystal structure are rather common. These defects can have various reasons and are mostly created at borders of crystal domains, such as the surface, or through impurities in the bulk material. In nanoparticles, the surface plays a major role as it, compared to the bulk material, makes up a much larger portion of the crystal. Surface defects can be created due to missing atoms or incomplete passivation of the surface through ligand molecules, as will be discussed in the upcoming **chapter 3.2**. These irregularities can introduce additional electronic states in the semiconductor nanoparticle band structure. This can for example create electronic states inside the bandgap, which are then called trap states, as shown in **Figure 4**.^{27,28}

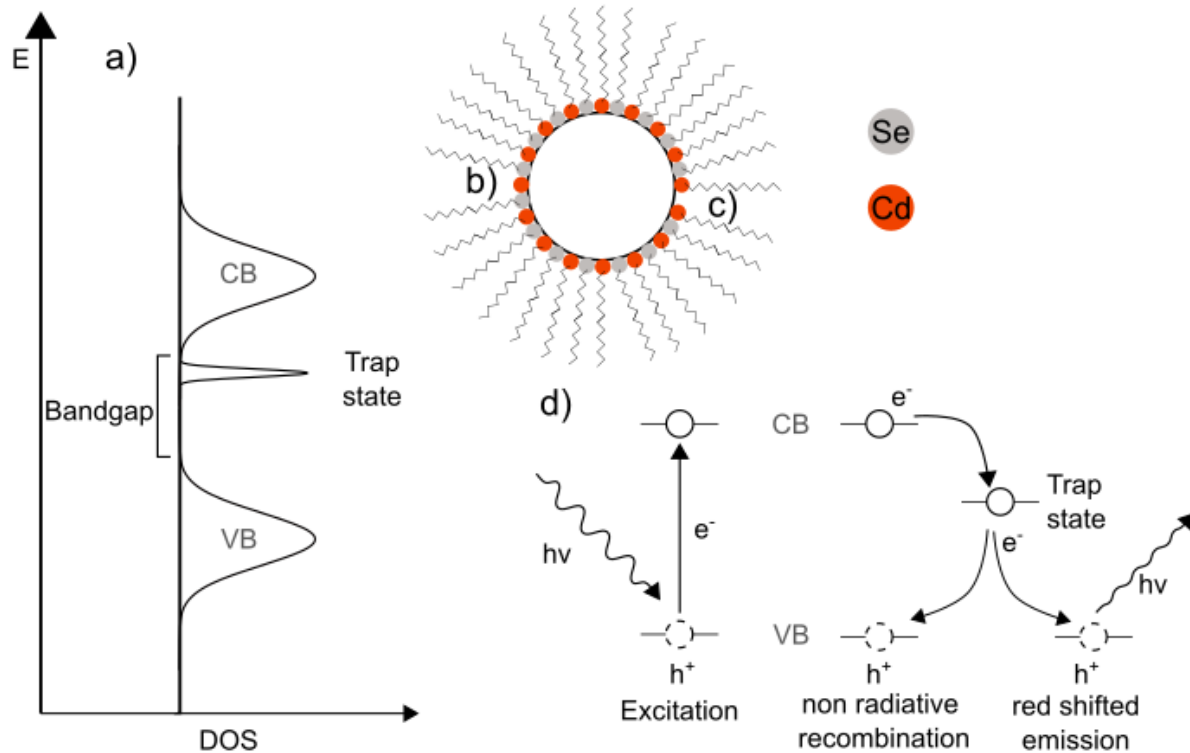


Figure 4: a) Schematic representation for DOS for an imperfect nanocrystal with trap states that are located inside the bandgap. Trap states can be induced due to unsaturated surface atoms, either through b) incomplete surface saturation with ligands or c) missing surface atoms. d) Trap states can allow for alternative, non-radiative recombination pathways or recombination under emission of light with a longer wavelength due to the lower energy difference.

These trap states can influence the optical properties of the QD through so-called trapping processes. Trap states provide secondary relaxation pathways that are either nonradiative or result in emission of light with longer wavelength, as the energy difference to the valence band is diminished. Both pathways result in a reduction of the main fluorescence efficiency of the nanocrystal. In such a trapping process, an electron assumes an interband trap state instead of recombining with the valence band hole under the emission of light. As the overall number of available electrons in one semiconductor nanocrystal is extremely low, a high number of trap states that possess a long lifetime can effectively deactivate the fluorescence of the nanoparticle for the duration of the trapping.²⁹ This effect is called blinking and is unwanted in fluorescence applications as it reduces the overall quantum yield of the nanoparticle.^{30–32}

To further understand the creation of surface trap states, we need to take a look at the role of surface ligands during the synthesis of the QDs and how they can contribute to the optical and electric properties of our QDs.

3.2 The Role of QD surface and surface ligands in optical properties

As shown above, the size and crystal structure of a semiconductor QD directly relates to its electronic and optical properties. Therefore, a great amount of effort in QD research is focused on precisely controlling these properties. This can be achieved in a variety of ways, for example through variation of the precursor chemicals, solvents or differences in the synthetic approach, such as hot injection or heat-up synthesis.^{4,33,34} This allows for particles of varying sizes and shapes, which can be stabilized by different surface molecules. In most cases, this native ligand shell contains long chained fatty acids, phosphine oxides or amines (**Figure 5 (a-c)**), that bind to the surfaces and provide colloidal stability, i.e. prohibition of aggregation, via steric and electrostatic repulsion of the particles.

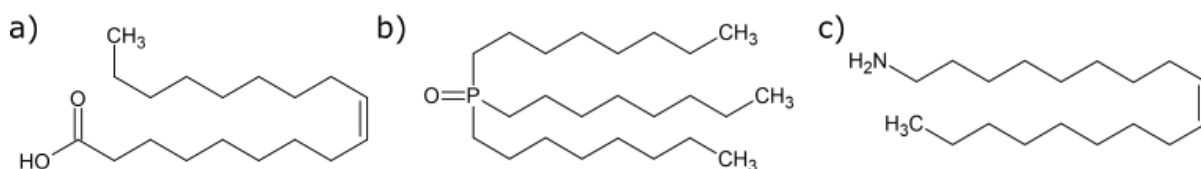


Figure 5: Illustration of different stabilizing agents and ligand molecules. a) Oleic acid, b) Trioctylphosphineoxide, c) Oleylamine.

Besides stabilization, the native ligand shell also provides a passivation of the QD surface to eliminate surface trap states as discussed in the previous chapter. Hereby, the assumption is that ligands bind to under-coordinated surface atoms and the resulting molecular orbitals hybridize with valence or conduction band states to passivate and eliminate surface traps, as shown in **Figure 6**.^{35,36}

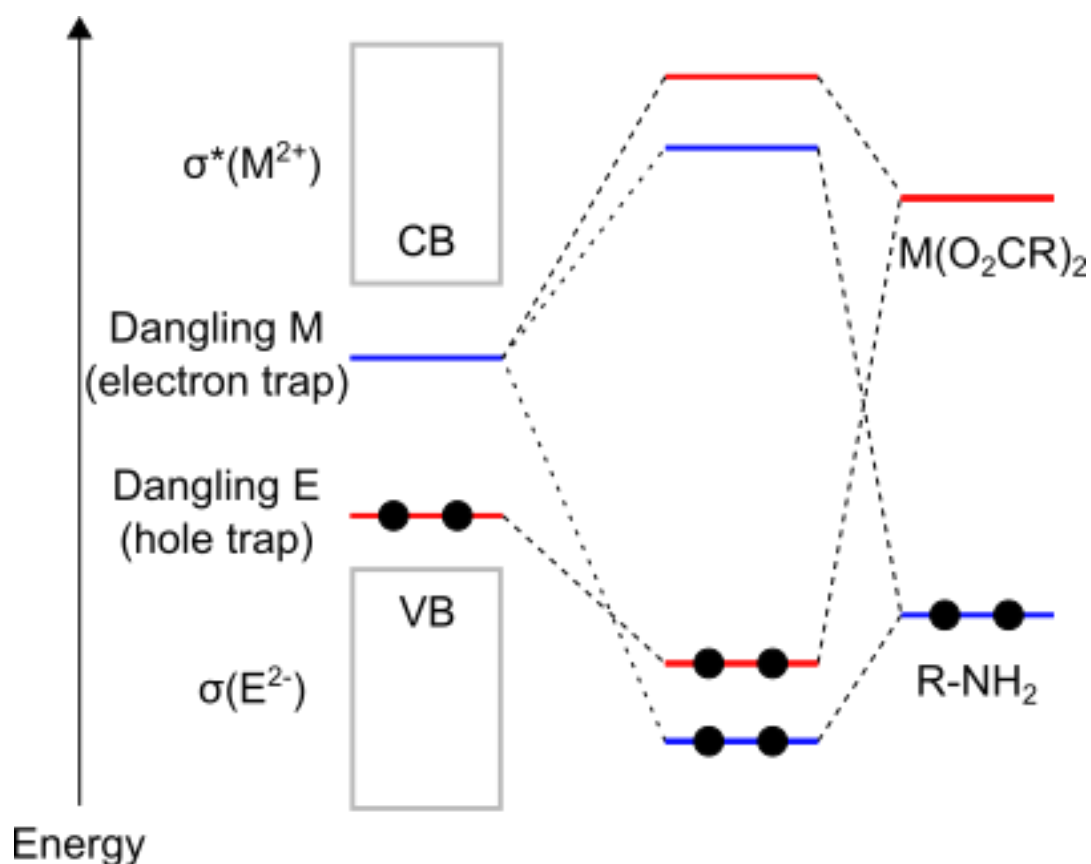


Figure 6: Schematic representation of trap state elimination through ligand molecules. Image taken from the work of A.J. Houtepen.³⁶ Copyright 2016 American Chemical Society.

Based on this model, ligands can be categorized into three different types according to the number of electrons the ligand uses to form a bond with the surface. **Figure 7** gives a schematic overview of the three different types of ligands and their bonding behavior.

L-Type ligands are two electron donors (Lewis acids) such as amines that bind with Lewis acidic surface sites. X-Type ligands such as carboxylates or trioctylphosphineoxide (TOPO) provide one electron to form a bond and Z-type ligands are two electron acceptors that can bind to electron donating surface sites.

Theoretical Background

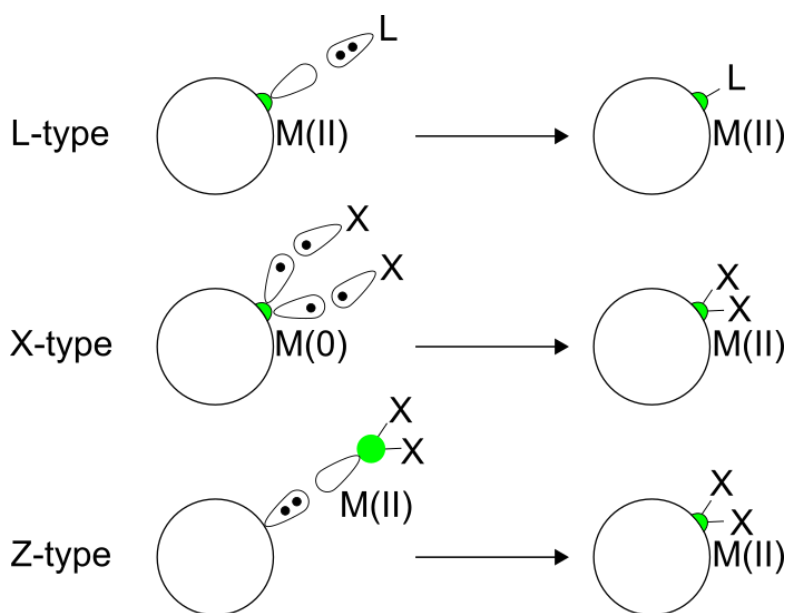


Figure 7: Schematic visualization of ligand types. a) L-type ligands as two electron donors. b) X-type ligands functioning as one electron donor. c) Z-type ligands act as two electron acceptors to form a bond. Image taken from the work of A.J. Houtepen.³⁶ Copyright 2016 American Chemical Society.

Through careful selection of the stabilizing ligands, surface trap states can be mostly eliminated and the overall fluorescence properties can be enhanced. The most used ligands in QD synthesis provide a good passivation of the nanoparticle surface, while also allowing for steric separation of the particles through their long-chained molecule structure.

In addition to the saturation of surface trap states, the low dielectric constant of the ligand shell on the QDs surface and the surrounding medium make stabilization of charges on the surface unfavorable, confining the exciton recombination to the particle core. In contrast, a chemical environment with a high dielectric constant has been shown to increase the likelihood of charge transfer to the particle surface and stabilizes surface trap states, diminishing the quantum yield of the QDs.^{37,38}

Complementary to the passivation of the QD surface through the native ligand shell, additional steps can be taken after the synthesis to optimize the optical properties and functionality of the QDs. An alternative way to passivate the QD surface and remove trap states is through growth of an inorganic passivation shell on the QD's surface. In the case of CdSe QDs, this is often done with a layer of cadmium sulfide, whose crystal structure is similar enough to allow for epitaxial growth avoiding defects, while the difference in the bandgap position is large enough to restrict the exciton to the QDs core. This enables a reliable inorganic saturation of dangling surfaces bonds effectively eliminating the majority of surface trap states.³⁹⁻⁴¹

3.3 CdSe based hybrid materials

By itself, a material produced from colloidal CdSe QDs can already be considered a hybrid system as it contains the inorganic QDs and their organic ligand shell. The native ligand shell of CdSe QDs after synthesis consists mainly of long chained inert molecules that provide surface saturation and colloidal stability in solution.^{4–6} On the other hand, these native ligands are themselves mostly inert and function as an isolating barrier between QDs and are not ideal for a variety of QD applications, which require electric conductivity, solubility in polar solvents or biocompatibility.^{42–45} This can be addressed through the exchange of the inert ligands with molecules with different anchoring groups, chain lengths, functional groups and polarities. The exchange of the native ligand shell with functional molecules allows for further modification of the optical and electric properties of the resulting hybrid material, while preserving the main properties of the QDs. In this chapter, we want to discuss different approaches for the exchange of the native ligand shell for functional molecules and provide a short overview of the physical properties that can be modified due to this exchange. As the focus of this work is centered around CdSe based hybrid materials, the ligand exchange methods discussed in the following will be on the example of CdSe QDs.

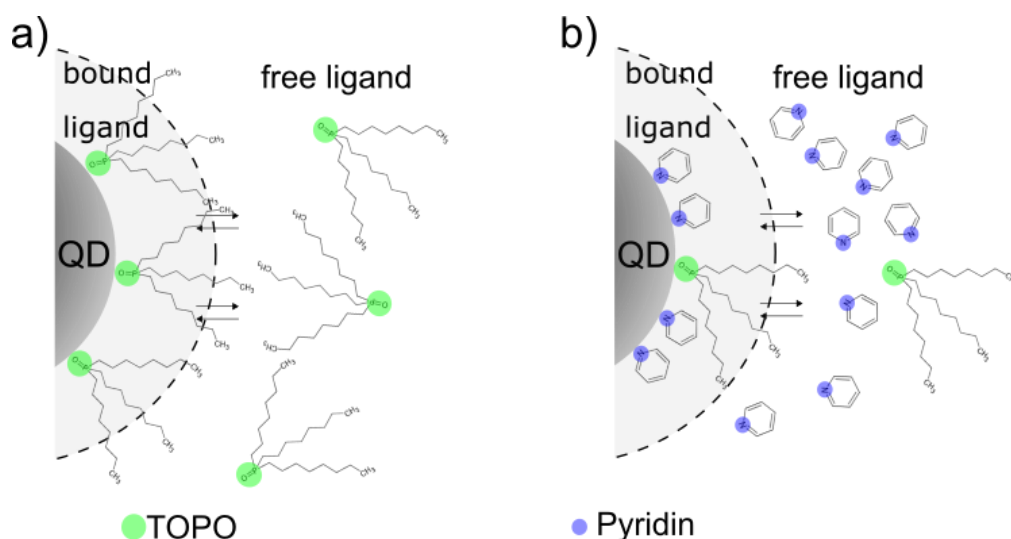


Figure 8: Schematic of ligand exchange using excess pyridine to displace the native Trioctylphosphine Oxide (TOPO) ligand shell. a) Equilibrium between bound TOPO ligands and unbound ligands in solution. b) Replacement of TOPO through excess pyridine in solution shifting the surface equilibrium towards pyridine stabilization.

The native ligand shell in a colloidal QD solution is the result of an equilibrium of ligand molecules that are attached to the surface and free molecules in solution, as shown in **Figure 8**. This equilibrium can be exploited to introduce new molecules into the ligand shell of the

Theoretical Background

QD by providing the new molecule in large excess into the solution, which shifts the equilibrium in favor of the excess molecule. One of the earliest examples for this direct exchange of ligands is the replacement of trioctylphosphine oxide type ligands through pyridine as a ligand, performed by the groups of Bawendi and Alivisatos, through heating of the QDs in pyridine as a solvent.^{3,46} The resulting ligand shell is a mixture of the native ligands and the excess molecule, where the displaced amount of native ligand molecules is mostly dependent on the affinity of the ligands to bind to the surface of the QDs, such that molecules with a higher binding affinity more easily replace ligands with a smaller one. The differences in binding affinity are dependent on a multitude of factors such as the QD surface composition and ligand binding type (**chapter 3.2**).

Another very successful approach, that is explored in this work, is to first displace the native ligand shell with small inorganic species, which has been mostly utilized to increase charge transport in QD films, as their native ligand shells usually provide great insulation of the QDs to each other. The group of Eychmüller et al. has published a simple two step procedure for the ligand exchange of CdSe QDs using ammonium iodide and n-butylamine, as shown in **Figure 9**.⁴

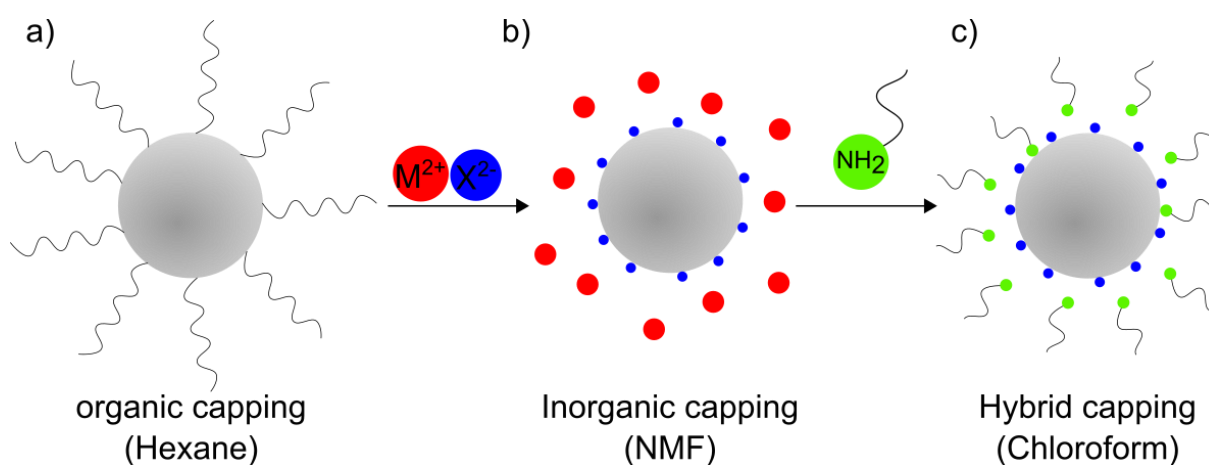


Figure 9: Schematic of ligand exchange of the native organic, long-chained ligand shell with a hybrid, organic-inorganic ligand shell. a) Native ligand shell of long-chained organic molecules stabilizing QDs in non-polar solvents (hexane). b) Transfer of QDs into N-methylamine formamide solvent through ligand exchange with Ammonium iodide salt resulting in inorganic stabilization. c) Transfer of QDs into chloroform solvent through ligand exchange using an excess of n-butylamine, creating a hybrid organic inorganic ligand shell. The modified graphic is taken from the work of Eychmüller et al. ⁴ Copyright 2017 American Chemical Society.

In this approach, the high affinity of iodine ions to bind to the QD surface is exploited to transfer the CdSe QDs from nonpolar to a highly polar solvent, while forming an

electrostatically stabilized QD solution. To further improve the stability and handling of the colloidal QD solution, a second exchange using an excess of butylamine is performed resulting in hybrid iodine/butylamine stabilized QDs. As butylamine has a rather weak binding affinity to the QD surface and is a volatile compound, it can be easily replaced by other molecules or even be removed through increasing temperatures. Functional molecules can then be introduced through the already described direct ligand exchange, by decorating the QDs with an excess of functional molecules. This exchange procedure using solvent transfer and electrostatic stabilization allows for the exchange with functional molecules that are otherwise unable to replace the native ligand shell due to their comparatively low binding affinity.

3.4 Properties of organic semiconductors on the example of Phthalocyanines

Phthalocyanines (Pc) are a well-known group of metal complexes that through their high stability and strong blue/green color scheme were initially used as pigments and are characterized by a planar structure of four isoindole units linked by nitrogen atoms, analogous to porphyrins as shown in **Figure 10**.

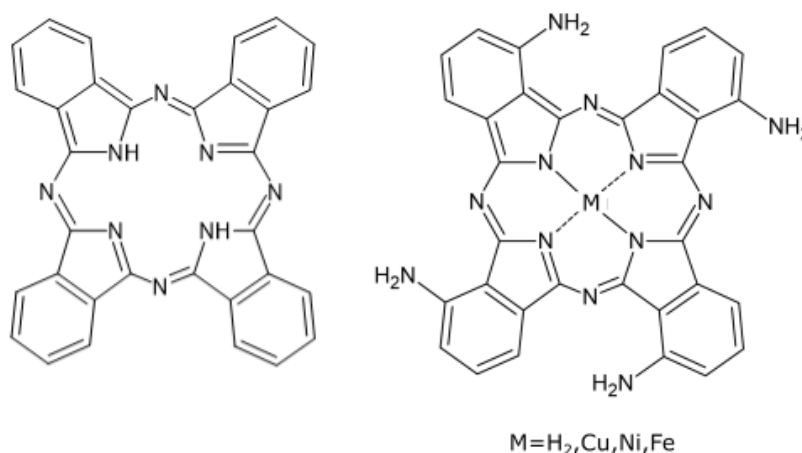


Figure 10: Schematic of unmodified metal-free phthalocyanine molecules (left) and 4,4',4'',4'''-tetraamino phthalocyanine (4APc) with varying metal centers (right).

They have become a subject of great interest in research for their high stability and chemical flexibility, that enables the preparation of a variety of differently substituted derivatives allowing to tailor their electronic, optical and physical properties to suit a variety of applications, such as solar cells, optical switching and cancer treatment.⁴⁷⁻⁴⁹ This flexibility is further increased through the variety of available different metal centers and their ability to

either function as electron accepting or donating complexes and has led to their further study as catalytic species.^{50,51}

In this chapter, we want to discuss the optical, electric and physical properties of 4,4',4'',4'''-tetraamino phthalocyanine (4APc) molecules with different metal centers and how they enable us to fine-tune the properties of CdSe based hybrid materials. The phthalocyanine species used in this work have been modified through the addition of four amino-groups to the outer rings of the molecule structure as shown in **Figure 10** to increase their binding affinity to the QD surface and increase the solubility in polar solvents. As the research of the physical, optical and electronic properties of these 4APc complexes is still in progress, we will mostly refer to the unsubstituted phthalocyanine complexes, as their properties are well documented and should give a good indication for the behavior of the substituted species.

3.4.1 Optical properties

The use of 4APc molecules in the CdSe based hybrid materials adds their specific absorption and emission properties to the material. The 4APc molecules possess a broader absorption range than CdSe QDs, which reaches into the near infrared spectrum at up to 780 nm for thin films, whereas CdSe QD are limited to the visible spectrum at around 630 nm. Phthalocyanine complexes usually exhibit two strong absorption bands, the so-called B-band at around 300-400 nm and the Q-band at around 650-700 nm, as shown in **Figure 11**

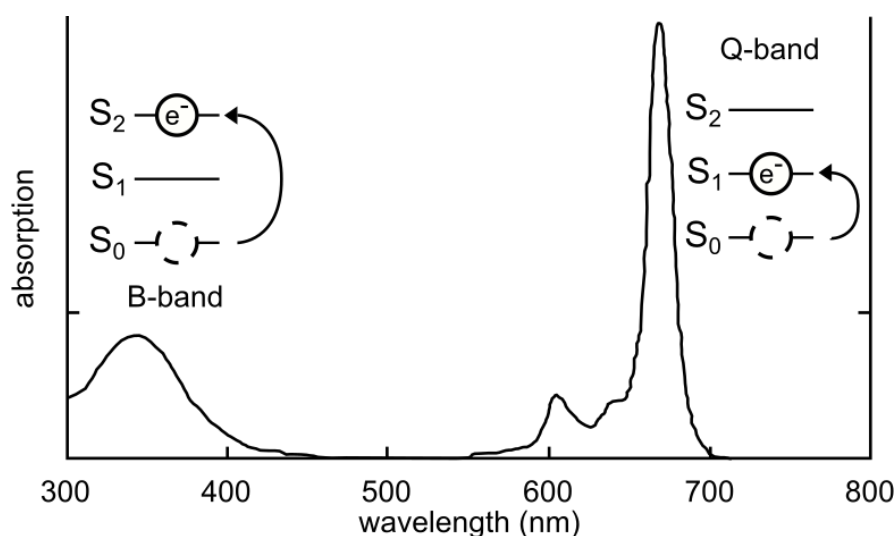


Figure 11: Absorption spectrum of zinc-phthalocyanine with distinct B- and Q-absorption bands. The B-band absorption is caused by the transition of electrons from the ground state (S_0) to the second excited state (S_2), while the Q-band absorption is related to the transition from the ground state (S_0) to the first excited state (S_1). Spectral data taken from "The Porphyrin Handbook" vol 16 Copyright 2003 Elsevier Inc.⁵²

These bands are the result of electron transitions in the pi-system of the molecule, where the B-band is caused by the transition from the highest occupied molecule orbital (HOMO) to the second excited state and the Q-band is the transition from the HOMO to the lowest unoccupied molecule orbital (LUMO). The Q-band mostly dominates the optical properties of the phthalocyanine molecule and is responsible for its green-blue coloration. The HOMO-LUMO transition responsible for the Q-band absorption can be shifted through change of the phthalocyanine complexes metal center, as theoretical models and absorption studies have shown (**Figure 12**).

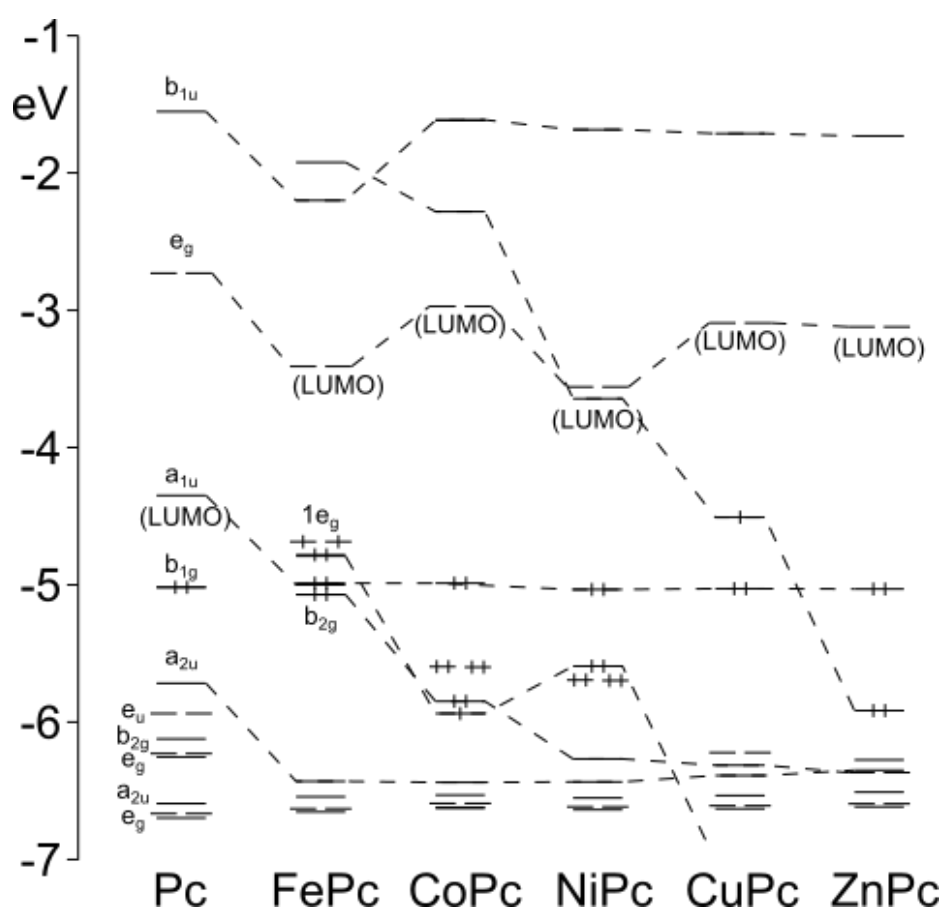


Figure 12: Schematic visualization of calculated molecule orbital energy levels in phthalocyanine complexes with varying metal central atoms. The energy levels of the molecule orbitals can change significantly by changing the central metal atom. Most noticeable here is the change in energy for the HOMO LUMO transition that governs the position of the Q-band absorption. Schematic taken from the work of Liao and Schreiner.⁵³ Copyright 2002 Wiley Periodicals LLC

The species discussed in this work (Fe, Ni, Cu and metal free) were chosen to represent the variety of electronic structures in phthalocyanines, with the calculated HOMO-LUMO transition energies ranging from 1.38 eV for iron phthalocyanine up to 1.53 eV for the metal

Theoretical Background

free phthalocyanine species.^{54,55} Additionally to the changes of the metal center, the addition of substituent groups to the ring system can further change the electronic and optical properties of the phthalocyanine complex. The addition of four Amino groups to the ring systems, as in the molecules used in this work has been studied by the example of tetra amino zinc phthalocyanine (Zn4APc) by the group of Liu et al.⁵⁶ These studies show a significant red shift of the Q-band absorption maxima of the tetra amino zinc phthalocyanine from 670 nm to 765 nm compared to zinc phthalocyanine without the NH₂ functionalization.

It has been shown by the Scheele group that the use of Zn4APC molecules in a CdSe based hybrid material even allows for the excitation with 847 nm laser sources that would normally not show interactions with CdSe QDs as it is above the first excitonic transition of the QDs and mostly outside of the absorption range of the QD material.⁵⁷ The broad absorption of the tetra amino phthalocyanines should allow for manipulation using higher wavelength laser excitation such as 633 nm and above that show low interaction with the QD material. Using this divergence in absorption properties should allow for the targeted excitation of both components and their specific fluorescence using different excitation wavelengths. Furthermore, the fluorescence of phthalocyanine molecules is sensitive to degradation under laser excitation in the presence of atmospheric oxygen and water, which makes phthalocyanines an ideal candidate for fluorescence patterning creating a negative fluorescence contrast under laser excitation (**see chapter 3.5**).^{58,59}

3.4.2 Dielectric properties

As already discussed in **chapter 3.2**, the optical and electrical properties of QDs are not only dependent on their material and size but are also dependent on their surrounding medium. To further elaborate on this, we now want to discuss the change of the dielectric environment that occurs through replacement of the native ligand shell of the CdSe QDs with 4APc molecules. The relative electric permeability or dielectric constant of the surrounding medium is an indication for the ability of a material to stabilize charges. The native ligand shell of synthesized CdSe is mostly comprised of long chained molecules, such as oleic acid or trioctylphosphineoxide, that show a generally low dielectric constant of 2.1 and 2.5, respectively.^{60,61} In comparison, phthalocyanines with their extended 16 electron pi-system have been shown to have a higher dielectric constant of 2.7 and higher, which is tunable through selection of the central metal atom of the complex. This enables us to create a

material where the QDs are placed in a dielectric environment with an adjustable dielectric constant ranging from 2.74 for zinc-phthalocyanine up to 8.9 for iron-phthalocyanine.^{62–67} This change in the chemical environment has to be considered when looking at the optical properties of the CdSe QDs in the resulting hybrid material, as it has been shown that the quantum confinement in the particle is dependent on the dielectric properties of the surrounding material or solvent.⁶⁸ The removal of the isolating shell and the change to an environment with higher dielectric constant has been shown to increase interparticle coupling and should be visible in a shift of the optical and electronic properties of the QDs.^{69–71} Furthermore, a chemical environment with a higher dielectric constant allows for easier transfer of charges to the particle surface, which can improve the electronic conductivity, but can also lead to the stabilization of trap state charges on the surface, diminishing the fluorescence quantum yield of the material (see chapter 3.1.3).^{37,38}

3.4.3 Catalytic properties

The flexibility of the electronic structure of phthalocyanine metal complexes through substitution of the metal center has also made them subject for catalytic studies, as they have been shown to function as either electron donor or acceptor centers enabling a variety of reactions.⁵⁰ In this work, we want to especially focus on the activation of oxygen through phthalocyanine complexes as both the diminishment of the phthalocyanine fluorescence and increase of the QD fluorescence under excitation are predicated on their respective oxidative processes. All metal-phthalocyanine complexes used in this work have been demonstrated to function as oxygen activating catalyst forming an oxygen binding intermediate allowing for the use of molecular oxygen as readily available oxidation agent. Although all metal phthalocyanine complexes show oxidative properties, most recent research focused on the use of Iron phthalocyanine-based complexes for oxidative purposes. As shown in **Figure 13** iron complexes allow for the bonding of oxygen species to the metal center of the complex and subsequent homo- or heterolytic cleaving of the oxygen-oxygen bond.⁷² In this process either radical or charged oxygen species are created and released from the complex. These reactive oxygen species (ROS) are then available as oxidation agents or can transform into further ROS through reaction with the environment.

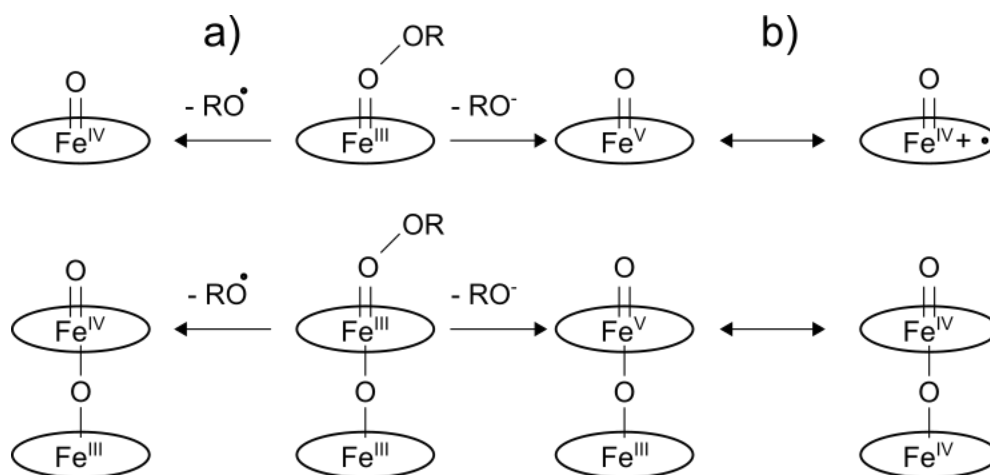


Figure 13: schematic for possible pathways for forming reactive oxygen species under a) homolytic oxygen cleavage and b) heterolytic oxygen cleavage on the example of mono- and binuclear iron complexes. The cleaving of the oxygen bond allows for the creation of radical and ionic oxygen species that can further react to form a variety of reactive oxygen species. Schematic taken from the work of Sorokin and Kudrik.⁷² Copyright 2011 Elsevier

3.5 Optical patterning using semiconductor materials

Recently, semiconductor QDs have been used as very efficient absorber materials in optical patterning processes.¹² As shown in previous chapters, CdSe QDs are ideal for this as they are available through a variety of synthetic methods that allow for precise control of size, shape and crystal structure of the particles and their resulting optical properties.^{4,33,34} There are a variety of methods that are currently used to produce fluorescence patterns from CdSe QDs, which can be divided in two general strategic approaches.

One approach to creating a pattern of interest is by manipulating the stabilizing ligand shell that surrounds the CdSe QDs and allows for solution processability. In this process, the stabilizing ligands undergo structural or chemical transformation under irradiation with UV light, electron beam or X-rays that drastically change the particles solubility due to cross linking or protonation.^{12,73–76} The spatial pattern can be achieved either through targeted control of the beam, directly writing the pattern into the material or application of a mask that contains the desired pattern. After irradiation, unaltered particles can be removed by a washing process leaving only the irradiated material to shape a pattern as shown in **Figure 14**.

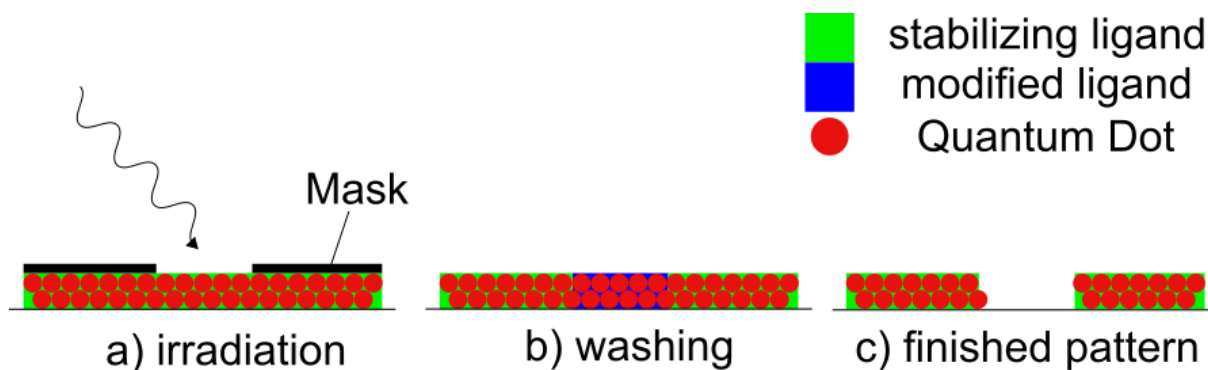


Figure 14: Schematic of optical patterning via ligand modification under irradiation to modify solution processability. a) Irradiation with a mask containing the desired pattern modifying the exposed stabilizing ligands. b) Washing with an appropriate solvent to remove the modified QDs. c) Finished pattern of unaltered QDs.

Another approach is the direct transformation of the optical properties of the absorber material to create a pattern. Photo-degeneration via optical irradiation of either the surface ligand or the surface of the QDs has been successfully applied to change the spatial properties of the fluorescence. For the first approach, CdSe QDs are functionalized with a photo sensitive fluorescence quencher such as polyviologen. Degradation of this molecule through irradiation will restore the initial fluorescence yield and result in a positive fluorescence contrast.⁷⁷

Furthermore, it has been shown that a thin oxide layer on top of the CdSe QDs is beneficial for the overall quantum yield during the photooxidation process. It has been shown that the above-bandgap optical excitation of CdSe QDs under ambient conditions leads to a smoothing of the surface by oxidation of defect centers. This eliminates trap states, as shown in **Figure 15** and, thus, improves the overall radiative recombination and quantum yield of the particles.⁷⁸⁻⁸¹ The creation of a cadmium oxide (CdO) layer on the particle surface further saturates any dangling bonds (see Chapter 3.2), resulting in a positive fluorescence contrast.

Theoretical Background

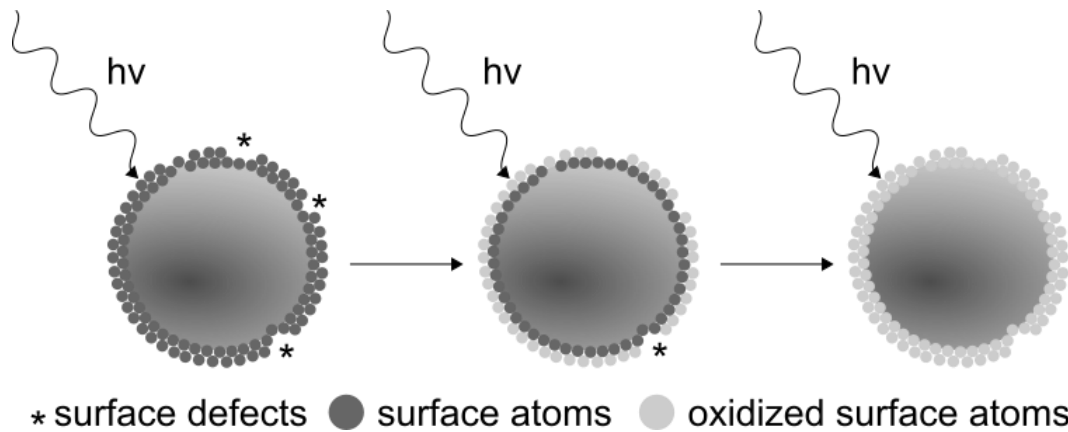


Figure 15: Visualization of gradual oxidation of surface atoms through targeted laser light excitation and resulting elimination of surface defects and resulting trap states.

Using this process, CdSe QD materials have been utilized to create optical patterns either using an optical mask to control the spatial resolution, or through targeted excitation with a focused laser beam.⁸² As shown in **Figure 16**, the targeted laser excitation can be used to directly write optical patterns in the CdSe QD material.

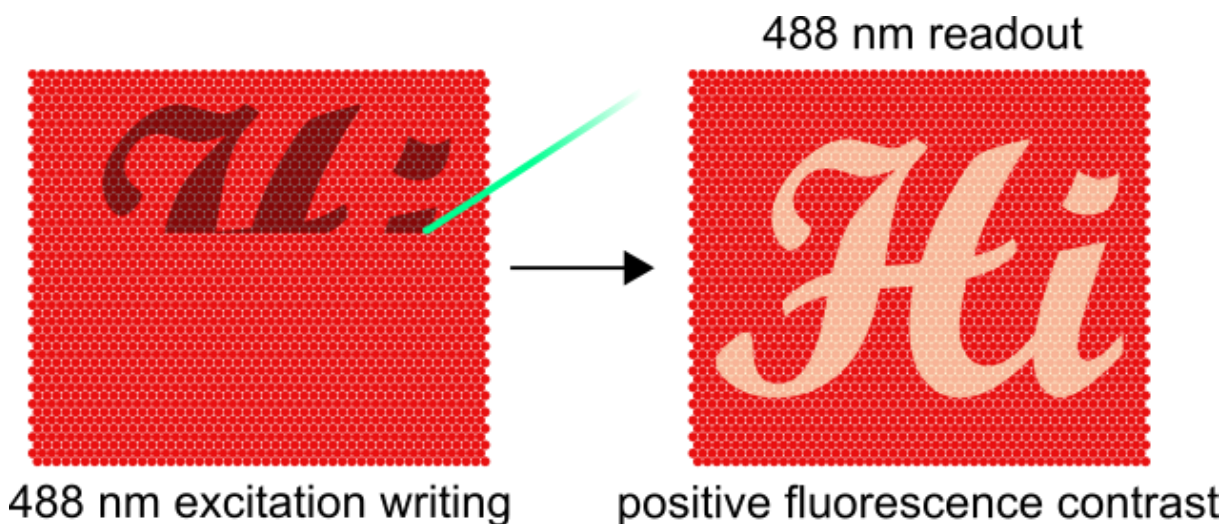


Figure 16: Schematic of positive fluorescence contrast writing with CdSe QDs. Excitation using 488 nm laser source resulting in a positive fluorescence contrast pattern.

The majority of CdSe based fluorescence patterning utilizes a positive fluorescence contrast because a negative contrast has been challenging to realize and often results in the destruction of the QD material.

To allow for a high-resolution patterning, while also providing the ability for wavelength-dependent excitation in the patterning and imaging process, a confocal laser microscopy setup using a 488 nm and 633 nm excitation laser is used in this work.

3.6 Confocal microscopy

The following section is meant to give the reader a brief overview of the theory of confocal microscopy and the concepts governing resolution limits. A more detailed discussion of all these aspects can be found in the references cited in this chapter and especially in the following books that have been used as reference:^{83,84}

- Pawel B. James, *Handbook of Biological confocal Microscopy*, 2nd Edition, Springer, Berlin, **1995**
- Gu Min, *Advanced Optical Imaging Theory*, 1st Edition, Springer, Berlin, **2000**

Microscopy has been one of the most essential tools of scientists for over a century, the ability to optically resolve even the smallest structures in our environment led to an immeasurable amount of scientific discoveries. The identification of ever smaller structures was driven by the constant improvement of the optical components used in microscopic setups, which resulted in ever higher spatial resolution.

In optical microscopy, the spatial resolution is limited by diffraction, so that even a point-like source will have a blurred image, which can be described by the so-called point spread function (PSF) of the optical system.^{85,86} The PSF limits the spatial distance Δx at which two point-like sources can be distinguished from a single source, thus determining the resolution of the microscope. The PSF for a perfect lens with a circular aperture can be described as a so-called airy disc, which is a circular diffraction image of the point like source with a central bright disk and weaker concentric dark and bright rings. This structure is a result of the refraction of the light and the resulting positive and negative interference of the scattered light resulting in this disc-like structure. Ernst Abbe defined the minimal distance Δx , based on the airy disk radius, to distinguish between two PSFs as:

$$\Delta x = 0.6098 \frac{\lambda}{n \sin \alpha} = 0.6098 \frac{\lambda}{NA} \quad 5$$

Δx is the distance of two separate objects at which they can still be distinguished from each other and λ is the wavelength of the light used. The Term $n \sin \alpha$ is also known as the numerical aperture (NA) and is a measure for the ability of an optical system to focus light, or the maximum collection angle of an optical system. According to Abbe, two point like sources can be distinguished if Δx is larger than the value given in equation 5. In **Figure 17**, a schematic representation of the PSF is shown.

Theoretical Background

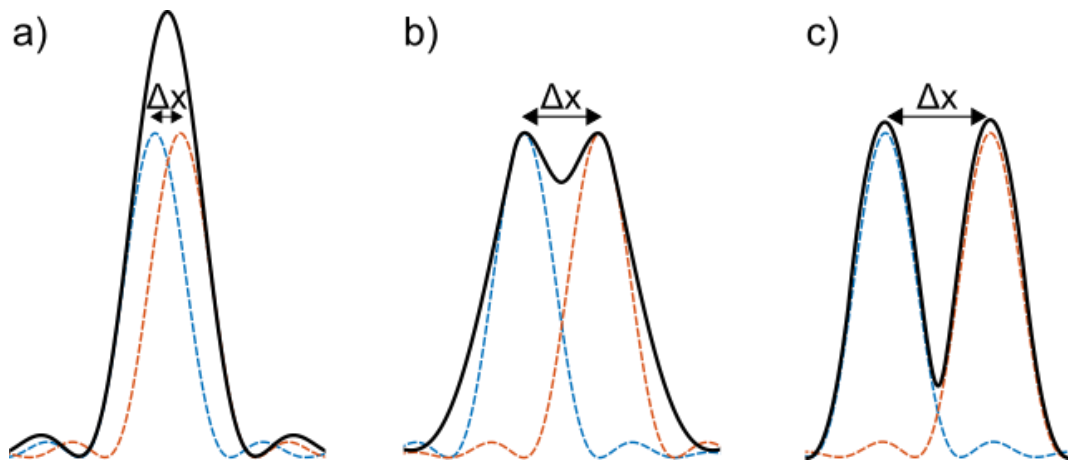


Figure 17: (a)-(c) show the line section produced by two different point-like sources (blue and red dashed line) together with their sum (black line). The distance between the maxima of both objects is defined by Δx . (a) The distance Δx is smaller than the value given by equation 5 and the 2 sources cannot be distinguished. (b) The distance Δx is chosen in a way that both sources can be distinguished, as the first minimum of the black curve is located at the maximum of the red curve and vice versa, this configuration is called the Rayleigh criterion. (c) The distance Δx is much larger and both sources can be clearly distinguished.

The case when two point-like sources cannot be distinguished from each other is represented in **Figure 17** (a), when the distance Δx between the two line sections (red and blue dashed line) of the Airy disc is smaller than the value given by **Equation 5** and their sum (black) appears as one point-like source. In **Figure 17** (b), Δx is chosen as the minimal distance under which the two point-like sources can be distinguished from each other. In this case, the maximum of the blue dashed curve coincides with the first minimum of the red dashed curve and illustrates the minimum distance defined by **Equation 5**, which is also called the Rayleigh criterion. Under consideration of the Rayleigh criterion, the PSF can be distinguished in the image plane (black line). **Figure 17** (c) illustrates the case of an even larger Δx between the two PSFs where both point-like sources can be easily distinguished from each other.

As we can see from **Equation 5** the spatial resolution of an objective lens depends on the refractive index n and the wavelength λ and can therefore be increased by decreasing the wavelength or increasing the refractive index. To change the refractive index, an oil immersion objective can be used as the refractive index of oil with ~ 1.5 is generally higher than the one of air ~ 1.0 , which is the normal surrounding medium in most microscopes.⁸⁷ The use of smaller wavelengths of light is usually limited due to the nature of the investigated objects and the wavelength range that it interacts with.

The Rayleigh criterion gives us a good impression of the resolution of an microscopy objective lens, nevertheless the value according to **Equation 5** tends to underestimate the lateral resolution.⁸⁸ Furthermore, these considerations only concern conventional microscopy and further steps can be taken to increase the optical resolution, for example in fluorescence microscopy. This has been shown by Marvin Minsky, who patented a microscopy setup to spatially filter the signal of the microscopy images by placing a Pinhole (PH) with a radius in the order of the Airy disc into the image plane in 1957.⁸⁹ This allows for a strong discrimination of out of focus light in the image beam, which is referred to as “the confocal principle” as shown in **Figure 18**.

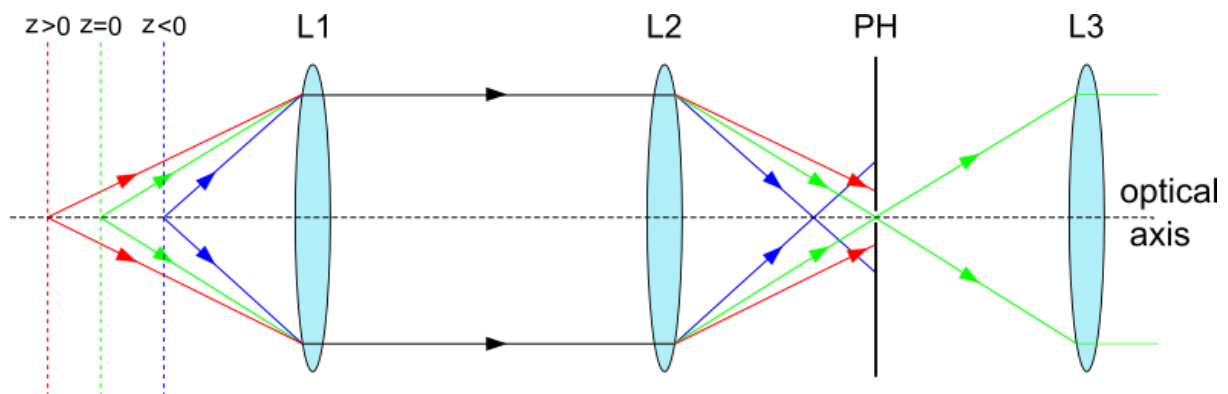


Figure 18: Schematic drawing of the confocal principle for achieving high axial resolution along the optical axis. In this method, a pinhole (PH) is placed in the image plane to reduce out-of-focus light ($z < 0$ in blue, $z > 0$ in red). This way, only light emerging from the focal plane ($z = 0$, shown in green) can pass the PH, while out of focus signal gets drastically reduced.

As shown in **Figure 18** the axial resolution is enhanced in confocal microscopy by placing a PH in the image plane (confocally). In this setup, the focus $z = 0$ and the one of the PH position are conjugated to each other and allow only light emerging from the object in the focus plane $z = 0$ (green beam) to pass the PH. This way, out-of-focus light from ($z \neq 0$, red and blue beam) outside the image plane, that would otherwise contribute to the image as noise, does not reach the detector. In confocal microscopy, the axial resolution is given by:

$$\Delta z = 2 \frac{n\lambda}{NA^2} \quad 6$$

Here, n is the refractive index, λ the wavelength of the beam and NA is the numerical aperture of the setup. The use of this PH in confocal microscopy can lead to an increase of lateral resolution of up to a factor of 1.4 and the spatial filtering significantly reduces out-of-focus

Experimental

light which is favorable in case of denser samples. Due to the focused excitation beam in confocal microscopy, the image of the sample must be obtained through scanning the sample or the beam and obtaining the image point by point. Sample scanning is done through the use of a piezo driven microcontroller stage, that moves the sample through the focal point in x-y direction, collecting the image point by point.

In the context of this work, a home-built confocal scanning fluorescence microscope as described in **chapter 4.1.2** is used to selectively excite a CdSe QD hybrid material and create optical patterns, which can be visualized by imaging the material after the patterning. The high spatial resolution of the scanning microscopy setup allows for the direct creation of detailed fluorescence contrast patterns on a μm scale without the use of an optical mask.⁷⁶ Furthermore, though the use of laser light as the excitation source, a wavelength-selective patterning process becomes possible, allowing for a positive and negative fluorescence response.

4 Experimental

4.1 Methods and Instruments

All measurements and preparations described in the following chapter are done by myself, if not further specified.

4.1.1 UV-vis Absorption spectroscopy

All absorption spectra in the spectral range from 200 nm to 800 nm are recorded using a *Cary Series 5000 UV/vis Spectrometer* from *Agilent Technologies*, using the inbuilt Software *Instrument Cary 5000 version 2.24*. All spectra are acquired under ambient conditions at room temperature (25°C) in a cuvette of 1 cm pathlength for solutions and *Menzel microscopy cover slides* (12x12 mm) for films and are evaluated using *OriginPro*, Version 8.0 from *Origin Labs*. To ensure consistency in the measurements, background spectra are taken beforehand using an empty cuvette or cover slide and subtracted utilizing the spectrometer software.

Size evaluation using absorption spectroscopy

To evaluate the size distribution of CdSe QDs in colloidal solution, the method published by the group of Peng et al. was used.⁹⁰ Here, 10 μL of the synthesized and fully cleaned QD solution in Hexane is diluted through addition of 3 mL of hexane. Absorption spectra are

acquired according to the procedure described above and the particle size is evaluated according to the formula:

$$D = (1.6122 * 10^{-9})\lambda^4 - (2.6575 * 10^{-6})\lambda^3 - (1.6242 * 10^{-3})\lambda^2 - (0.4277)\lambda + 41.57 \quad 7$$

With D (nm) as the diameter of the nanoparticle and λ (nm) as the wavelength of the first excitonic absorption peak of the solution spectra as seen in **Figure 19**. Similarly, the concentration of the solution can be determined through the extinction coefficient of the sample with the formula:

$$\epsilon = 5857(D)^{2.65} \quad 8$$

Using the QD diameter D taken from **equation 7** the extinction coefficient ϵ of the solution is calculated. The concentration c of the solution can then be calculated using Lambert Beer's law:

$$c = \frac{A}{\epsilon} \quad 9$$

With A as the absorption intensity of the first excitonic absorption peak of the solution and the calculated extinction coefficient ϵ .

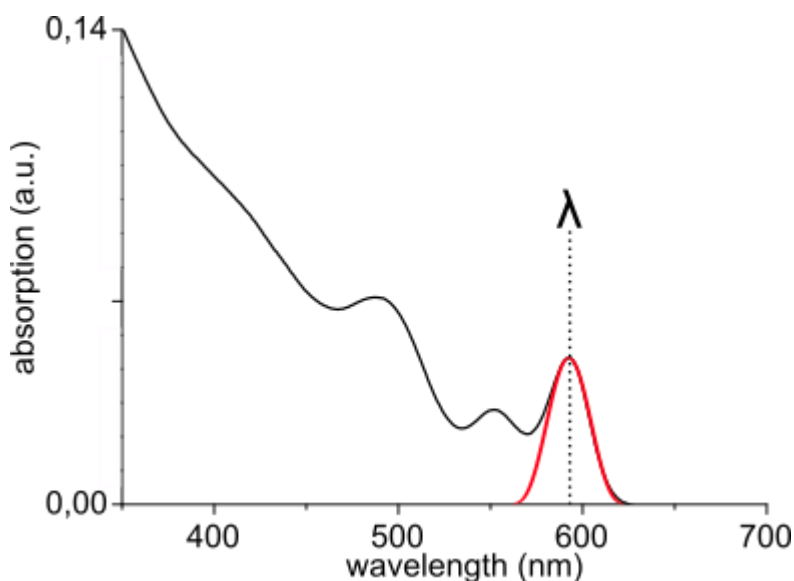


Figure 19: Absorption spectrum of colloidal CdSe QDs. Using a Lorentzian fit to determine the wavelength of the first excitonic absorption peak, to determine size and concentration of the colloidal QDs.

4.1.2 Confocal fluorescence microscopy

All fluorescence experiments were performed with a home-built inverted confocal microscope as seen in **Figure 20** by myself and Jonas Hiller.^{91,92}

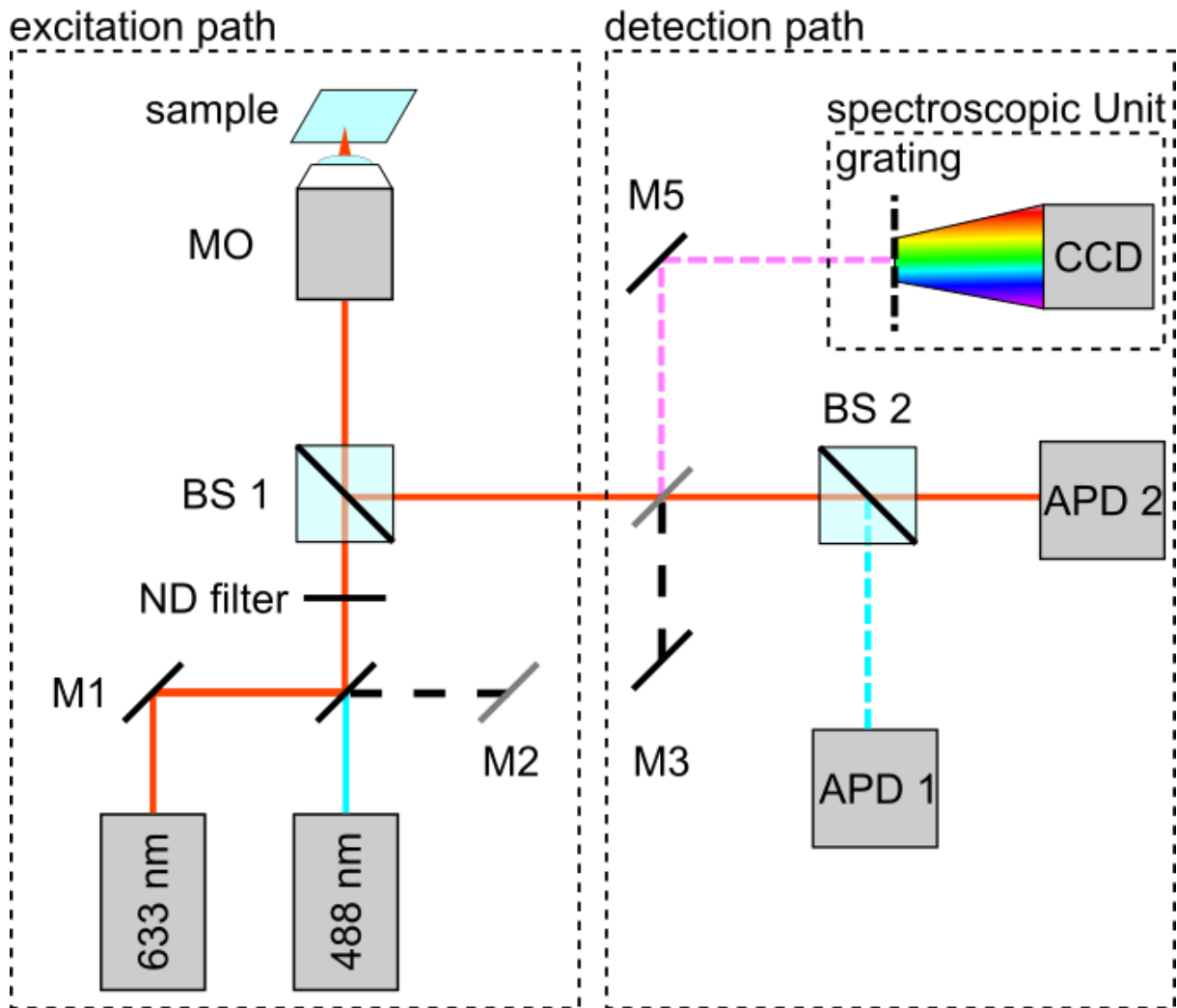


Figure 20: Schematic drawing of the experimental microscopy setup. The dashed rectangles indicate the excitation and the detection beam path. M1-5: mirrors, BS: beam splitter, MO: microscope objective, APD 1,2: avalanche photodiodes, CCD: charged coupled device sensor. The excitation beam path consists of a 488 nm and a 633 nm laser diode as excitation sources, which are operated in CW mode. The excitation light source can be switched through use of mirror (M2) and is focused with an immersion oil objective lens (NA=1.25) onto the sample which is scanned through the focus. The same objective lens is used to collect the detected signal, which is guided through a beam splitter (BS) to the detection path. The detected signal can either be guided to a spectroscopic unit or two different avalanche photodiodes (APD 1,2) for imaging.

The microscopy setup can be divided into two major parts, the excitation and detection beam path indicated in **Figure 20** by the dashed rectangles. An *iBeam-Smart* (488 nm) and a *DL100* (633 nm) diode laser with a *SYS DC110* control unit from *Toptica Photonics* served as excitation light source and a mirror (M2) allows to switch between these laser sources. The excitation laser beams were focused on the hybrid nanocomposite film with a high numerical aperture objective lens (NA=1.25), which is also used to collect the detected signal. The laser sources were used in continuous wave mode and the laser intensity in the diffraction limited focus was approximately 9 kW/cm² for 488 nm and 0.4 kW/cm² for 633 nm. In the detection beam

path, the mirrors M3 and M4 can be used to guide the collected signal either to a spectroscopic unit or to two avalanche photodiodes (APD 1,2). Luminescence patterns are recorded by raster scanning the sample through the focus and using an APD for detection. Spectra are recorded using an Acton-SpectraPro SP-2300 with a coupled Andor iDus DV401A CCD Camera. This microscopy setup allows for spot sizes of $1,39 \cdot 10^{-13} \text{m}^2$ (488 nm) and $2,46 \cdot 10^{-13} \text{m}^2$ (633 nm) and theoretically enables pattern writing and read out in a resolution close to the diffraction limit.

4.1.3 Atomic force microscopy imaging

Atomic force microscopy (AFM) images are taken using the *Scan Asyst, Peakforce-HR* function of the *Bruker Multimode 8 AFM microscope* using a *NanoScope V Controller*. Samples are prepared using dip-coating and drop-casting procedure with 15x15 mm silicon chips as a substrate.

4.1.4 Scanning/Transmission electron microscopy imaging

Scanning Electron microscopy (SEM) and Scanning transmission electron microscopy (STEM) images are recorded with a *Hitachi SU8030* Scanning electron microscope by Elke Nadler and Andre Maier. SEM samples are prepared using dip-coating and drop-casting procedure with 15x15 mm silicon chips as a substrate. TEM samples are prepared through drying 10 μL of a 7 μM CdSe QD solution in hexane on a carbon coated TEM grid.

4.1.5 Raman spectroscopy

Raman spectra are recorded using a Horiba Jobin Yvon Labram HR 800 spectrometer in the group of Prof. Dr. Frank Schreiber. The scattered light was detected by a CCD-1024 \times 256-OPEN-3S9 detector. A He:Ne laser 633 & 532 nm laser excitation were used to excite the sample. Samples are prepared using dip-coating and drop-casting procedure with 15x15 mm silicon chips as a substrate.

5 Synthesis

Parts of this chapter have been already published by myself in the Article: "Simultaneous positive and negative optical patterning with dye-sensitized CdSe quantum dots".⁹³ Specifically the Segments: 5.1.2 "Hot Injection Synthesis of CdSe with mixed Ligands", 5.2 "Phase transfer of QDs using Ammonium Iodide and hybrid ligand shell with n-butylamine" and 5.3 "Hybrid nanocomposite film preparation using dip coating" which were performed and written by myself.

5.1 Synthesis of phthalocyanine linker molecules

This Synthesis is performed by Markus Katzenmeyer

Copper-4,4',4'',4'''-tetranitrophthalocyanine (Cu4APc) is synthesized according to the procedure described by Jung et. al.⁹⁴

Metal free 4,4',4'',4'''-tetranitrophthalocyanine (H₂4APc) is synthesized according to a procedure described by Alzeer et al.⁹⁵ Zinc-phthalocyanine is here cooked in pyridine-HCl for 17 h at 120°.

Nickel-4,4',4'',4'''-tetranitrophthalocyanine (Ni4APc) and iron-4,4',4'',4'''-tetranitrophthalocyanine (Fe4APc) are purchased from ABCR GmbH.

CdSe Synthesis

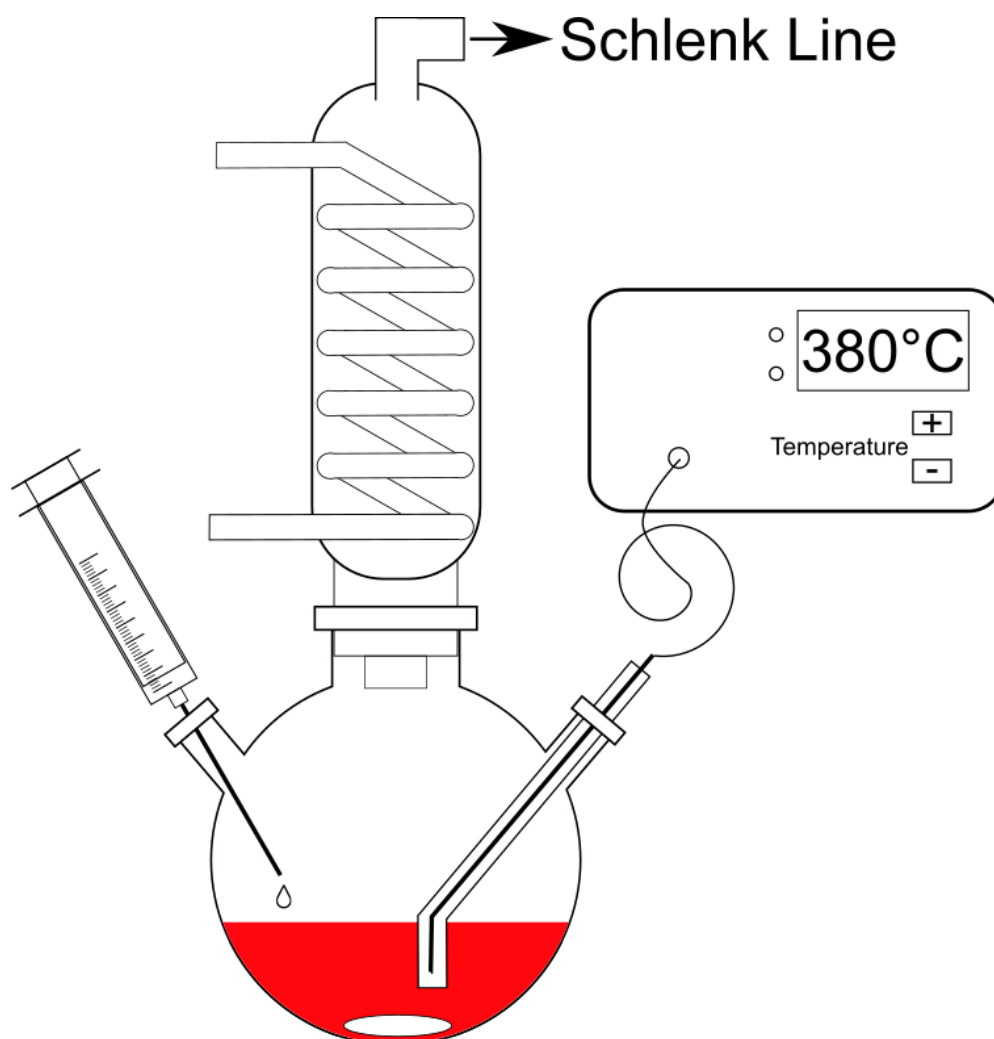


Figure 21: Schematic of experimental setup for CdSe particle synthesis. Setup includes a Three-necked round bottom flask with magnetic stirring, temperature controller, injection valve and Dimroth cooler connected to a Schlenk line.

5.1.1 Hot Injection Synthesis of CdSe with TOPO Ligands

The CdSe QDs are prepared according to the method described by Bawendi et al.⁵ A 50 mL three-necked round bottom flask is loaded with 3 g trioctylphosphine oxide (TOPO), 280 mg octadecylphosphonic acid (ODPA), 60 mg cadmium Oxide (CdO) and is heated under vacuum for 1 h at 150°C. The degassed reaction mixture is put under a nitrogen atmosphere and heated up to 320°C under stirring, until it forms a clear solution. CdO residue is removed through carefully swirling the reaction flask. After the reaction mixture reaches a stable temperature of 320°C again, 1 mL trioctylphosphine is injected and the mixture is heated up to 380°C. At 380°C a degassed solution of 0.5 mL of 1 M selenium in trioctylphosphine (TOPSe)

Synthesis

is quickly injected into the mixture, which instantaneously turns red and the heating mantle is kept at 380°C for a certain time to control the size of the QDs, which is summarized in **Table 1**. After removing the heating mantle, the mixture is cooled down to room temperature. When the temperature of the reaction mixture is below 60°C, 10 mL ethanol are added to precipitate the QDs. The precipitated mixture is moved into a centrifuge vial and rotated with 2600 g for 10 min after which the supernatant is discarded. The particles are cleaned by redispersing them in 2 mL Hexane and precipitating them two times using Acetone and once using Ethanol. The precipitated mixture is centrifuged with 2600 g for 10 min. The cleaned particles are dried under vacuum, redispersed in 3 mL of hexane and stored under nitrogen atmosphere.

QD-Size	Reaction time in min (at 380°C)
3.0 ± 0.1 nm / 3.0 nm	0 (remove heating after injection)
3.5 ± 0.1 nm / 3.5 nm	1.5
4.0 ± 0.1 nm / 4.1 nm	3
4.5 ± 0.2 nm / 4.6 nm	5

Table 1 : Reaction times and resulting nanoparticles size distribution for a range of CdSe particles from 3.0 nm to 4.5 nm.

Characterization

Particle sizes are initially determined using the method published by Peng et al.⁹⁰ The mean particle size in the solution is determined by correlating the first maximum of the UV-vis absorption (**Figure 22a**) of the colloidal particle solutions with a STEM image-based size investigation. These results are confirmed by manual counting of at least 100 particles using the software *ImageJ* (**Figure 22b**) and applying a Gaussian fit resulting in the size distributions listed in **Table 1**. The obtained size distribution is in good agreement with the results of the UV-vis absorption measurement and shows only a small deviation from the mean value.

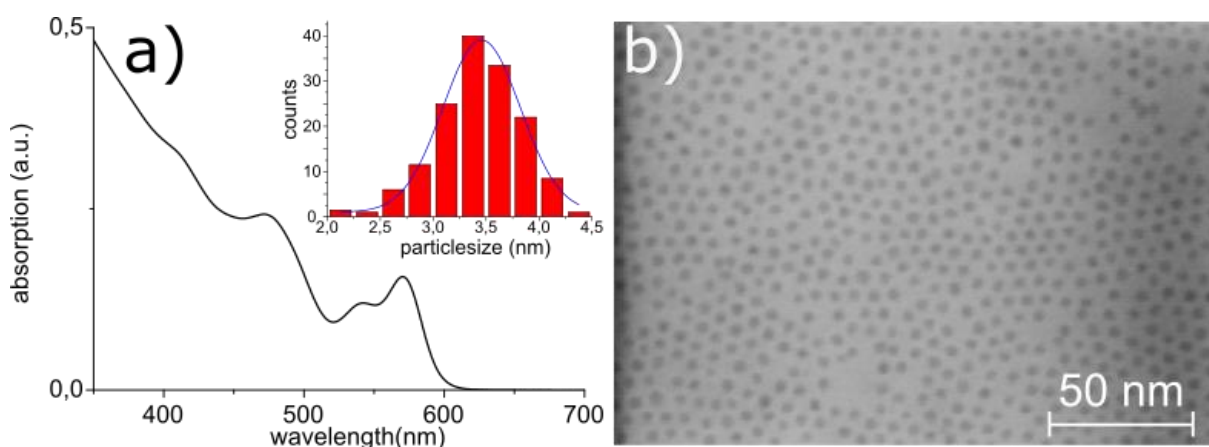


Figure 22: a) UV-vis absorption spectra of 3.5 ± 0.1 nm CdSe NP with size distribution analysis (inset) using STEM images b).

5.1.2 Hot Injection Synthesis of CdSe with mixed Ligands

The CdSe QDs are prepared using a modified literature procedure described by Eychmüller et al.⁴ A three-necked round-bottom flask is loaded with 167.7 mg of CdO, 8 g of TOPO, 2.2 mL of oleic acid (OA), 8 g of hexadecylamine (HAD), 45.8 mL 1-octadecene (ODE) and kept under vacuum for 2 h. The mixture is stirred and heated up to 300°C in a nitrogen atmosphere until a clear solution is formed. Before injection, the mixture is cooled down to 275°C and kept at this temperature for 0.5 h. Degassed solutions of 1.6 mL (1 M) TOPSe, 6.4 mL trioctylphosphine (TOP) and 8.0 mL of ODE are quickly injected into the reaction mixture, which turns to a dark red color. After 25 min of reaction time at 275°C, the heating is removed and the mixture is quickly cooled using a stream of pressurized air. When the temperature of the mixture falls below 100°C, the QDs are precipitated by adding 10 mL of ethanol. The precipitated mixture is centrifuged, the supernatant discarded and the particles redissolved in hexane.

To further remove synthesis educts and excess ligands, the particles dissolved in hexane are precipitated using acetone, centrifuged and then redissolved in hexane. This step is repeated twice-using ethanol for precipitation. The cleaned particles are dissolved in hexane and stored in a nitrogen atmosphere.

Characterization

The particle size of 4.7 ± 0.2 nm is determined using the method published by Peng et al.⁹⁰ The mean particle size in the solution is determined by correlating the first maximum of the UV-vis absorption (**Figure 23 a**) of colloidal particle solutions with a SEM image-based size investigation. These results are confirmed by manual counting of at least 100 particles using the software *ImageJ* (**Figure 23b**) and applying a Gaussian fit. The obtained size distribution is in good agreement with the results of the UV-vis absorption measurement and shows only a small deviation from the mean value.

Synthesis

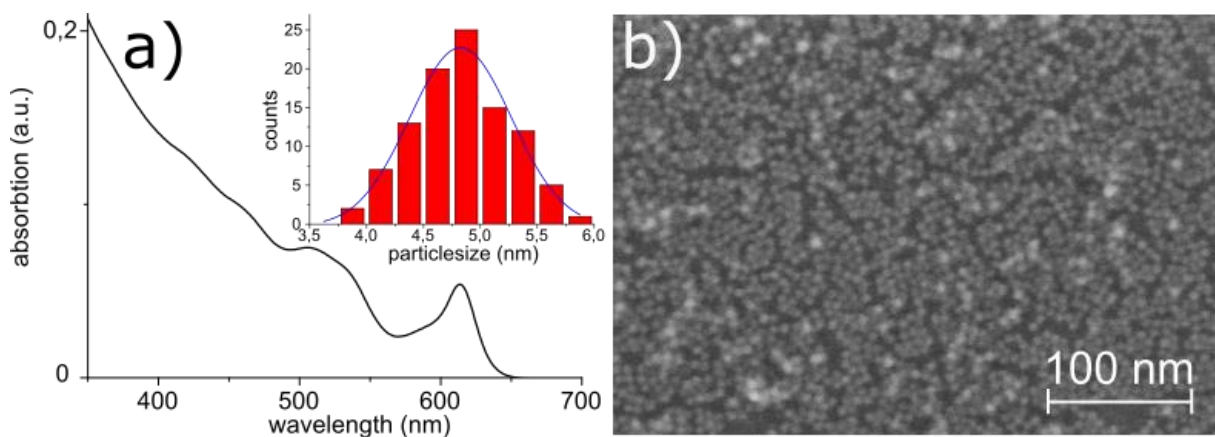


Figure 23: a) UV-vis absorption spectra of 4.7 ± 0.2 nm CdSe NP with size distribution analysis (inset) using SEM images b).

5.1.3 Heat Up Synthesis of CdSe with OA and MA Ligands

The CdSe QDs are synthesized according to a method described by Cao et al.⁶ For preparing the Cd-precursor, a three-necked round bottom flask is loaded with 22.5 mg CdO, 80 mg myristic acid, 5 mL ODE and heated to 100°C under vacuum for 10 min. The mixture is heated up to 240° C in a nitrogen atmosphere and constantly stirred until it forms a clear solution. Residue of CdO is removed through careful swirling of the reaction flask. The mixture is left to cool down to 60°C without removing the heating mantle.

After adding 13 mL ODE, the reaction mixture is heated to 90° C and left under vacuum for 1 h. The reaction mixture is cooled down to 60° C and selenium oxide and cadmium acetate are added according to **Table 2**. The reaction mixture is heated up to 240° C in a nitrogen atmosphere at a rate of 10° C/min, while slowly turning red. Upon reaching 240° C, a mixture of 2 mL ODE and 1 mL OA is slowly added over 5 min, while maintaining the reaction temperature of 240° C. After a reaction time according to **Table 2**, the heating mantle is removed and the mixture is left to cool down to room temperature.

The nanoparticle reaction mixture is cleaned according to the method described by Dempsey et al to remove residual ODE and excess ligand molecules.⁹⁶ After cooling down, 40 ml of toluene are added to the reaction mixture and the solution is split into eight equal parts. Each part is precipitated, by adding 5 mL acetone and centrifuging at 2600 g for 10 min. The white precipitate is removed, and the portions combined again. The particles are precipitated using 100 mL of methanol and centrifuging at 2600 g for 10 min. The supernatant is carefully removed from the red colored oily precipitate and the particles are redispersed in 20 mL of toluene. The particles are further cleaned by adding 20 mL methanol and centrifuging at

2600 g for 10 min. The supernatant is discarded, and 14 mL dichloromethane (DCM) are added to the oily precipitate. The mixture is cleaned by precipitating five times with 14 mL ethanol and centrifuging at 14000 g for 10 min, discarding the supernatant and redispersing the precipitate in 14 mL DCM. The final precipitate is cleaned by removing the supernatant and adding 7 mL acetone. The mixture is sonicated shortly to disperse the precipitate and centrifuged at 14000 g rpm for 5 min, this step is repeated four times to remove residual ODE. The cleaned particles are dried under vacuum for 5 min, redissolved in 4 mL of hexane and stored under nitrogen atmosphere.

NP Size (SEM/UV-vis)	CdAc ₂ in mg	Oleic Acid Injection	Reaction Time after OA injection
3.0 ± 0.1 nm / 3.0 nm	-	at reaching 240°C	25 min
3.5 ± 0.1 nm / 3.6 nm	-	5 min after reaching 240°C	60 min
4.3 ± 0.2 nm / 4.3 nm	4 mg	at reaching 240°C	60 min

Table 2: Reaction times and resulting nanoparticles size distribution for a range of CdSe particles from 3.0 nm to 4.3 nm.

Characterization

Particle sizes are initially determined using the method published by Peng et al.⁹⁰ The mean particle size in the solution is determined by correlating the first maximum of the UV-vis absorption (**Figure 24a**) of colloidal particle solutions with a SEM image-based size investigation. These results are confirmed by manual counting of at least 100 particles using ImageJ (**Figure 24b**) and applying a Gaussian fit resulting in the size distributions listed in **Table 2**. The obtained size distribution is in good agreement with the results of the UV-vis absorption measurement and shows only a small deviation from the mean value.

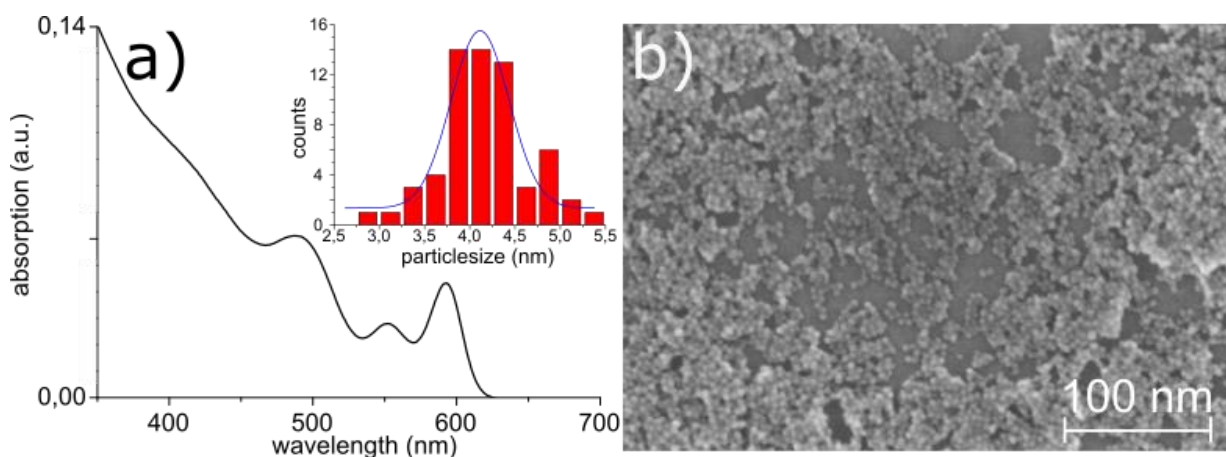


Figure 24: a) UV-vis absorption spectra of 4.1 ± 0.1 nm CdSe NP with size distribution analysis (inset) using SEM image b).

5.2 Phase transfer of QDs using Ammonium Iodide and hybrid ligand shell with n-butylamine

The CdSe QDs are stripped of their native ligand shell using a modified procedure described by Eychmüller et al.⁴ 50 mg of ammonium iodide are dissolved in 1 mL of *N*-methylformamide (NMF) in a 12 mL vial and the QD solution in hexane (10 mg/L) is added on top to create a two-phase system. The two-phase system is stirred vigorously for 30 min during which the QDs transfer from the top to the bottom phase that changes from colorless to dark red.

After letting the system separate, the red bottom phase containing the QDs is removed and the now colorless top phase is discarded. The QDs dissolved in NMF are rinsed 3 times using 2 mL hexane and then precipitated using toluene to remove excess iodide. In case of incomplete precipitation, small amounts of acetone can be added (acetone: toluene, 1: 10). The precipitated QDs are centrifuged and redispersed in 500 µL of fresh NMF. The supernatant is discarded.

The QDs in NMF are precipitated using 200 µL n-butylamine (BA), centrifuged and the supernatant discarded. The pellet is then redissolved in chloroform or tetrahydrofuran (THF) and stored in a nitrogen atmosphere.

NMR spectra

¹³C NMR spectra are acquired to investigate the exchange from the long-chained native TOPO, OA and HDA ligand shell after the synthesis to mainly n-butylamine stabilized particles. As we can clearly see, the spectra (**Figure 25**) show a very different peak profile before (blue) and after the exchange (red). The native particle spectra feature 4 peaks (2-5) at 128.7 ppm (2), 127.6 ppm (3), 124.8 ppm (4) and 20.1 ppm (5) that can be assigned to C-Atoms in long alkyl chains, such as oleic acid, which was added to stabilize our particles. These Peaks also show small satellite peaks (**Figure 25a**), which we attribute to a mixed signal of oleic Acid (OA) and remaining hexadecylamine (HAD) and trioctylphosphine oxide (TOPO). We further observe a peak at 137.5 ppm (1), which we assign to the double bonded carbon from remaining octadecene solvent from the synthesis. After the ligand exchange (red), those peaks can no longer be observed and instead four Peaks at 42.0 ppm (6), 36.0 ppm (7), 20.0 ppm (8) and 13.9 ppm (9) appear, which can be clearly attributed to the 4 carbon atoms of n-butylamine as the new stabilizing agent.

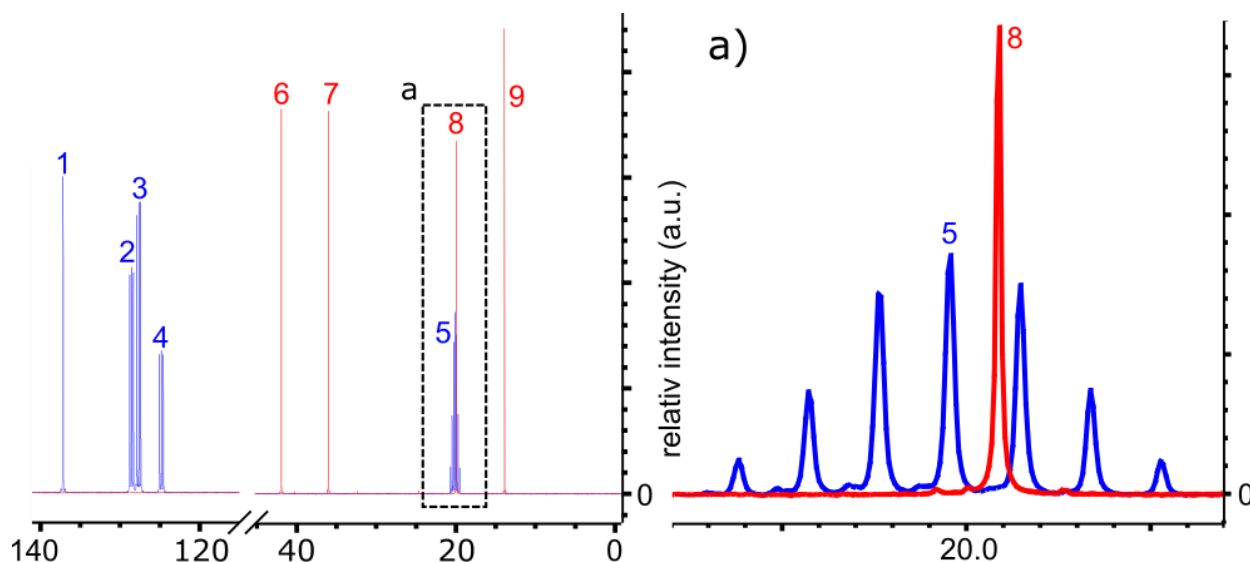


Figure 25: ^{13}C NMR spectra of CdSe particle solution before (blue) and after (red) ligand exchange procedure. Clear indication of long chained molecules before the exchange (1-5) being replaced by n-butylamine (6-9). Small satellite signals (blue/magnified) indicate a mixture of long chained molecules in the native ligand shell.

	C_{13} shift (ppm)	Multiplett	Assignment
1	137.5	s	octadecene
2	129.2	t	Oleic acid
3	126.9	t	Oleic acid
4	124.8	t	Oleic acid
5	20.2	m	Alkyl chains mainly oleic acid
6-9	42.0, 36.0, 20.0, 13.9	s	n-Butylamine

Table 3: Peak assignment of ^{13}C NMR-spectra (Fig), showing a ligand shell consisting of mainly oleic acid (2-5) before the ligand exchange and n-Butylamine after the exchange.

5.3 Sample preparation

The hybrid nanocomposite films are prepared on functionalized 12 mm glass microscope cover slides or alternatively 15 mm doped silicon wafer with a 200 nm silicon oxide surface layer. The glass substrates are cleaned by submersion in an aqueous solution of chromo sulfuric acid for 3h and subsequently rinsed using deionized water and methanol. The silicon substrates are cleaned with an optical wipe and acetone. The substrate is then cleaned by sonication in acetone, hexane and ethanol for 5 minutes each and put into a plasma cleaner for 10 min. The cleaned substrates are functionalized by submerging them in a solution of 100 μL (3-mercaptopropyl) trimethoxy silane (MPTMS) in 5 mL hexane overnight. The solution is then discarded, and the substrate is washed twice using hexane and dried at 60°C for 5 min.

5.3.1 Hybrid nanocomposite film preparation using dip coating

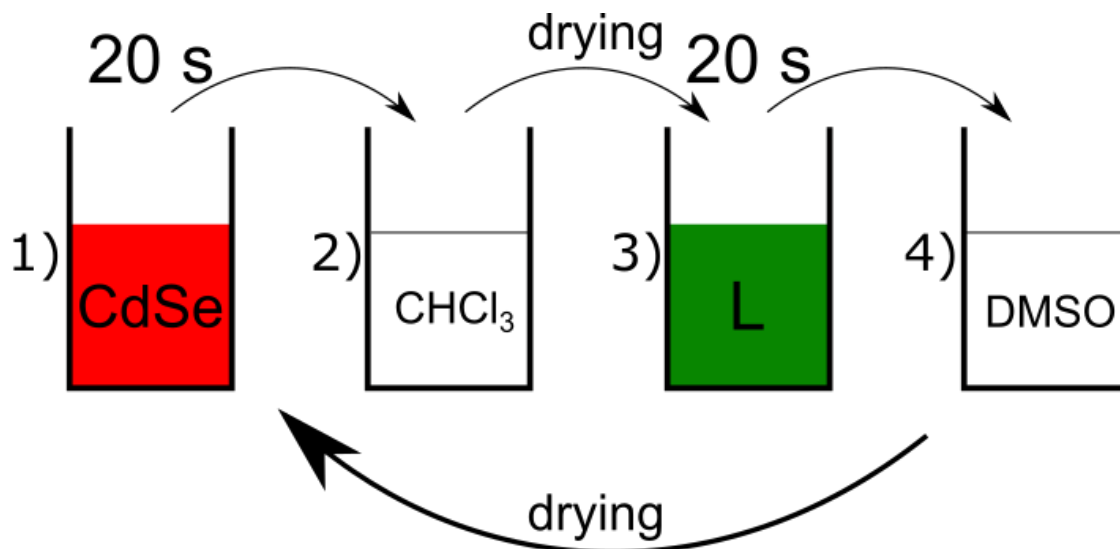


Figure 26: Schematic for dip coating procedure to obtain phthalocyanine functionalized CdSe films on glass or silicon oxide surfaced substrates. Dipping into a CdSe particle solution (1) for 20s followed by washing in Chloroform (2). Subsequent dipping in a ligand solution in DMSO (3) for 20s and cleaning in DMSO (4). This sequence is repeated as often as needed.

For dip coating, the functionalized substrate is submerged in a chloroform QD solution for two minutes, washed twice using fresh chloroform and dried on a hot-plate at 100°C. During this first submerging, the CdSe QDs can bind to the MPTMS molecules on the functionalized substrate surface and any unbound particles and excess n-butylamine are washed away afterwards. The substrate is then placed in a saturated solution of Fe4APc in dimethyl sulfoxide (DMSO) for 20 s, washed twice using fresh DMSO and dried on a hot-plate at 100°C. This functionalizes the particles with 4APc molecules which can now function as further binding sites for additional particle layers. The previous steps are repeated by dipping the substrate into the particle or ligand solution for 20 s and washing it in the corresponding solvent afterwards and drying at 100°C at the end of a cycle. This cycle is repeated at least 20 times in total to obtain a sufficiently thick film (~100 nm). The film is then annealed at 150°C for 30 min.

For preparation of the reference material containing only QDs, the exact same steps are employed, substituting the 4APc solutions with the pure solvents and adding additional cycles to compensate for the lack of a linker molecule, which leads to a visibly slower buildup of the QD film.

5.3.2 Hybrid nanocomposite film preparation using drop casting

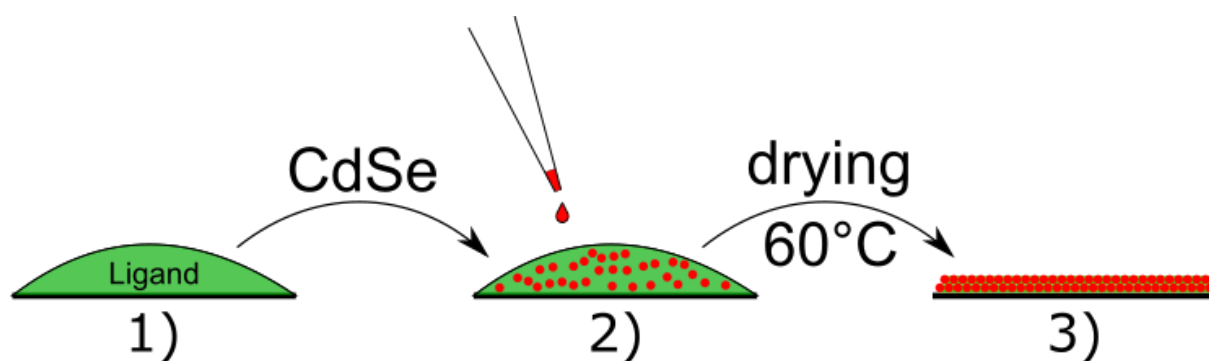


Figure 27: Schematic for drop casting procedure to obtain phthalocyanine functionalized CdSe films on glass or silicon oxide surfaced substrates. Deposition of ligand solution in DMF on the substrate (1), with subsequent addition of CdSe particle solution in THF (2), which is then dried (3) resulting in functionalized CdSe films.

For drop casting silicon substrates (15x15 mm), the functionalized substrate is placed on a hot-plate. The substrate is covered with 120 μL of a saturated Fe4APc solution in *N,N'*-dimethylformamide (DMF) and 80 μL of a 7 μM CdSe QD solution in THF. The substrate with the QD phthalocyanine mixture is dried at 60°C for 30 min. To remove excess ligand, the substrate is washed twice using DMF and annealed at 150°C for 30 min. For drop casting onto the smaller glass substrates (12x12 mm), the used amounts are adjusted to 60 μL of a 7 μM QD solution in THF and 100 μL of a saturated Fe4APc solution.

6 Results

Parts of this chapter have been already published by myself in the Article: "Simultaneous positive and negative optical patterning with dye-sensitized CdSe quantum dots".⁹³ All associated measurements and preparations were performed and described by myself.

6.1 Synthesis of CdSe based hybrid materials

One of the more recent approaches in the field of semiconductor nanoparticle materials is to exchange the native ligand shell on the QD surface for functional molecules to modify the properties of the QD material and make them more attractive for specific applications in optics and electronics.⁴⁷⁻⁴⁹ CdSe QDs as used in this work are one of the best researched and well-known representatives of semiconductor QDs and are signified by their distinct absorption and emission spectra in the visible spectral range. A prominent target of investigation for changes in the optical properties of the CdSe QDs has been the modification with organic semiconductor molecules such as phthalocyanines. Previous works use the incorporation of modified phthalocyanine molecules into the ligand shell of CdSe QDs in solution, modifying the optical response of the hybrid material, suggesting a coupling of the two semiconductor components.⁹⁷⁻⁹⁹ Another approach is to use chemical vapor deposition to place a layer of phthalocyanine molecules on top of a CdSe QD film to form a hybrid system, where the two semiconductor materials are separated by the ligand shell of the QDs but show optical coupling between the components.^{100,101} Expanding on those CdSe-phthalocyanine hybrid materials, the aim of this work is a new approach to directly chemically couple phthalocyanine onto the QD surface, replacing the native ligand shell and preparing well-structured thin films to characterize their structural and optical properties.

To create our functional hybrid materials, we replace the native ligand shell with 4,4',4'',4'''-tetranitrophthalocyanine (4APc) molecules. Preliminary tests have shown that a direct exchange, as published by Scheele et al, is not possible with a CdSe QD based system, due to the difficulties with replacing the most common surface ligands such as oleic acid and phosphine oxide ligands.^{102,103} To facilitate the addition of 4APc species to the surface, the native ligands are first removed using the method published by Eychmüller et al. and replaced by a mixture of ammonium iodide and n-butylamine, which grants stability in polar solvents. Further, n-butylamine is easily exchanged with 4APc molecules due to its volatility. This

represents a new approach to easily functionalize CdSe QDs with phthalocyanine molecules and incorporate them into a QD organic hybrid semiconductor material.

6.1.1 Structural analysis using SEM images and AFM

The CdSe QD based hybrid material films discussed in this chapter are prepared using the previously described drop casting and dip coating procedures (**chapter 5.3**). Silicon wafers (15x15 mm) with a 200 nm silicon oxide layer are used for preparation of SEM and AFM imaging samples and Menzel microscope cover slides (12x12 mm) are used as substrates for optical measurements. All images presented in the coming chapters are obtained from CdSe QD films functionalized with Fe4APc molecules with a QD size of 4.7 ± 0.2 nm, as they are also used in the patterning experiments in the coming **chapter 6.2**.

Visually, both the dip coating (**Figure 28 a,c**) and drop casting technique (**Figure 28 b,d**) lead to complete and even coverage of the substrate with the CdSe QD hybrid material. Both, the silicon (a,b) and glass substrates (c,d), seem equally suited for the film preparation. The drop casted films show a slightly different coloration, which can be attributed to the larger amount of material that is deposited on the substrate surface using the drop casting method and the larger thickness of the material.

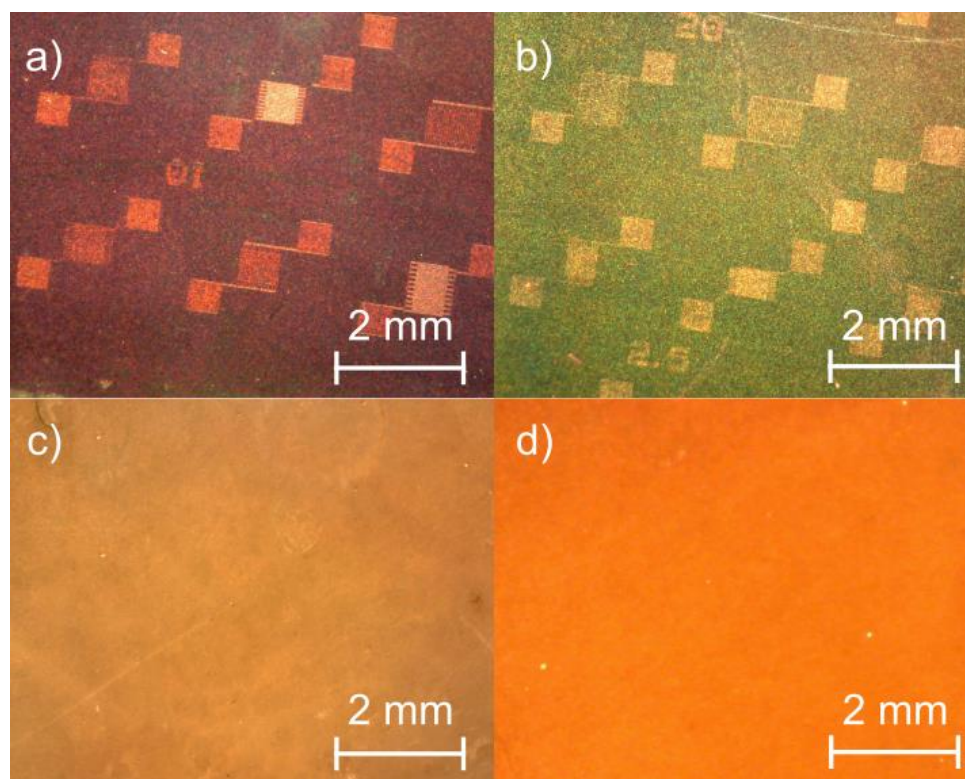


Figure 28: Images of completely covered silicon (a,b) and glass substrates (c,d) using dip coating (a,c) and drop casting (b,d) preparation.

Results

Figure 29 shows SEM images of the CdSe hybrid material films on silicon substrates prepared by dip coating (a,b) and drop casting (c,d). The dip coating procedure results in a homogenous coverage of the whole substrate as seen in (a) containing only a few differentiable layers, which shows only occasional small holes (b). In comparison, the films created using the drop casting method continue showing an uninterrupted coverage of the whole substrate, but the film structure is visibly less homogenous (c) and shows visible depressions and small cracks on the nm scale in the hybrid material (d). Upon closer investigation, the film shows no preferred structural motive and the particle structure seems entirely random without overarching structural domains as observed by other groups.^{104,105} Evaluating the shape and size of the nanoparticles appears consistent with the data obtained from the as synthesized colloidal particle solutions in **chapter 5.1.2**, containing spherical particles with a size of 4.7 ± 0.2 nm. This indicates the retention of the initial physical particle properties throughout the ligand exchange and film preparation procedure without any sintering effects through the heat treatment during preparation.

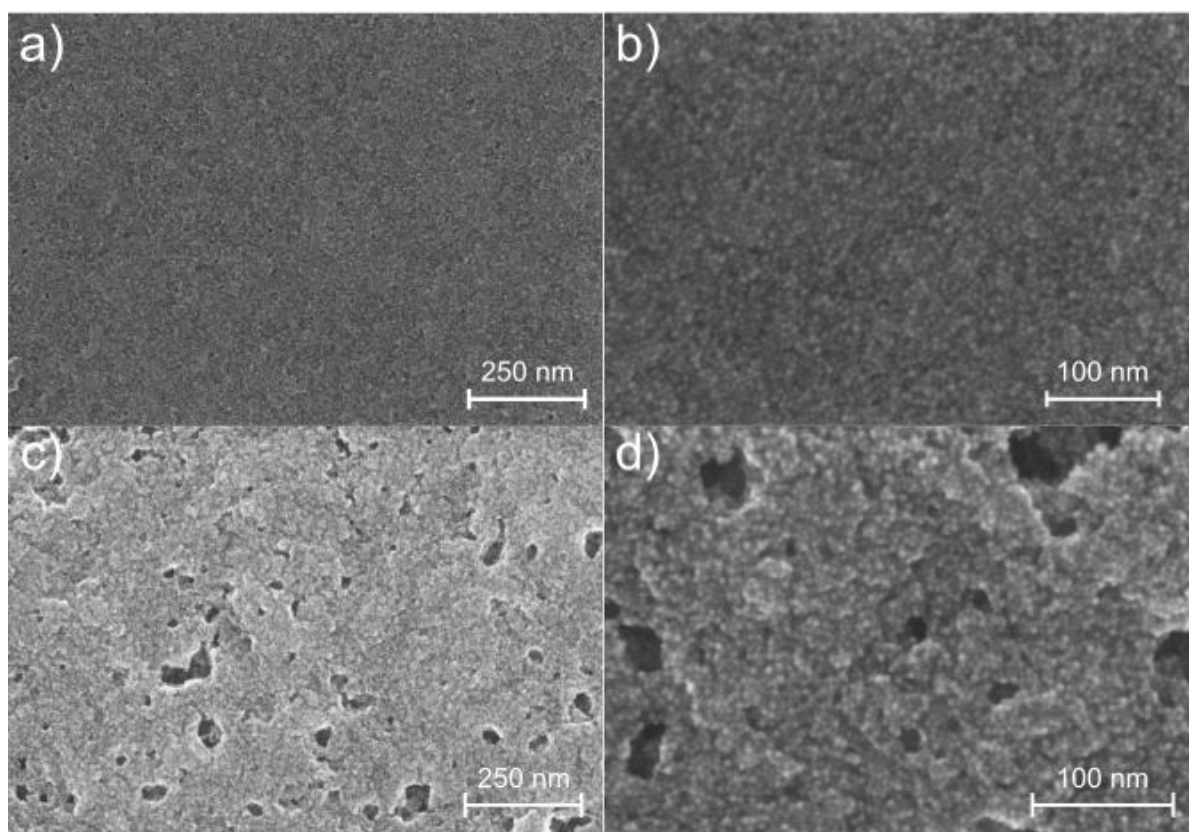


Figure 29: SEM images of hybrid material thin films created through drop casting using CdSe QDs and Fe4APc molecules. a) Image of complete coverage of the substrate with the QD hybrid material showing cracks and material indentations due to drying effects. b) No obvious ordered structure motive or overarching structural domains can be observed.

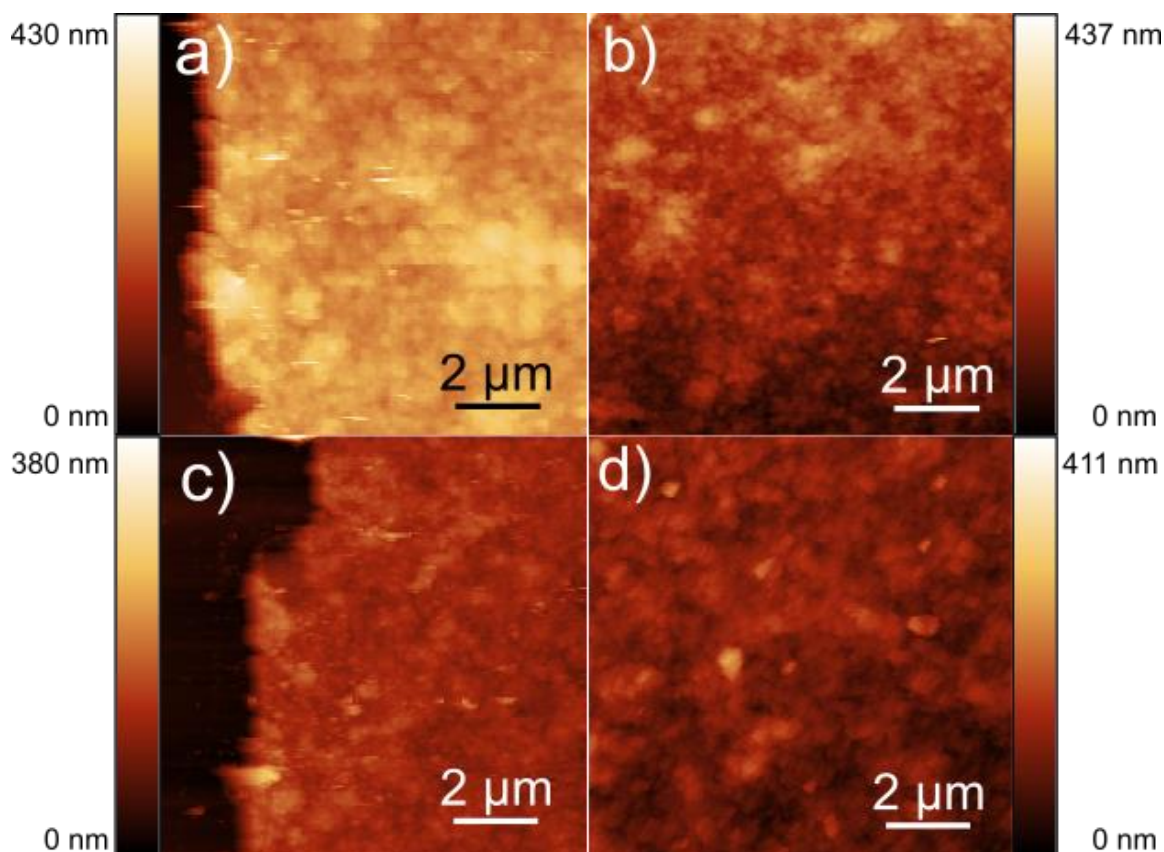


Figure 30: AFM images of CdSe hybrid films created through dip coating (a,b) and drop casting (c,d). For film thickness evaluation, an incision is made and the height difference from substrate to film is measured on the border (a,c). Roughness is evaluated by measuring the root mean square value of the height difference in an undisturbed $10 \times 10 \mu\text{m}$ area (b,d).

In order to further investigate the film structure and thickness, AFM images of the substrates are acquired as shown in **Figure 30**. Images are acquired from the previously described SEM image substrates, which are prepared using dip coating (a,b) and drop casting (c,d). To evaluate the film thickness, an incision to the substrate surface is made (a,c) and the height difference to the substrate surface is measured on the films edge and presented in **Table 4**. The AFM images are further used to investigate the roughness of the hybrid QD films and compare the root mean square (RMS) value of the height differences in a $10 \times 10 \mu\text{m}$ area of undisturbed QD hybrid material film as shown in **Figure 30 b,d**.

Results

	Dip coating (20 cycles)	Drop casting
Thickness	115 nm ± 8 nm	232 nm ± 12 nm
Roughness (RMS)	24.3 ± 3 nm	31.2 ± 3 nm

Table 4: Comparison of CdSe hybrid material film thickness and surface roughness (root mean square) depending on the preparation method.

Film preparation using 20 cycles of dip coating with Fe4APc as ligand results in a film consisting of at least 24 nanoparticle layers. The film shows an average height of 115 nm ± 8 nm and an average root mean square (RMS) roughness of 24.3 ± 3 nm using an average of 20 measurements of the films surface, as exemplarily shown in **Figure 30 a,b**.

We can obtain a good coverage using the drop casting method resulting in a thicker film consisting of at least 50 nanoparticle layers. The film shows an average height of 232 nm ± 12 nm and a larger RMS roughness of 31.2 ± 3 nm using an average of 20 measurements of the films surface area of 10 by 10 μm, as shown in **Figure 30 c,d**.

Both the drop casting and dip coating method allow us to completely cover the substrate with a homogeneous film of QD hybrid material. The dip coating approach allows for the controlled layer by layer assembly of the QD hybrid material film.¹⁰⁶ The thickness of the film is controlled by the number of dip coating cycles that are applied and the binding affinity of the 4APc species. This results in a generally more homogeneous film showing fewer and smaller structural defects and an overall lower surface roughness. In comparison, the drop casted films are generally thicker and show a rougher surface with nm scale cracks and depressions leading to a higher surface roughness, compared to films prepared via dip coating (**Table 4**). The larger thickness of the drop casted films is easily explained by the larger amount of QD material that is used in the preparation compared to the dip coating approach. Films of a larger thickness can be prepared via dip coating through additional dip cycles in the preparation of the substrate, whereas a reduction in QD solution volume or concentration below a certain threshold in the drop casting method leads to poor substrate coverage or an unevenly distributed film (**Figure 31**).

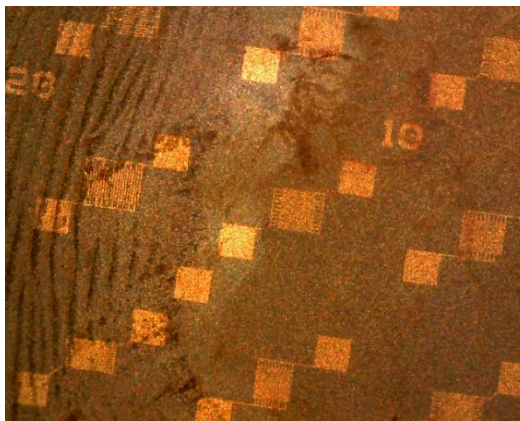


Figure 31: Image of in homogeneously and partially covered silicon substrate due to insufficient CdSe QD particle amount.

6.1.2 UV-vis absorption

As a basic characterization of the finished films, UV-Vis spectra are acquired (**Figure 32**). Throughout the ligand exchange procedure (**Figure 32a 1,2**) and in films without phthalocyanine (**Figure 32a 3**), the absorption spectra remain unchanged which indicates the preservation of the original size and shape of the nanoparticles, as particularly the position of the first excitonic transition ($1S_h-1S_e$) at 612 nm is very sensitive towards changes of the morphology. The UV-Vis spectra also show that n-butylamine stabilized particles are successfully functionalized with phthalocyanine (**Figure 32b 4**), resulting in a very broad absorption around 688 nm due to the electronic transition from the highest occupied molecule orbital (HOMO) to the lowest unoccupied molecular orbital (LUMO). The resulting spectrum of the functionalized film (**Figure 32b 5**) displays both the electronic transition from the HOMO to the LUMO of the phthalocyanine molecule and the $1S_h-1S_e$ transition of the CdSe QDs, which is also slightly shifted from 612 nm to 615 nm (**Figure 32b inset**). This small redshift in the $1S_h-1S_e$ absorption can be attributed to the change in the dielectric environment of the QDs as butylamine is replaced by phthalocyanine molecules, which have a larger dielectric constant than the native ligand shell. Overall, the absorption spectra of the colloidal QD solutions and prepared QD hybrid films indicate the preservation of the initial QD properties, while successfully functionalizing them with 4APc molecules.

Results

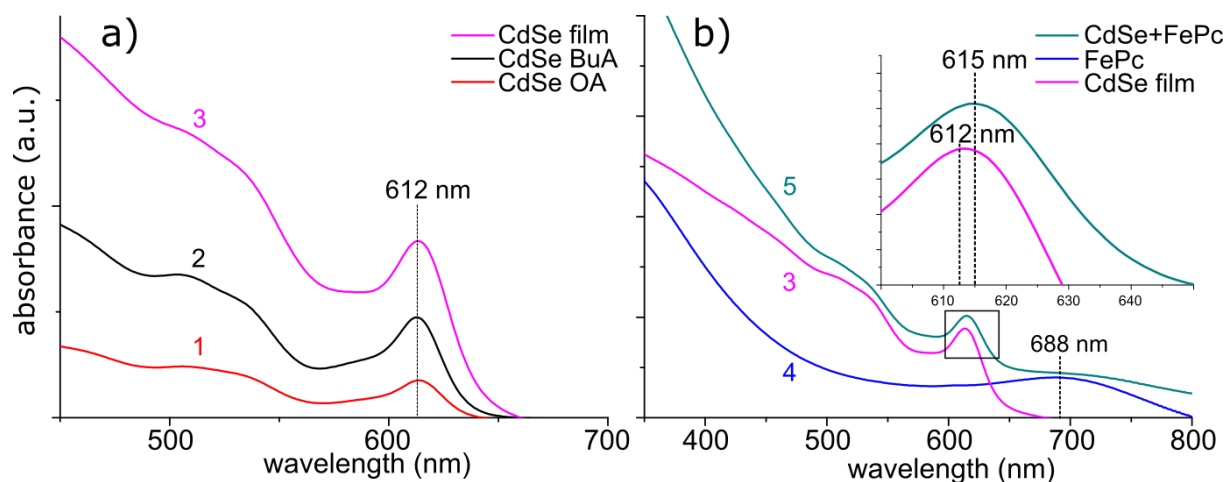


Figure 32: a) Comparison of UV-Vis absorption spectra of native CdSe particle solution (1) after ligand exchange with butylamine (2) and prepared as unfunctionalized film (3). b) Comparison of UV-Vis spectra of an unfunctionalized CdSe particle film (3), a spectrum of Fe-phthalocyanine (4) and a CdSe particle film functionalized with Fe-phthalocyanine (5).

6.1.3 Raman spectroscopy

To further monitor the ligand exchange with different 4APc species, Raman spectra are acquired after the film preparation using dip coating (**Figure 34**). All spectra are dominated by the extremely strong signal of the longitudinal optical phonon mode of CdSe (1) at 207 cm^{-1} and its first and second overtone at 415 cm^{-1} (2) and 621 cm^{-1} (3) assigned in **Table 5**.^{107,108} After functionalization with different 4APc species (Ni, Cu, Fe and metal free) (**Figure 33**) additional Raman signals between $680 - 1600\text{ cm}^{-1}$ can be observed, which are characteristic for vibrations of the phthalocyanine molecules and stretching motions of the ring structure and are assigned according to the literature sources (**Table 5 4-15**).¹⁰⁹⁻¹¹¹ The difference in the variety of Raman signals and their intensity can be attributed to the degree of functionalization of the QD film with the 4APc molecule. The different 4APc show varying binding affinities to the QDs surface resulting in films of different optical thickness, which is directly correlated to the intensity of the observed Raman signals. The difference in signal intensity between CdSe and the functionalizing phthalocyanine molecules can be mainly attributed to a strong difference in overall material concentration as the functionalized films are thoroughly washed after the ligand exchange to eliminate any unbound excess ligand molecules, and n-butylamine/iodine capped CdSe particles have been observed to exhibit a strong phonon resonance.¹¹² The presence of phthalocyanine signal after intensive washing is a good indication for strong binding of the molecule to the QD surface.

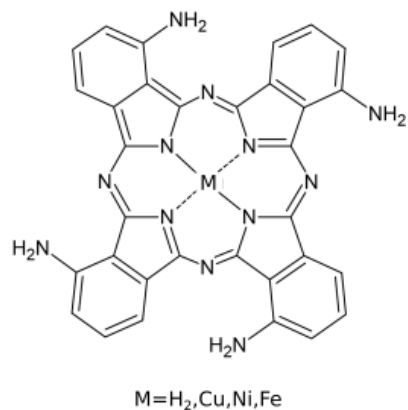
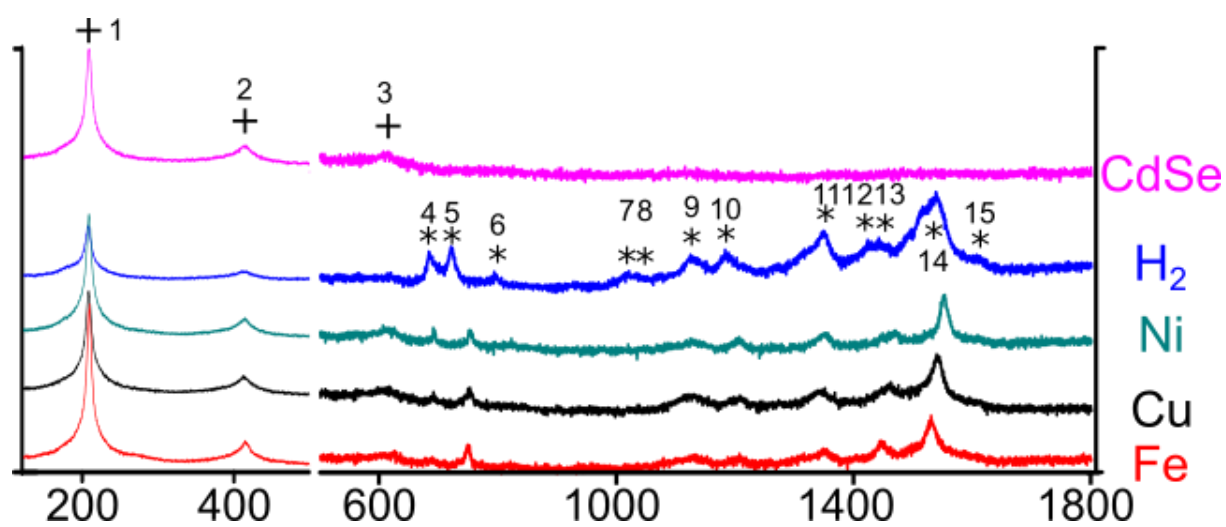


Figure 33: Schematic structure of 4,4',4'',4''' tetraaminophthalocyanine (4APc) molecules, containing different metal center atoms of Copper (Cu), Nickel (Ni), Iron (Fe) and as metal free variant (H₂).



Results

Figure 34: Comparison of Raman spectra of unfunctionalized CdSe films and after ligand exchange with various phthalocyanine species containing Fe, Ni, Cu metal centers and the metal free variant (H₂).

<i>Peak</i>	<i>CdSe</i>	<i>CdSe + Fe4APc (1/cm)</i>	<i>CdSe + Ni4APc (1/cm)</i>	<i>CdSe + Cu4APc (1/cm)</i>	<i>CdSe + 4APc (1/cm)</i>	<i>Assignment</i>
1	207	207	207	207	207	CdSe Phonon
2	415	415	415	415	415	CdSe Phonon
3	621	621	621	621	621	CdSe Phonon
4			691	690	684	Bridging C-N-C sym. deform. Pyrrole ring OP bend
5		721	724	721	722	Macrocycle stretch/central ring twisting
6			748		750	Central ring contraction
7					1019	C-H deformation aryl C-C stretch
8					1024	C-H deformation aryl C-C stretch
9		1126	1124	1123	1126	Macrocycle stretch/ C-H bend
10		1185	1182	1183	1186	pyrrole ring breathing
11		1353	1351	1355	1350	indole
12		1443	1441	1440	1442	indole
13		1511		1530	1516	N-H macrocycle ring stretch benzene
14			1551	1608	1538	Macrocycle in plane stretch
15			1611		1605	NH ₂ deformation

Table 5: Raman spectroscopy signal assignment of the main features in CdSe and phthalocyanine hybrid film spectra according to literature.^{107–111}

6.1.4 Summary

Using n-butylamine stabilized CdSe QDs according to the exchange method by Eychmüller et al., we can exchange the native particle ligand shell and replace it with different 4APc species. Using either dip coating or drop casting, the 4APc functionalized QDs are used to create homogeneous CdSe hybrid material films using glass cover slides and silicon as substrates.

The substrates are analyzed using SEM imaging to ascertain the substrate coverage on a nm scale and show complete coverage of the whole substrate for either preparation method. The layer-by-layer preparation of the QD hybrid film through dip coating generally results in a smoother film with fewer structural defects. The characterization of the hybrid films using AFM imaging further supports this by showing a lower surface roughness of the dip coating films, compared to the drop casting method. Additionally, AFM images are used to measure the average film thickness of $232 \text{ nm} \pm 12 \text{ nm}$ for drop casted films and $115 \text{ nm} \pm 8 \text{ nm}$ for dip coated samples using 20 cycles of dip coating. Using the dip coating approach, the film thickness can be controlled through the number of dip coating cycles that are employed, whereas drop casted films show an insufficient or inhomogeneous coverage below a QD solution concentration of $2.4 \text{ } \mu\text{L}$ ($7 \text{ } \mu\text{M}$) per mm^2 of substrate surface.

UV-Vis absorption spectra throughout the preparation process show the retention of the initial QD properties, indicating that the original size and shape are maintained. A slight red shift in the first absorption minimum of the QDs in the hybrid material can be attributed to a change in the dielectric environment, further confirming the functionalization with the 4APc molecules. For further investigation of the functionalization in the finished film, Raman spectra are acquired. The functionalization of the QDs with 4APc species can be confirmed and the Raman signals are assigned according to literature.

6.2 Optical patterning

Using the QD hybrid material described in the previous chapter, it is possible to receive a wavelength dependent fluorescence response under photoexcitation due to the distinct difference in resonance of the two semiconductor components. CdSe QDs are known to profit from photoactivation of the quantum yield during above bandgap excitation, under ambient conditions.^{78–80,113,114} While conversely the conjugated π -system of the 4APc molecules tends to get degraded by near resonant excitation of the HOMO-LUMO transition, leading to the extinction of its fluorescence, resulting in a negative fluorescence contrast.^{58,59} This effect is used to create optical patterns with a confocal scanning microscopy setup using a 488 nm and 633 nm laser source for optical excitation as shown in **Figure 35**.

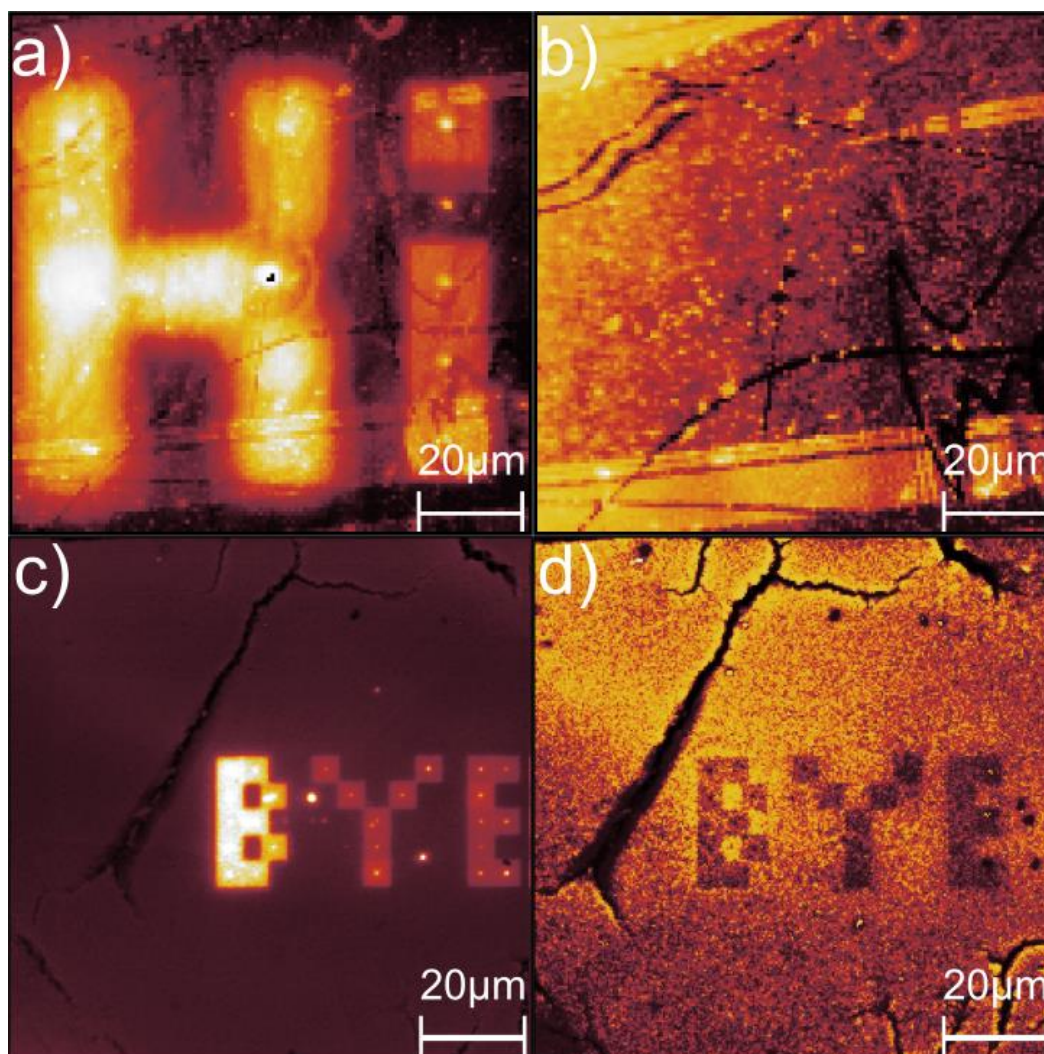


Figure 35: Optical write/read-out experiments on thin films of CdSe QDs functionalized with Fe4APc. (a) 488 nm write/488 nm read. (b) 488 nm write/633 nm read. Both panels show the same part of the sample, which was optically patterned under the same conditions. (c) A different part of the sample optically patterned at 633 nm and read-out at 633 nm. (d) The same patterned sample region as in (c), but under 488 nm read-out. Adapted with permission from ref ⁹³. Copyright 2019 AIP Publishing.

Using a $5\mu\text{m}$ scan window as the basic pixel unit of our image, a pattern is written in the CdSe hybrid film due to photoactivation of the QDs at a wavelength of 488 nm with a laser intensity of approximately 9 kW/cm^2 . To read out the written pattern, the whole area of the picture is scanned using the same 488 nm laser with much lower intensity and the fluorescence signal is recorded as shown in **Figure 35 a**. The readout using the 488 nm laser is mostly sensitive to the spatial distribution of the $1S_h-1S_e$ transition in the CdSe QDs, which absorbs predominantly at this wavelength. In contrast, only a small portion of laser light is expected to be absorbed by the phthalocyanine molecules as their absorption cross-section at 488 nm is comparably small. Conversely, this leads to a readout with 633 nm excitation that predominantly probes the spatial variation of the HOMO-LUMO recombination of the phthalocyanine molecules so that the changes in the fluorescence of the QDs cannot be detected, as seen in **Figure 35 b**. Excitation using the 633 nm laser is used to create a negative fluorescence contrast due to bleaching of the fluorescence resulting from the HOMO-LUMO recombination of the phthalocyanine. The negative fluorescence contrast is then probed through scanning the area using a low intensity 633 nm excitation (**Figure 35 d**). When the same area is probed using 488 nm excitation, a positive fluorescence contrast in the CdSe QDs is observed induced through the below bandgap excitation (**Figure 35 c**). In total, this leads to four different experiments that can be observed in **Figure 35**: 488 nm write/488 nm read (**a**), 488 nm write/633 nm read (**b**), 633 nm write/488 nm read (**c**) and 633 nm write/633 nm read (**d**). It must be noted that (**a**)/(**b**) and (**c**)/(**d**) are fluorescence contrast images from the same area of the sample which are patterned under the same conditions. All patterns created using this approach are irreversible and stable for a long time, especially if samples are stored under nitrogen atmosphere and exclusion of light. Preliminary investigations show that QD hybrid films with Fe4APc functionalized 4.7 nm QDs show the most promising results in the patterning experiment and were used for all further investigations mentioned in this chapter.

6.2.1 Positive fluorescence contrast patterning

During fluorescence excitation using a 488 nm laser source, the CdSe QDs in the hybrid material show a steady increase in overall fluorescence emission. To evaluate the fluorescence emission development, spectra are taken every 10 s over a 15 minutes time interval. As shown in **Figure 36**, the CdSe emission continuously increases over the duration of the measurement and the center wavelength undergoes a constant blueshift. This can be attributed to the

Results

elimination of surface trap states due to oxidation of the QDs under ambient conditions as shown in the literature.^{78–81} The creation of a small oxide shell on the QDs surface has been shown to be beneficial to the overall quantum yield through further passivation of the QD surface. Furthermore, the continued oxidation of the particle leads to a blue shift in the emission due to shrinking of the effective QD size, increasing the quantum confinement and shifting the fluorescence emission to lower wavelengths.¹¹⁵

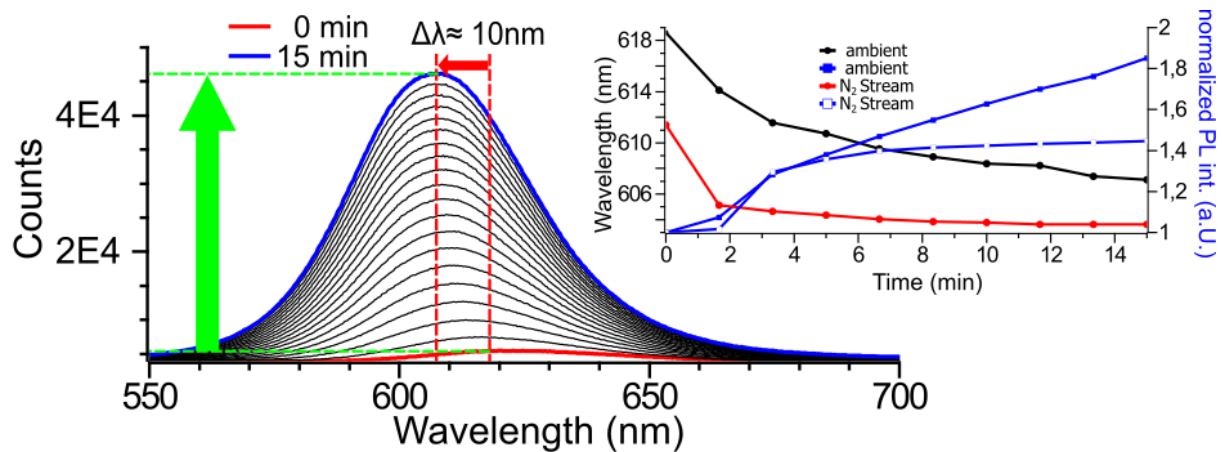


Figure 36: Fluorescence spectra over time under 488 nm excitation of a CdSe QD (4.7 nm) film functionalized with Fe4APc molecules. Overview during 15 min excitation, spectra are taken every 10 s of excitation time. A continued increase of the fluorescence intensity is visible, together with a blue shift of the emission peak of about 10 nm. Inset: Overview of the fluorescence intensity (blue lines, right scale) and center wavelength of the emission (red and black line, left scale) development during excitation over 15 min.

When the sample is placed under a nitrogen stream during the experiment, a clear reduction of the oxidation speed can be observed (**Figure 36 Inset blue lines**) due to the elimination of environmental oxygen and water. The initial oxidation under the nitrogen stream can be attributed to oxygen contamination during the sample transfer, this process slows down after the oxygen is consumed, whereas the oxidation under ambient conditions continues.

If the excitation is continued indefinitely, a point is reached where the quantum yield does not increase any further. Further excitation of the QD hybrid film leads to an overall decrease of the fluorescence emission and the QD spectra start to become irregular as shown in (**Figure 37**). This can be continued until the CdSe QD fluorescence is completely bleached. When compared with the spatial distribution of the fluorescence on the substrate, we can observe that the QDs are so far oxidized, that they no longer function as a fluorescence emitter resulting in an overall negative fluorescence contrast in the spatial readout (**Figure 37 b**).

Additionally, the fluorescence of the Fe4APc molecules under excitation, as seen in the 633 nm readout (**Figure 37 b**) is diminished, resulting in a negative fluorescence contrast.

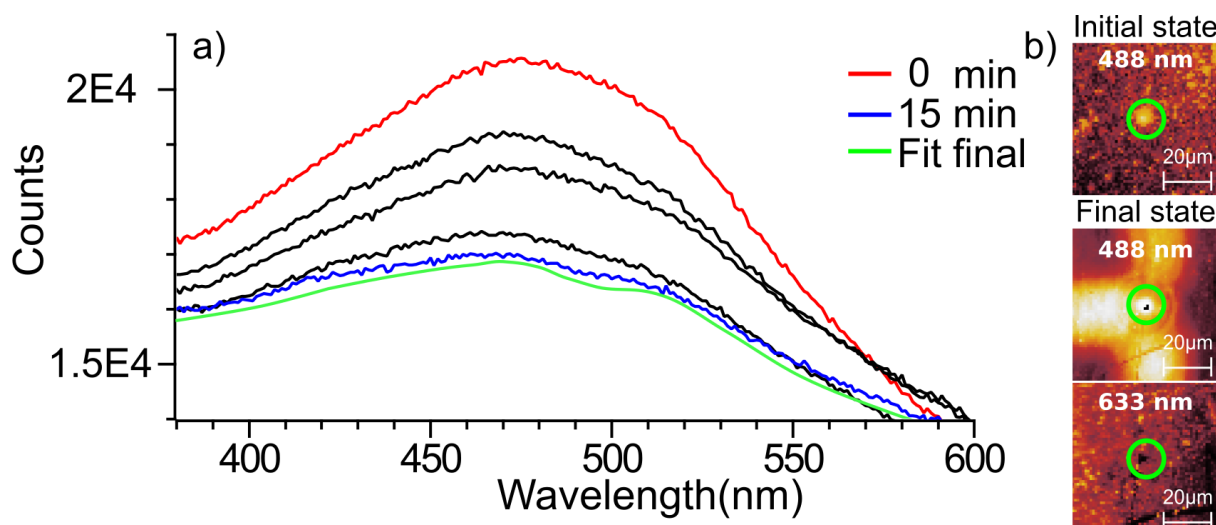


Figure 37: a) Fluorescence spectra over time under 488 nm excitation. Overview during 15 min excitation, spectra are acquired every 10 s of excitation time. Continuous decrease of the fluorescence intensity due to break down of the CdSe QDs. A fit of the final spectra no longer corresponds to the usual Lorentzian fit model of the CdSe QDs. b) Spatial scan of the fluorescence intensity under different readout wavelengths showing fluorescence enhancement in the initial state of the material and negative fluorescence contrast after excitation due to destruction of the CdSe QD hybrid material.

Using an unfunctionalized CdSe film, a similar fluorescence increase and blue shift in the spectra can be observed. If we compare the fluorescence intensity change of a n-butylamine/iodine stabilized QD film vs Fe4APc functionalized QDs in the hybrid material (**Figure 38**) under identical excitation conditions, we observe a faster development of the fluorescence enhancement in the presence of the Fe4APc molecule as shown in **Figure 38 b**.

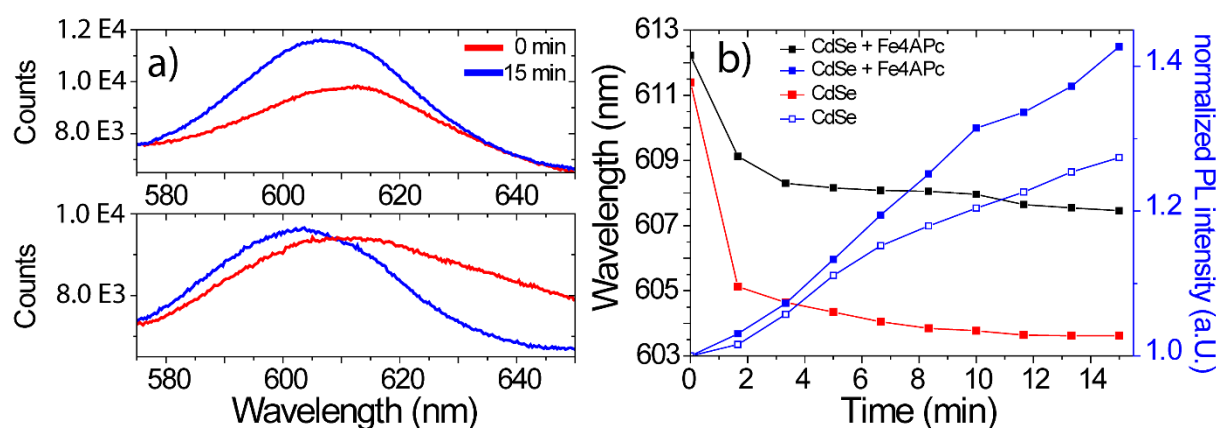


Figure 38: a) Fluorescence spectra of CdSe-Fe4APc (top) QDs and of CdSe-I/BA QDs (bottom) under 488 nm excitation for 0 min (red) and 15 min (blue). b) Fluorescence intensity increase (right axis) and spectral shift (left axis) of the same samples as those analyzed in a) for consecutive time intervals. Adapted with permission from ref⁹³. Copyright 2019 AIP Publishing.

6.2.2 Negative fluorescence contrast

In the fluorescence spectrum of the CdSe-Fe4APc QD film under 633 nm excitation, we observe the excitation of the distinct phonon bands of the CdSe QDs below 650 nm (**Figure 39 a,b asterisk**) for the hybrid film (a) and the unfunctionalized CdSe QD film (b). The CdSe phonon bands remain stable over the minute excitation period and do not contribute to the negative fluorescence contrast observed in the 633 nm spatial readout. Furthermore, the unfunctionalized CdSe film does not exhibit a negative fluorescence contrast in the 633 nm spatial readout of the sample.

As a second component of the spectra, we can observe the broad fluorescence of the Fe4APc molecules in the range of 650 nm to 800 nm, due to the radiative recombination of the HOMO-LUMO transition of the phthalocyanine, which rapidly diminishes over the excitation period. This applies especially to the fluorescence intensity around 700 nm, where the neat Fe4APc film exhibits strong phonon bands (**Figure 39 a Inset**). This decrease in fluorescence intensity can be attributed to the instability of Fe4APc molecules under near resonance excitation in ambient conditions, leading to the oxidation of the functional molecule and subsequent elimination of its fluorescence response.

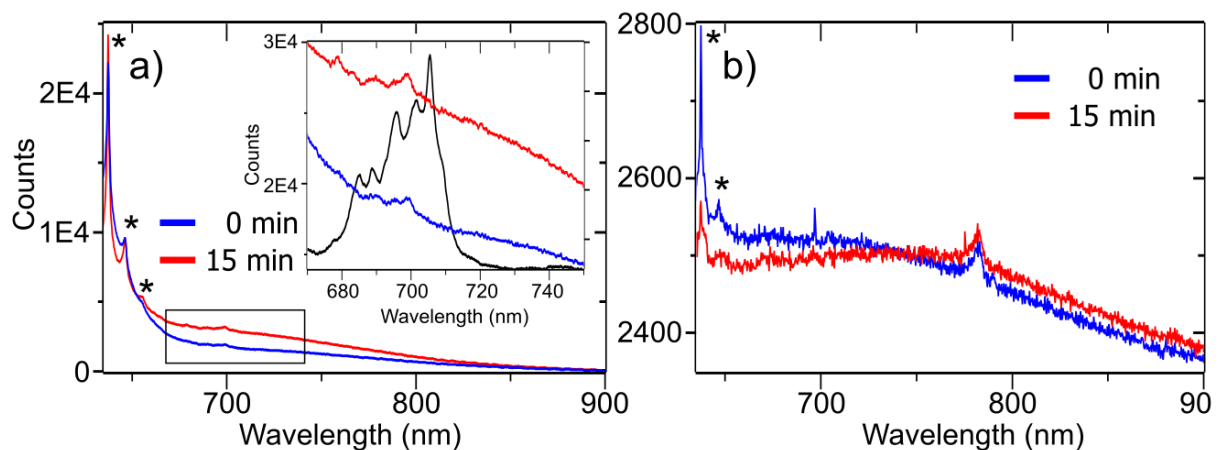


Figure 39: (a) Fluorescence spectra under 633 nm excitation of the hybrid material after 0 min (blue) and 15 min (red) continuous excitation. Phonon modes of the CdSe lattice are signaled by asterisks. At this wavelength only the phthalocyanine is excited, which leads to a broad fluorescence signal. The spectral region of the fluorescence from the phthalocyanine due to radiative recombination of the HOMO-LUMO transition is highlighted with a black square. The inset magnifies this spectral region and provides the fluorescence spectrum of the neat phthalocyanine in black for comparison. (b) Fluorescence spectra under 633 nm excitation of CdSe QDs functionalized with OA/HDA after 0 min (blue) and 15 min (red) continuous excitation. Adapted with permission from ref ⁹³. Copyright 2019 AIP Publishing.

As shown in **Figure 40 b**, the Fe4APc molecules contained in the QD hybrid material deteriorate at a faster rate compared to a film of the neat molecules. One of the major factors in this is again the accessibility of ambient oxygen for the oxidation process as shown by a much lower decomposition rate of the experiment under nitrogen atmosphere (**Figure 40 b**). Any initial oxidation under the nitrogen stream can be attributed to oxygen contamination during the sample transfer.

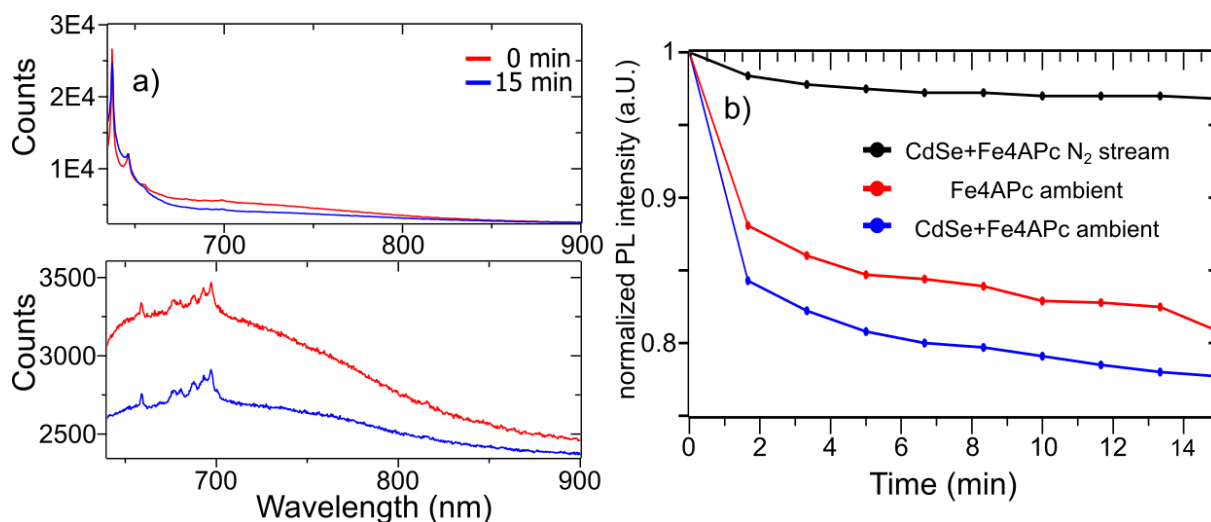


Figure 40: a) Fluorescence spectra of CdSe-Fe4APc (top) and of Fe4APc neat molecules (bottom) under 633 nm excitation for 0 min (red) and 15 min (blue). b) Fluorescence intensity decrease of the same samples as those analyzed in a) for consecutive time intervals.

6.2.3 Summary

In this chapter, Fe4APc functionalized CdSe QD hybrid films are used as optical patterning material, allowing for two wavelength dependent optical resonances to be exploited. It is shown that these two different components can be exploited during an optical write/read patterning experiment to create complex patterns on the micrometer scale, simultaneously employing positive and negative fluorescence contrast depending on the read/write laser wavelength. This is enabled by the fluorescence enhancement of the QDs under near-resonant excitation in combination with the fluorescence bleaching of the HOMO-LUMO transition during excitation of the phthalocyanine moiety. For further investigation of the wavelength dependent fluorescence patterning, emission spectra are taken over the whole excitation period under ambient conditions and with the sample placed in a nitrogen stream.

Investigating the fluorescence enhancement under 488 nm excitation shows a consistent increase of the emission intensity and a blueshift of the center wavelength emission. These

Discussion

processes are attributed to the steady oxidation of the QDs surface leading to the elimination of surface trap states thus enhancing the overall quantum yield. The blue shift is a result of the shrinking of the QDs size due to oxidation, which leads to a higher quantum confinement. The oxidation of the QDs was further verified by placing the sample in a nitrogen stream, which led to a significant reduction of the fluorescence enhancement through elimination of ambient oxygen and water.

Constant monitoring of the 4APc fluorescence elimination under 633 nm excitation shows no significant change in the excitation of the CdSe QD, while the broad 4APc fluorescence gets diminished. We attribute this to the destruction of the 4APc molecules under excitation in ambient conditions as unfunctionalized QDs under the same conditions show no negative fluorescence contrast whatsoever under 633 nm readout. This is verified by the significantly slower diminishment of the fluorescence in the nitrogen stream, eliminating ambient oxygen and water. Furthermore, the presence of 4APc molecules in the QD hybrid film not only enables a negative fluorescence contrast under 633 nm excitation, but also enhances the contrast during positive patterning.

Overall, we can show that this CdSe QD hybrid material allows for a new approach in optical patterning, enabling the wavelength dependent use of negative and positive fluorescence contrast to create complex optical patterns on a μm scale.

7 Discussion

In this work, we show an easy and versatile approach for functionalizing CdSe based QDs with 4,4',4'',4'''-tetraaminophthalocyanine molecules, while observing the optical properties of the material from the QDs synthesis throughout the functionalization and preparation of thin films (**chapter 6.1**). For the film preparation, dip coating and drop casting procedures are established and the resulting films are investigated using AFM and SEM imaging and to determine their coverage, homogeneity, thickness and general structure. Incorporation of the 4APc organic semiconductor molecules into the QD hybrid material structure is further verified through Raman spectroscopy.

Utilizing the divergence in optical properties of the two semiconductor moieties in the hybrid material optical patterns are fabricated through wavelength dependent excitation of the different components. The dual functionality of the material is used to produce optical

patterns on the μm scale, simultaneously employing a positive or negative fluorescence contrast. To further elucidate the temporal progression of this process, continuous emission spectra are acquired and the intensity and speed of the contrast development under varying conditions is investigated (**chapter 6.2**).

Preparation of 4APc functionalized CdSe hybrid material films

Preliminary experiments have shown that a direct exchange, as performed on lead sulfide QDs by the Scheele group, is not possible due to the high stability of the native ligand shell surrounding the synthesized CdSe QDs.^{102,103} We establish a new synthetic approach using a method published by Eychmüller et al., exploiting the binding affinity of inorganic halide species to the CdSe surface, to remove the native ligand shell and stabilize the QDs in a polar solvent through a n-butylamine/iodide hybrid functionalization.⁴ The volatility of the n-butylamine hybrid functionalization allows for the direct exchange with 4APc molecules in solution, allowing for the further processability of the material into QD hybrid nanostructures. This approach allows for direct binding of the 4APc molecules to the QD surface compared to similar hybrid materials, which are prepared without removal of the native ligand shell. These materials have been prepared through layered deposition of the material via CVD, molecular beam epitaxy, or coordination of the phthalocyanine molecule into the native ligand shell in solution under use of specialized phthalocyanine derivatives.^{97,98,100,101}

Furthermore, as shown via NMR spectroscopy this hybrid stabilization of the QDs can be used for CdSe QDs obtained through a variety of synthetic routes, covering the most common stabilizing agents currently used in CdSe synthesis.^{4,6,34} The n-butylamine/iodide stabilized QDs provides us with a universal approach for functionalization of CdSe QD with organic semiconductor molecules. Through dip coating, QD hybrid material films are prepared that through investigation via SEM and AFM imaging show a complete and homogeneous coverage of either glass or silicon oxide on silicon wafer substrates. The dip coating method enables the assembly of the QD hybrid material from solution, through layer by layer deposition of QDs interlinking them with our functional 4APc molecule similar to the process first described by Bethell (**Figure 41**).¹⁰⁶ In this process, the QDs are initially coordinated to the substrate by MPTMS functionalization. The stabilizing n-butylamine/iodide ligands are removed through washing with DMSO and subsequent heating of the film. The QD surface is then functionalized

Discussion

with phthalocyanine, providing new coordination centers and allowing for the binding of additional QDs.

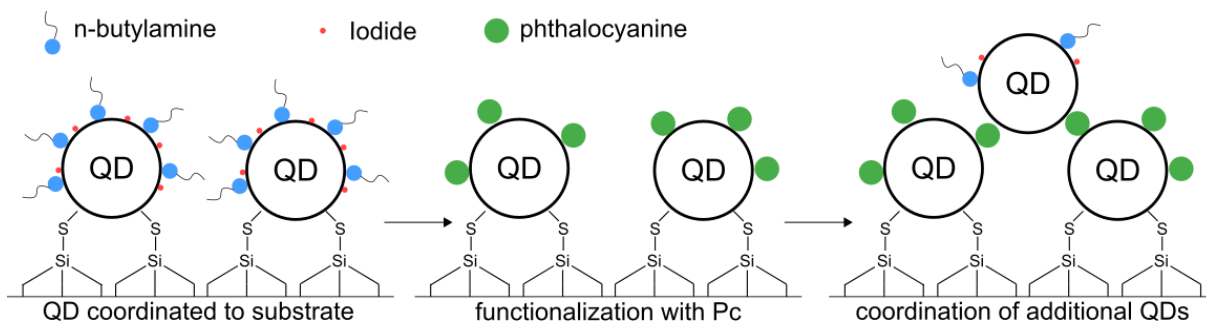


Figure 41: Schematic visualization of layer by layer deposition of n-butylamine/iodide stabilized CdSe QD on an MPTMS functionalized substrate. The initial QD layer is coordinated to the substrate via the MPTMS functionalization. The QDs are immobilized through washing and drying, removing the hybrid ligands. Functionalization with phthalocyanine enables coordination of additional QD layers.

This method results in homogeneous, tightly packed films with a surface roughness comparable to films of similar thickness, prepared from colloidal QDs reported in literature.^{116–118} Additionally, SEM imaging and UV-Vis absorption spectroscopy show that the initial size and shape of the QDs are retained throughout the preparation, allowing for the fabrication of a material that combines both components without altering their respective properties (**Figure 29, Figure 32**). This is further verified by Raman spectroscopy, showing a distribution of the QDs and 4APc molecules throughout the entire film (**chapter 6.1.3**). The assigned signals from literature vary only in the intensity between the different 4APc species, which can be explained through their varying binding affinity to the particle surface resulting in a higher concentration of molecules present in the film. This is further underlined by the observation that the films exhibit stronger Raman signals from their respective 4APc molecule as well as the fact that they are visually thicker and show a larger absorption in the UV-vis spectra. In this case, the larger binding affinity of the molecules leads to a higher functionalization degree of the QD surface, increasing the probability for coupling of further QDs to the surface in the next deposition cycle. In comparison, films prepared using the drop casting method are obtained through mixing of the QD and 4APc solutions on the substrate and the film is precipitated through drying of the solvent. The dried films are washed to remove access 4APc molecules and exhibit identical UV-Vis absorption and Raman spectra. Structurally, they are slightly less homogeneous on the nm scale with small cracks and depressions, resulting in an increase of overall surface roughness from 24.3 ± 3 nm to

31.2 ± 3 nm. The generally thicker films obtained through drop casting are also more susceptible to cracking during the drying process, which is generally avoided through the layer by layer approach of the dip coating procedure. Despite these disadvantages, the drop casting method presents the opportunity to prepare homogeneous films through simple mixing of stock solutions and subsequent drying. This allows for the large-scale preparation of samples in a short amount of time. The nanometer scale holes and depressions in the drop casted film are below the resolution limit of our patterning process and therefore negligible, which makes the drop casting approach viable for the preparation of patterned samples.

Optical patterning using Fe4APc functionalized CdSe QD films

The functionalization of CdSe QDs with Fe4APc molecules allows for the creation of optical patterns, simultaneously employing a positive and negative fluorescence contrast dependent on the excitation wavelength used in the write/read process. The divergence in optical absorption and electronic structure allows for the wavelength selective emission excitation of the two different moieties (**Figure 42**). Excitation using a 488 nm source is used to obtain the fluorescence of the CdSe QDs due to their higher absorption cross-section. In comparison, the energetically lower HOMO-LUMO transition of the Fe4APc molecules is excited using the 633 nm laser source.

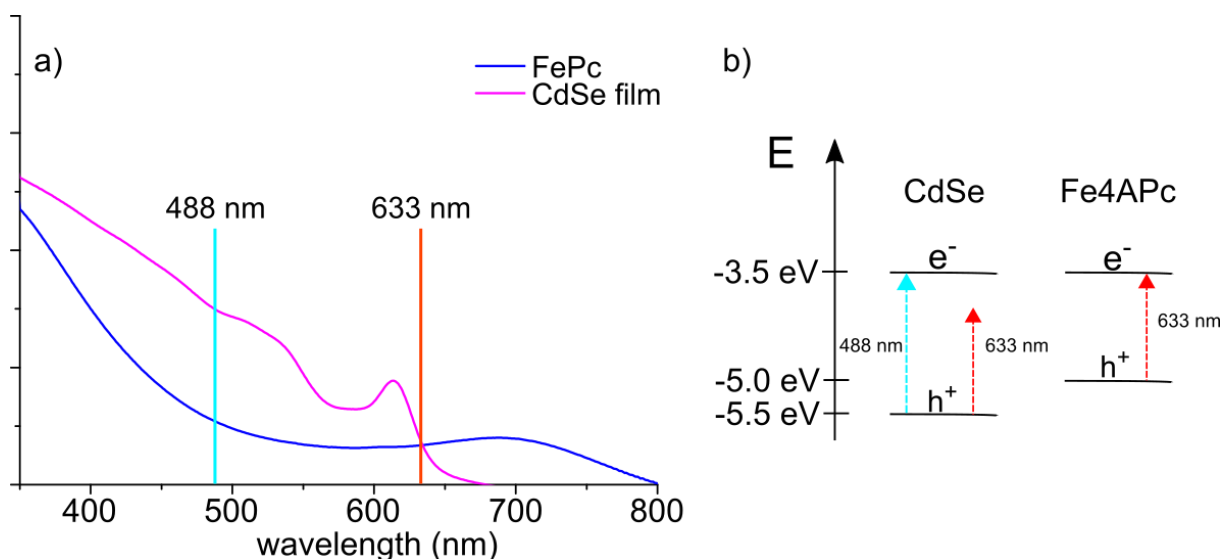


Figure 42: Comparison of UV-Vis absorption properties and electronic structure of the CdSe QDs and Fe4APc molecules of the hybrid material. a) UV-Vis absorption spectra of CdSe QDs and 4APc films with the two different laser excitation wavelengths. b) comparison of the $1S_h-1S_e$ transition of the QDs and the HOMO-LUMO transition of Fe4APc using different laser wavelengths. Energy levels for the HOMO/LUMO transition of Fe4APc and the CdSe QDs are taken from theoretical energy level calculations and measurements.^{23–25,53,119}

Discussion

In general, optical patterning using CdSe QDs aims to exploit the increase in quantum yield that can be observed at near resonant excitation of the QD under ambient conditions. In addition, functional molecules for the creation of patterns may be employed. Additional functionalization of the QDs is either used to influence the solution processability of the material allowing a photolithography like process, or to act as a switchable fluorescence quencher.^{73,75,120} Irradiation of the fluorescence quencher in turn restores the initial QY of the CdSe material resulting in the optical pattern. In contrast, the functionalization of CdSe with Fe4APc molecules as presented in this work adds additional patterning possibilities. It introduces a negative fluorescence contrast obtained through the fluorescence bleaching during excitation of the HOMO-LUMO transition of the molecules.^{58,59}

The positive fluorescence contrast of the QDs under 488 nm excitation can be clearly attributed to the oxidation of the QDs surface and the subsequent elimination of trap states.⁷⁸⁻⁸¹ This is further supported by the long-term stability of the obtained patterns and the irreversibility of the enhancement. In contrast, the temporary enhancement through surface coordination of water and oxygen seems unlikely, as no recovery of the enhancement can be observed during excitation in a nitrogen atmosphere.¹¹⁴ Furthermore, we observe that the functionalization of the CdSe QDs with Fe4APc enhances the development of a positive fluorescence contrast through oxidation of the surface, compared to unfunctionalized QDs (**Figure 38**). The oxidation of the QDs surface is attributed to the photo-induced production of reactive oxygen species (ROS).¹²¹⁻¹²³ Hereby, the exciton created by the above bandgap excitation reacts with surface bound oxygen molecules to create ROS, which in turn can oxidize the surface atoms of the QD. However, the exact nature of the ROS species and the mechanism of the surface oxidation are still being discussed in literature. Similar to this, phthalocyanine metal complexes are well known photooxidation agents, generating ROS under photoexcitation. Especially iron phthalocyanine has been of great research interest due to its catalytic functionality in organic oxidation reactions.⁵⁰ From this we propose that the functionalization with Fe4APc provides a second pathway for the generation of ROS, which results in the observed faster oxidation of the QDs (**Figure 43**).

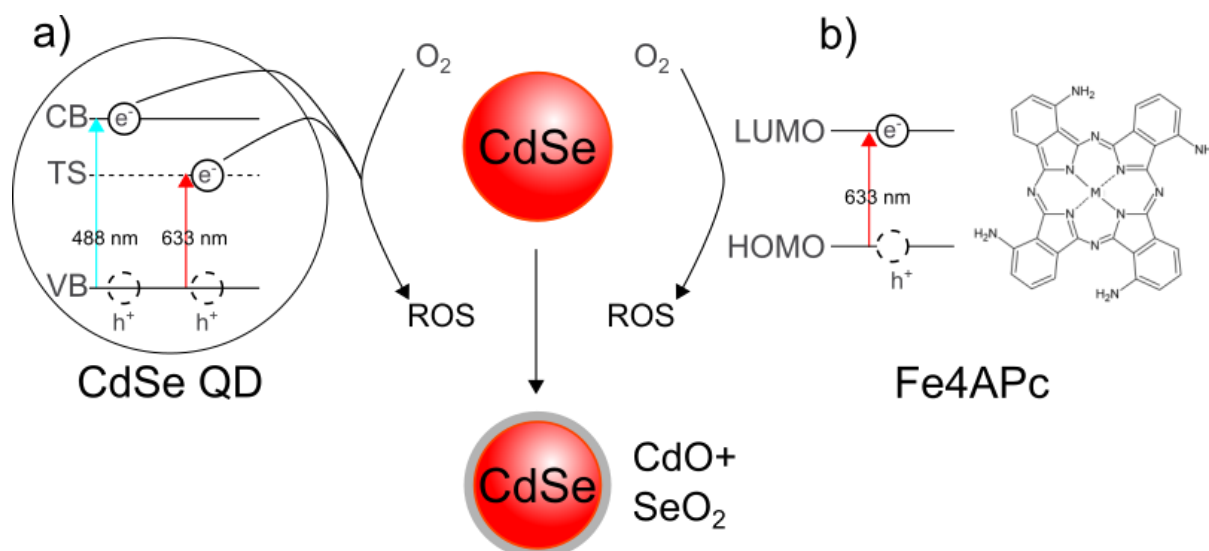


Figure 43: Schematic visualization of ROS generation through CdSe QDs and Fe4APc molecules under laser excitation. **a)** Generation of ROS through interaction with the exciton of the QD. The exciton can be formed through excitation of electrons to the conduction band at 488 nm excitation or below bandgap excitation through trap states (TS) at 633 nm. **b)** Generation of ROS through interaction of oxygen with the exciton of the HOMO-LUMO transition of phthalocyanine at 633 nm excitation. The generation of ROS near the QD surface results in the steady oxidation of the QD.

This is supported by the observed strong enhancement of the QD fluorescence, through below bandgap excitation of the particles using a 633 nm laser source. Below bandgap excitation of the QDs allows only for the formation of excitons using energetically lower trap states and reducing the overall efficiency due to the very low absorption cross-section of the QD material at 633 nm, whereas the Fe4APc molecules efficiency with its energetically lower HOMO-LUMO transition should not be impeded and its absorption cross-section is maximized at 633 nm. We suggest that under 633 nm excitation, the majority of the generated ROS species originates from the iron-phthalocyanine complex, leading to the observed strong fluorescence enhancement of the QDs, even at below bandgap excitation. Specialized measurements for the generation of ROS under varying excitation wavelengths need to be performed to further corroborate this.

The second aspect in the functionalization of the QDs with Fe4APc molecules is the change of the dielectric constant in the environment of the QDs. The phthalocyanine species used in this work have a generally larger dielectric constant from $\epsilon = 2.74$ to $\epsilon = 8.9$ compared to the native ligand shell $\epsilon \sim 2.5$ of the QDs, whereby iron phthalocyanine stands out with the largest dielectric constant of $\epsilon = 8.9$. It has been shown that a change in the QDs environment to a higher dielectric constant is beneficial to increase the quantum yield by stabilizing surface

Conclusion

charges from trap states and enabling the coordination of oxygen to the surface trap state.¹²⁴ This further facilitates the creation of ROS through the exciton from the trap state excitation on the QD surface.

The generation of ROS species through Fe4APc under 633 nm excitation was further exploited to generate a negative fluorescence contrast, slowly degrading the molecules through the ROS and diminishing the fluorescence of the HOMO-LUMO transition of the molecule. This is supported by the reduction of the oxidation speed under elimination of ambient oxygen and water during excitation in a nitrogen stream. We observe that the molecule fluorescence of the neat Fe4APc is more resistant to oxidation than in the QD hybrid material. It has been shown that the stacked configuration of phthalocyanine molecules in well-ordered films and molecule dimers reduces the generation of ROS significantly, resulting in the higher oxidation stability of the neat Fe4APc film.^{125–127} Furthermore, in the QD hybrid film a low concentration of Fe4APc molecules is distributed over a large active QD surface providing better access of ambient oxygen to the molecules than in the neat molecule film. Coordination of the phthalocyanine molecules to the QDs surface also puts strain on the ring structure of the molecule, making it more susceptible to oxidation.

8 Conclusion

In this work, we present a simple and direct approach for the preparation of functionalized CdSe QD hybrid materials. Through a two-step exchange procedure using n-butylamine/iodide hybrid stabilized QD as an intermediate, we are able to prepare homogenous films of QD hybrid material using dip-coating and drop-casting. This shows that phthalocyanine molecules can be used in this procedure to functionalize and interlink the CdSe QDs in the assembly, leading to a hybrid material.

AFM and SEM imaging are used to investigate the structural properties, such as surface roughness and thickness of the films, in relation to the preparation method. This showed that the careful, layer by layer assembly through dip coating allows for preparation of well-structured highly homogenous QD films. The drop casting approach in comparison allows for quick preparation of films through simple mixing of stock solution, while leading only to a slight increase in the overall roughness of the films. UV-Vis absorption and Raman

spectroscopy are used to show the presence of 4APc molecules throughout the QD hybrid material film.

Hybrid material films prepared on glass slides are employed to create optical patterns using a confocal microscopy setup, allowing for resolutions of the patterns close to the diffraction limit. Due to the divergence in optical resonance of the two components, this hybrid material allows for wavelength dependent optical patterning. Positive and negative optical patterning is achieved simultaneously during writing or reading. While patterning using a positive fluorescence contrast has been well established in literature, negative fluorescence contrast has been challenging and often suffers from low pattern stability. The QD hybrid material is an ideal candidate to address this challenge. Optical writing resonant to the excitonic transition of the QDs results in a positive fluorescence contrast, while writing near resonantly to the HOMO-LUMO transition of the organic dye leads to negative contrast. Furthermore, we are able to show that the functionalization of CdSe QDs with 4APc species also shows synergistic effects, providing not only additional optical properties but further enhancing the QDs capabilities.

9 Outlook

This work only presents the foundation for further investigations, and additional applications of the prepared materials would have exceeded the scope of this dissertation. The preparation methods presented in this work for CdSe based QD hybrid materials could easily be expanded upon to include other functional molecules. Preliminary tests have shown that the used 4APc species can be substituted by functional porphyrins or other dyes. The readily replaced hybrid n-butylamine/iodide stabilization of the QDs allows for functionalization with different molecules species, provided they possess an appropriate binding group and are processible in DMF or DMSO. This should allow for access to a wide variety of additional CdSe QD based hybrid materials.

Additionally, the phthalocyanines are commonly used to functionalize CdSe for a variety of other applications, such as photocatalysis, solar cells and medical applications.⁴⁷⁻⁴⁹ The CdSe QD hybrid materials presented in this work could be further investigated for use in these applications. Especially the use as heterogenic catalytic material for oxidative reaction merits

Outlook

further investigation, as the oxidation capabilities of the hybrid material have already been demonstrated in this work.

The patterning process presented in this work is realized through manual scanning excitation of a $5 \mu\text{m}^2$ area, functioning as a pixel of the complete image, which can then be revealed through low intensity excitation and recording of the whole image area. In a subsequent experiment, we aim to further increase the complexity and resolution of the patterned images, as the confocal microscopy setup should allow for a resolution close to the diffraction limit. Preliminary results using a programmable laser controller for the creation of the patterns result in highly complex optical patterns on the nanometer scale, as shown in **Figure 44**. Through the homogeneity of the material response, the patterning process could be further enhanced to incorporate pixels with different excitation writing durations, therefore allowing a scaling of the fluorescence contrast within the image.

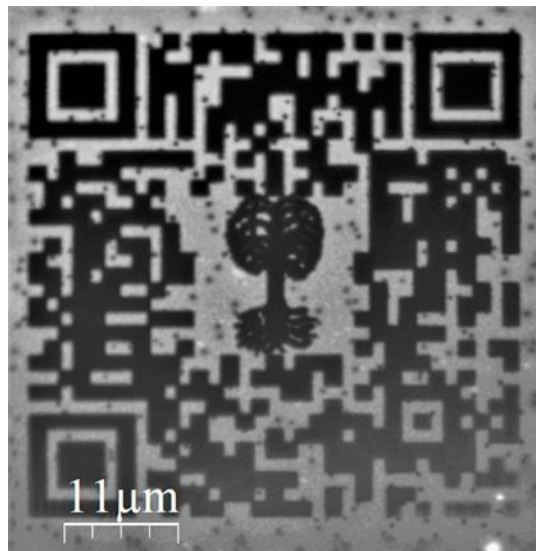


Figure 44: Refractive imaging of a laser printed pattern using a CdSe QD based hybrid material substrate. The automated printing process allows for the production of complex patterns on a nm scale in a short amount of time.

10 Acknowledgements

It should be quite clear that a work such as this dissertation is not done by one person alone. For this reason, I would like to take the opportunity and thank all the people involved with this project.

My thanks and appreciation first have to go to Prof. Dr. Marcus Scheele for not only allowing me to prove myself on this project, helping me to further my scientific career but also for his continued scientific support and for generally being a very nice boss to work for.

Great appreciation also has to go to Prof. Dr. Alfred Meixner for his support as my second advisor and the cooperation opportunities with his working group, without which this work would probably be impossible to achieve.

A big thanks go to Frank Wackenhut for his help in understanding the intricacies of confocal fluorescence microscopy, his willingness to discuss every small and large question of mine in great detail, and of course for the use of his ever evolving HydraFit Programs.

Further thanks go to Kai Braun for his introduction into the Meixner Groups Atomic force microscopy and his continued willingness to discuss almost all scientific topics with me, by offering his expertise and also some political ones.

Here I also want to thank my college, Krishan Kumar, for his continued efforts in his work with CdSe based hybrid materials and our discussions about the latest developments in our research, which were of great help in finishing this work.

I owe a lot of thanks to Alexander André who helped me find my professional footing at the beginning of my thesis by introducing me to most of the inner workings of my then-new group and helping me with the basics of field effector measurements. I also very much appreciated our scientific and movie centered discourse.

Many thanks have to go to Michelle Weber for her efforts in using electrochemistry to understand the electronic properties of CdSe hybrid materials and the resulting publications from our cooperation.

In this context, I want to also thank Kai Wurst for continuing to further my understanding of electrochemistry and being a very pleasant colleague to share an office with.

I want to also voice my appreciation for Andre Maier and Elke Nadler for their expertly recorded SEM images used in this work and the interesting discussions during those long measurement sessions.

Acknowledgements

A lot of thanks have to go to Jonas Hiller, for his immense help in the long hours of recording the fluorescence contrast images with the microscopy setup and his near-endless enthusiasm for the subject even during routine measurements. Although I can't pass up the opportunity, to remind him to focus his attention more on reaching his own goals instead of involving himself with every other possible project.

My thanks are of course not only limited to the professional cooperation with all my aforementioned colleagues but also goes towards our everyday interactions. Though shared group retreats, conference and even movie nights in the break room I had the opportunity to get to know an incredible amount of new and very welcoming people in Tübingen, which made my stay here all the more pleasant.

I want to also thank my family for their unending support over the long time of my academic endeavors, leading up to this point.

At last, I want to thank all the people that I have not yet mentioned, as a mention of the sheer amount of helpful and supportive colleagues and friends I have interacted with in my time in Tübingen could continue this paragraph for a few more pages.

11 List of figures

Figure 1: Left-Schematic visualization of the “particle in a box” concept for the first three quantum numbers n as wavefunctions. The Potential barriers $V(x)$ for $x < 0$ and $x > L$ are assumed to be infinitely high. Right-Schematic visualization of the resulting Energy levels of excited particles in a box for the first eight quantum numbers, showing the increasing distance between energy levels with higher quantum numbers. 15

Figure 2: Schematic visualization of the semiconductor density of states (DOS) correlated to the energy E . The density of states below the fermi Energy level E_F are filled with electrons, while the energy levels above are unoccupied and can be populated by exciting electrons. a) DOS of bulk semiconductor material with electron filled valence band (VB) and unoccupied conduction band (CB). b) Splitting of CB and VB into a molecule orbital-like DOS inside semiconductor nanocrystals. c) Excitation of electrons by light from the VB in the CB. d) Relaxation of electrons under light emission from the CB to the VB. 16

Figure 3: Theoretically calculated density of states in CdSe bulk material and a 1 nm radius nanocrystal of CdSe. The Zero is the vacuum Energy. The theoretical calculations show a clear change in the band structure of the QD compared to the bulk material. The CBM of the nanoparticle at -2.17 eV and the VBM of -6.27 result in a calculated bandgap of 4.1 eV compared to the smaller calculated bandgap of the bulk material of 1.72 eV (CBM - 3.52 eV, VBM -5.24 eV). This figure has been taken from the work of L.W. Wang and A. Zunger as an abridged version.²⁶ Copyright 1996 The American Physical Society. 18

Figure 4: a) Schematic representation for DOS for an imperfect nanocrystal with trap states that are located inside the bandgap. Trap states can be induced due to unsaturated surface atoms, either through b) incomplete surface saturation with ligands or c) missing surface atoms. d) Trap states can allow for alternative, non-radiative recombination pathways or recombination under emission of light with a longer wavelength due to the lower energy difference. 19

Figure 5: Illustration of different stabilizing agents and ligand molecules. a) Oleic acid, b) Trioctylphosphineoxide, c) Oleylamine. 20

Figure 6: Schematic representation of trap state elimination through ligand molecules. Image taken from the work of A.J. Houtepen.³⁶ Copyright 2016 American Chemical Society. 21

List of figures

Figure 7: Schematic visualization of ligand types. a) L-type ligands as two electron donors. b) X-type ligands functioning as one electron donor. c) Z-type ligands act as two electron acceptors to form a bond. Image taken from the work of A.J. Houtepen.³⁶ Copyright 2016 American Chemical Society. 22

Figure 8: Schematic of ligand exchange using excess pyridine to displace the native Trioctylphosphine Oxide (TOPO) ligand shell. a) Equilibrium between bound TOPO ligands and unbound ligands in solution. b) Replacement of TOPO through excess pyridine in solution shifting the surface equilibrium towards pyridine stabilization. 23

Figure 9: Schematic of ligand exchange of the native organic, long-chained ligand shell with a hybrid, organic-inorganic ligand shell. a) Native ligand shell of long-chained organic molecules stabilizing QDs in non-polar solvents (hexane). b) Transfer of QDs into N-methylamine formamide solvent through ligand exchange with Ammonium iodide salt resulting in inorganic stabilization. c) Transfer of QDs into chloroform solvent through ligand exchange using an excess of n-butylamine, creating a hybrid organic inorganic ligand shell. The modified graphic is taken from the work of Eychmüller et al.⁴ Copyright 2017 American Chemical Society. 24

Figure 10: Schematic of unmodified metal-free phthalocyanine molecules (left) and 4,4',4'',4'''-tetraamino phthalocyanine (4APc) with varying metal centers (right). 25

Figure 11: Absorption spectrum of zinc-phthalocyanine with distinct B- and Q-absorption bands. The B-band absorption is caused by the transition of electrons from the ground state (S_0) to the second excited state (S_2), while the Q-band absorption is related to the transition from the ground state (S_0) to the first excited state (S_1). Spectral data taken from "The Porphyrin Handbook" vol 16 Copyright 2003 Elsevier Inc.⁵² 26

Figure 12: Schematic visualization of calculated molecule orbital energy levels in phthalocyanine complexes with varying metal central atoms. The energy levels of the molecule orbitals can change significantly by changing the central metal atom. Most noticeably here is the change in energy for the HOMO LUMO transition that governs the position of the Q-band absorption. Schematic taken from the work of Liao and Schreiner.⁵³ Copyright 2002 Wiley Periodicals LLC 27

Figure 13: schematic for possible pathways for forming reactive oxygen species under a) homolytic oxygen cleavage and b) heterolytic oxygen cleavage on the example of mono-

and binuclear iron complexes. The cleaving of the oxygen bond allows for the creation of radical and ionic oxygen species that can further react to form a variety of reactive oxygen species. Schematic taken from the work of Sorokin and Kudrik.⁷² Copyright 2011 Elsevier

30

Figure 14: Schematic of optical patterning via ligand modification under irradiation to modify solution processability. a) Irradiation with a mask containing the desired pattern modifying the exposed stabilizing ligands. b) Washing with an appropriate solvent to remove the modified QDs. c) Finished pattern of unaltered QDs. 31

Figure 15: Visualization of gradual oxidation of surface atoms through targeted laser light excitation and resulting elimination of surface defects and resulting trap states. 32

Figure 16: Schematic of positive fluorescence contrast writing with CdSe QDs. Excitation using 488 nm laser source resulting in a positive fluorescence contrast pattern. 32

Figure 17: (a)-(c) show the line section produced by two different point-like sources (blue and red dashed line) together with their sum (black line). The distance between the maxima of both objects is defined by Δx . (a) The distance Δx is smaller than the value given by equation 5 and the 2 sources cannot be distinguished. (b) The distance Δx is chosen in a way that both sources can be distinguished, as the first minimum of the black curve is located at the maximum of the red curve and vice versa, this configuration is called the Rayleigh criterion. (c) The distance Δx is much larger and both sources can be clearly distinguished. 34

Figure 18: Schematic drawing of the confocal principal for achieving high axial resolution along the optical axis. In this method, a pinhole (PH) is placed in the image plane to reduce out-of-focus light ($z < 0$ in blue, $z > 0$ in red). This way, only light emerging from the focal plane ($z = 0$, shown in green) can pass the PH, while out of focus signal gets drastically reduced. 35

Figure 19: Absorption spectrum of colloidal CdSe QDs. Using a Lorentzian fit to determine the wavelength of the first excitonic absorption peak, to determine size and concentration of the colloidal QDs. 37

Figure 20: Schematic drawing of the experimental microscopy setup. The dashed rectangles indicate the excitation and the detection beam path. M1-5: mirrors, BS: beam splitter, MO: microscope objective, APD 1,2: avalanche photodiodes, CCD: charged coupled

79

List of figures

device sensor. The excitation beam path consists of a 488 nm and a 633 nm laser diode as excitation sources, which are operated in CW mode. The excitation light source can be switched through use of mirror (M2) and is focused with an immersion oil objective lens (NA=1.25) onto the sample which is scanned through the focus. The same objective lens is used to collect the detected signal, which is guided through a beam splitter (BS) to the detection path. The detected signal can either be guided to a spectroscopic unit or two different avalanche photodiodes (APD 1,2) for imaging. 38

Figure 21: Schematic of experimental setup for CdSe particle synthesis. Setup includes a Three-necked round bottom flask with magnetic stirring, temperature controller, injection valve and Dimroth cooler connected to a Schlenk line. 41

Figure 22: a) UV-vis absorption spectra of 3.5 ± 0.1 nm CdSe NP with size distribution analysis (inset) using STEM images b). 42

Figure 23: a) UV-vis absorption spectra of 4.7 ± 0.2 nm CdSe NP with size distribution analysis (inset) using SEM images b). 44

Figure 24: a) UV-vis absorption spectra of 4.1 ± 0.1 nm CdSe NP with size distribution analysis (inset) using SEM image b). 45

Figure 25: ^{13}C NMR spectra of CdSe particle solution before (blue) and after (red) ligand exchange procedure. Clear indication of long chained molecules before the exchange (1-5) being replaced by n-butylamine (6-9). Small satellite signals (blue/magnified) indicate a mixture of long chained molecules in the native ligand shell. 47

Figure 26: Schematic for dip coating procedure to obtain phthalocyanine functionalized CdSe films on glass or silicon oxide surfaced substrates. Dipping into a CdSe particle solution (1) for 20s followed by washing in Chloroform (2). Subsequent dipping in a ligand solution in DMSO (3) for 20s and cleaning in DMSO (4). This sequence is repeated as often as needed. 48

Figure 27: Schematic for drop casting procedure to obtain phthalocyanine functionalized CdSe films on glass or silicon oxide surfaced substrates. Deposition of ligand solution in DMF on the substrate (1), with subsequent addition of CdSe particle solution in THF (2), which is then dried (3) resulting in functionalized CdSe films. 49

Figure 28: Images of completely covered silicon (a,b) and glass substrates (c,d) using dip coating (a,c) and drop casting (b,d) preparation. 51

Figure 29: SEM images of hybrid material thin films created through drop casting using CdSe QDs and Fe4APc molecules. a) Image of complete coverage of the substrate with the QD hybrid material showing cracks and material indentations due to drying effects. b) No obvious ordered structure motive or overarching structural domains can be observed.

52

Figure 30: AFM images of CdSe hybrid films created through dip coating (a,b) and drop casting (c,d). For film thickness evaluation, an incision is made and the height difference from substrate to film is measured on the boarder (a,c). Roughness is evaluated by measuring the root mean square value of the height difference in an undisturbed 10x10 μm area (c,d).

53

Figure 31: Image of in homogeneously and partially covered silicon substrate due to insufficient CdSe QD particle amount.

55

Figure 32: a) Comparison of UV-Vis absorption spectra of native CdSe particle solution (1) after ligand exchange with butylamine (2) and prepared as unfunctionalized film (3). b) Comparison of UV-Vis spectra of an unfunctionalized CdSe particle film (3), a spectrum of Fe-phthalocyanine (4) and a CdSe particle film functionalized with Fe-phthalocyanine (5).

56

Figure 33: Schematic structure of 4,4',4'',4''' tetraaminophthalocyanine (4APc) molecules, containing different metal center atoms of Copper (Cu), Nickel (Ni), Iron (Fe) and as metal free variant (H_2).

57

Figure 34: Comparison of Raman spectra of unfunctionalized CdSe films and after ligand exchange with various phthalocyanine species containing Fe, Ni, Cu metal centers and the metal free variant (H_2).

58

Figure 35: Optical write/read-out experiments on thin films of CdSe QDs functionalized with Fe4APc. (a) 488 nm write/488 nm read. (b) 488 nm write/633 nm read. Both panels show the same part of the sample, which was optically patterned under the same conditions. (c) A different part of the sample optically patterned at 633 nm and read-out at 633 nm. (d) The same patterned sample region as in (c), but under 488 nm read-out. Adapted with permission from ref⁹³. Copyright 2019 AIP Publishing.

60

Figure 36: Fluorescence spectra over time under 488 nm excitation of a CdSe QD (4.7 nm) film functionalized with Fe4APc molecules. Overview during 15 min excitation, spectra are

81

List of figures

taken every 10 s of excitation time. A continued increase of the fluorescence intensity is visible, together with a blue shift of the emission peak of about 10 nm. Inset: Overview the of fluorescence intensity (blue lines, right scale) and center wavelength of the emission (red and black line, left scale) development during excitation over 15 min. 62

Figure 37: a) Fluorescence spectra over time under 488 nm excitation. Overview during 15 min excitation, spectra are acquired every 10 s of excitation time. Continuous decrease of the fluorescence intensity due to break down of the CdSe QDs. A fit of the final spectra no longer corresponds to the usual Lorentzian fit model of the CdSe QDs. b) Spatial scan of the fluorescence intensity under different readout wavelengths showing fluorescence enhancement in the initial state of the material and negative fluorescence contrast after excitation due to destruction of the CdSe QD hybrid material. 63

Figure 38: a) Fluorescence spectra of CdSe-Fe4APc (top) QDs and of CdSe-I⁻/BA QDs (bottom) under 488 nm excitation for 0 min (red) and 15 min (blue). b) Fluorescence intensity increase (right axis) and spectral shift (left axis) of the same samples as those analyzed in a) for consecutive time intervals. Adapted with permission from ref ⁹³. Copyright 2019 AIP Publishing. 63

Figure 39: (a) Fluorescence spectra under 633 nm excitation of the hybrid material after 0 min (blue) and 15 min (red) continuous excitation. Phonon modes of the CdSe lattice are signaled by asterisks. At this wavelength only the phthalocyanine is excited, which leads to a broad fluorescence signal. The spectral region of the fluorescence from the phthalocyanine due to radiative recombination of the HOMO-LUMO transition is highlighted with a black square. The inset magnifies this spectral region and provides the fluorescence spectrum of the neat phthalocyanine in black for comparison. (b) Fluorescence spectra under 633 nm excitation of CdSe QDs functionalized with OA/HDA after 0 min (blue) and 15 min (red) continuous excitation. Adapted with permission from ref ⁹³. Copyright 2019 AIP Publishing. 64

Figure 40: a) Fluorescence spectra of CdSe-Fe4APc (top) and of Fe4APc neat molecules (bottom) under 633 nm excitation for 0 min (red) and 15 min (blue). b) Fluorescence intensity decrease of the same samples as those analyzed in a) for consecutive time intervals. 65

Figure 41: Schematic visualization of layer by layer deposition of n-butylamine/iodide stabilized CdSe QD on an MPTMS functionalized substrate. The initial QD layer is coordinated to the substrate via the MPTMS functionalization. The QDs are immobilized through washing and drying, removing the hybrid ligands. Functionalization with phthalocyanine enables coordination of additional QD layers. 68

Figure 42: Comparison of UV-Vis absorption properties and electronic structure of the CdSe QDs and Fe4APc molecules of the hybrid material. a) UV-Vis absorption spectra of CdSe QDs and 4APc films with the two different laser excitation wavelengths. b) comparison of the $1S_h-1S_e$ transition of the QDs and the HOMO-LUMO transition of Fe4APc using different laser wavelengths. Energy levels for the HOMO/LUMO transition of Fe4APc and the CdSe QDs are taken from theoretical energy level calculations and measurements.^{23-25,53,119} 69

Figure 43: Schematic visualization of ROS generation through CdSe QDs and Fe4APc molecules under laser excitation. a) Generation of ROS through interaction with the exciton of the QD. The exciton can be formed through excitation of electrons to the conduction band at 488 nm excitation or below bandgap excitation through trap states (TS) at 633 nm. b) Generation of ROS through interaction of oxygen with the exciton of the HOMO-LUMO transition of phthalocyanine at 633 nm excitation. The generation of ROS near the QD surface results in the steady oxidation of the QD. 71

Figure 44: Refractive imaging of a laser printed pattern using a CdSe QD based hybrid material substrate. The automated printing process allows for the production of complex patterns on a nm scale in a short amount of time. 74

12 References

- (1) WILLIAMS, J. A.; RINDONE, G. E.; MCKINSTRY, H. A. Small-Angle X-Ray Scattering Analysis of Nucleation in Glass: III, Gold Ruby Glasses. *J. Am. Ceram. Soc.* **1981**, *64* (12), 709–713. <https://doi.org/10.1111/j.1151-2916.1981.tb15891.x>.
- (2) Kortan, A. R.; Hull, R.; Opila, R. L.; Bawendi, M. G.; Steigerwald, M. L.; Carroll, P. J.; Brus, L. E. Nucleation and Growth of CdSe on ZnS Quantum Crystallite Seeds, and Vice Versa, in Inverse Micelle Media. *J. Am. Chem. Soc.* **1990**, *112* (4), 1327–1332. <https://doi.org/10.1021/ja00160a005>.
- (3) Murray, C. B.; Norris, D. J.; Bawendi, M. G. Synthesis and Characterization of Nearly Monodisperse CdE (E = Sulfur, Selenium, Tellurium) Semiconductor Nanocrystallites. *J. Am. Chem. Soc.* **1993**, *115* (19), 8706–8715. <https://doi.org/10.1021/ja00072a025>.
- (4) Sayevich, V.; Guhrenz, C.; Dzhagan, V. M.; Sin, M.; Werheid, M.; Cai, B.; Borchardt, L.; Widmer, J.; Zahn, D. R. T.; Brunner, E.; Lesnyak, V.; Gaponik, N.; Eychmüller, A. Hybrid N -Butylamine-Based Ligands for Switching the Colloidal Solubility and Regimentation of Inorganic-Capped Nanocrystals. *ACS Nano* **2017**, *11* (2), 1559–1571. <https://doi.org/10.1021/acsnano.6b06996>.
- (5) Dabbousi, B. O.; Rodriguez-Viejo, J.; Mikulec, F. V.; Heine, J. R.; Mattoussi, H.; Ober, R.; Jensen, K. F.; Bawendi, M. G. (CdSe)ZnS Core–Shell Quantum Dots: Synthesis and Characterization of a Size Series of Highly Luminescent Nanocrystallites. *J. Phys. Chem. B* **1997**, *101* (46), 9463–9475. <https://doi.org/10.1021/jp971091y>.
- (6) Chen, O.; Chen, X.; Yang, Y.; Lynch, J.; Wu, H.; Zhuang, J.; Cao, Y. C. Synthesis of Metal-Selenide Nanocrystals Using Selenium Dioxide as the Selenium Precursor. *Angew. Chemie Int. Ed.* **2008**, *47* (45), 8638–8641. <https://doi.org/10.1002/anie.200804266>.
- (7) Brus, L. Electronic Wave Functions in Semiconductor Clusters: Experiment and Theory. *J. Phys. Chem.* **1986**, *90* (12), 2555–2560. <https://doi.org/10.1021/j100403a003>.
- (8) Talapin, D. V.; Lee, J.-S.; Kovalenko, M. V.; Shevchenko, E. V. Prospects of Colloidal Nanocrystals for Electronic and Optoelectronic Applications. *Chem. Rev.* **2010**, *110* (1), 389–458. <https://doi.org/10.1021/cr900137k>.
- (9) Robel, I.; Subramanian, V.; Kuno, M.; Kamat, P. V. Quantum Dot Solar Cells. Harvesting Light Energy with CdSe Nanocrystals Molecularly Linked to Mesoscopic TiO₂ Films. *J. Am. Chem. Soc.* **2006**, *128* (7), 2385–2393. <https://doi.org/10.1021/ja056494n>.

- (10) Sukhanova, A.; Nabiev, I. Fluorescent Nanocrystal Quantum Dots as Medical Diagnostic Tools. *Expert Opin. Med. Diagn.* **2008**, *2* (4), 429–447. <https://doi.org/10.1517/17530059.2.4.429>.
- (11) Li, X.; Wang, H.; Wu, H. Phthalocyanines and Their Analogs Applied in Dye-Sensitized Solar Cell. In *Functional Phthalocyanine Molecular Materials*; Jiang, J., Ed.; Springer Berlin Heidelberg: Berlin, Heidelberg, 2010; pp 229–273. https://doi.org/10.1007/978-3-642-04752-7_8.
- (12) Palazon, F.; Prato, M.; Manna, L. Writing on Nanocrystals: Patterning Colloidal Inorganic Nanocrystal Films through Irradiation-Induced Chemical Transformations of Surface Ligands. *J. Am. Chem. Soc.* **2017**, *139* (38), 13250–13259. <https://doi.org/10.1021/jacs.7b05888>.
- (13) Malak, S. T.; Smith, M. J.; Yoon, Y. J.; Lin, C. H.; Jung, J.; Lin, Z.; Tsukruk, V. V. Programmed Emission Transformations: Negative-to-Positive Patterning Using the Decay-to-Recovery Behavior of Quantum Dots. *Adv. Opt. Mater.* **2017**, *5* (1), 1600509. <https://doi.org/10.1002/adom.201600509>.
- (14) Cartwright, H. *Physical Chemistry. By Peter Atkins, Oxford University Press: Oxford, U.K. Xvi Includes CD. ISBN 0-19-850101-3. Student Solutions Manual and Instructors Solutions Manual Are Also Available*; Wiley-VCH: Weinheim, 2001; Vol. 6. <https://doi.org/10.1007/s00897010493a>.
- (15) Göpel, W.; Ziegler, C. *Einführung in Die Materialwissenschaften: Physikalisch-Chemische Grundlagen Und Anwendungen*; Vieweg+Teubner Verlag: Wiesbaden, 1996. <https://doi.org/10.1007/978-3-322-93440-6>.
- (16) Wedler, G.; Freund, H. J. *Lehrbuch Der Physikalischen Chemie. 6. Auflage.*; Weinheim, 2012. <https://doi.org/10.1002/ange.201300430>.
- (17) Harris, R. D.; Bettis Homan, S.; Kodaimati, M.; He, C.; Nepomnyashchii, A. B.; Swenson, N. K.; Lian, S.; Calzada, R.; Weiss, E. A. Electronic Processes within Quantum Dot-Molecule Complexes. *Chem. Rev.* **2016**, *116* (21), 12865–12919. <https://doi.org/10.1021/acs.chemrev.6b00102>.
- (18) Yoffe, A. D. Semiconductor Quantum Dots and Related Systems: Electronic, Optical, Luminescence and Related Properties of Low Dimensional Systems. *Adv. Phys.* **2001**, *50* (1), 1–208. <https://doi.org/10.1080/00018730010006608>.

References

- (19) Singh, V. A.; Ranjan, V.; Kapoor, M. Semiconductor Quantum Dots: Theory and Phenomenology. *Bull. Mater. Sci.* **1999**, *22* (3), 563–569. <https://doi.org/10.1007/BF02749969>.
- (20) Baban, C.; Rusu, G. I.; Prepelita, P. On the Optical Properties of Polycrystalline CdSe Thin Films. *J. Optoelectron. Adv. Mater.* **2005**, *7* (2), 817–821.
- (21) Baban, C.; Rusu, G. . On the Structural and Optical Characteristics of CdSe Thin Films. *Appl. Surf. Sci.* **2003**, *211* (1–4), 6–12. [https://doi.org/10.1016/S0169-4332\(03\)00299-X](https://doi.org/10.1016/S0169-4332(03)00299-X).
- (22) Muthukumarasamy, N.; Jayakumar, S.; Kannan, M. D.; Balasundaraprabhu, R.; Ramanathaswamy, P. Structural and Optical Properties of Hot Wall Deposited CdSe_{0.15}Te_{0.85} Thin Films. *J. Cryst. Growth* **2004**, *263* (1–4), 308–315. <https://doi.org/10.1016/j.jcrysgr.2003.11.081>.
- (23) Erni, R.; Browning, N. D. Quantification of the Size-Dependent Energy Gap of Individual CdSe Quantum Dots by Valence Electron Energy-Loss Spectroscopy. *Ultramicroscopy* **2007**, *107* (2–3), 267–273. <https://doi.org/10.1016/j.ultramic.2006.08.002>.
- (24) Gupta, P.; Ramrakhiani, M. Influence of the Particle Size on the Optical Properties of CdSe Nanoparticles. *Open Nanosci. J.* **2009**, *3* (1), 15–19. <https://doi.org/10.2174/1874140100903010015>.
- (25) Hamizi, N. A.; Johan, M. R. Synthesis and Size Dependent Optical Studies in CdSe Quantum Dots via Inverse Micelle Technique. *Mater. Chem. Phys.* **2010**, *124* (1), 395–398. <https://doi.org/10.1016/j.matchemphys.2010.06.053>.
- (26) Wang, L.-W.; Zunger, A. Pseudopotential Calculations of Nanoscale CdSe Quantum Dots. *Phys. Rev. B* **1996**, *53* (15), 9579–9582. <https://doi.org/10.1103/PhysRevB.53.9579>.
- (27) Cordones, A. A.; Leone, S. R. Mechanisms for Charge Trapping in Single Semiconductor Nanocrystals Probed by Fluorescence Blinking. *Chem. Soc. Rev.* **2013**, *42* (8), 3209. <https://doi.org/10.1039/c2cs35452g>.
- (28) Jones, M.; Lo, S. S.; Scholes, G. D. Quantitative Modeling of the Role of Surface Traps in CdSe/CdS/ZnS Nanocrystal Photoluminescence Decay Dynamics. *Proc. Natl. Acad. Sci.* **2009**, *106* (9), 3011–3016. <https://doi.org/10.1073/pnas.0809316106>.
- (29) Abdellah, M.; Karki, K. J.; Lenngren, N.; Zheng, K.; Pascher, T.; Yartsev, A.; Pullerits, T.

- Ultra Long-Lived Radiative Trap States in CdSe Quantum Dots. *J. Phys. Chem. C* **2014**, *118* (37), 21682–21686. <https://doi.org/10.1021/jp506536h>.
- (30) Chen, Y.; Vela, J.; Htoon, H.; Casson, J. L.; Werder, D. J.; Bussian, D. A.; Klimov, V. I.; Hollingsworth, J. A. “Giant” Multishell CdSe Nanocrystal Quantum Dots with Suppressed Blinking. *J. Am. Chem. Soc.* **2008**, *130* (15), 5026–5027. <https://doi.org/10.1021/ja711379k>.
- (31) Spinicelli, P.; Buil, S.; Quélin, X.; Mahler, B.; Dubertret, B.; Hermier, J.-P. Bright and Grey States in CdSe-CdS Nanocrystals Exhibiting Strongly Reduced Blinking. *Phys. Rev. Lett.* **2009**, *102* (13), 136801. <https://doi.org/10.1103/PhysRevLett.102.136801>.
- (32) Rosen, S.; Schwartz, O.; Oron, D. Transient Fluorescence of the Off State in Blinking CdSe/CdS/ZnS Semiconductor Nanocrystals Is Not Governed by Auger Recombination. *Phys. Rev. Lett.* **2010**, *104* (15), 157404. <https://doi.org/10.1103/PhysRevLett.104.157404>.
- (33) Chen, O.; Chen, X.; Yang, Y.; Lynch, J.; Wu, H.; Zhuang, J.; Cao, Y. C. Synthesis of Metal-Selenide Nanocrystals Using Selenium Dioxide as the Selenium Precursor. *Angew. Chemie - Int. Ed.* **2008**, *47* (45), 8638–8641. <https://doi.org/10.1002/anie.200804266>.
- (34) Chen, O.; Zhao, J.; Chauhan, V. P.; Cui, J.; Wong, C.; Harris, D. K.; Wei, H.; Han, H.-S.; Fukumura, D.; Jain, R. K.; Bawendi, M. G. Compact High-Quality CdSe–CdS Core–Shell Nanocrystals with Narrow Emission Linewidths and Suppressed Blinking. *Nat. Mater.* **2013**, *12* (5), 445–451. <https://doi.org/10.1038/nmat3539>.
- (35) Kirkwood, N.; Monchen, J. O. V.; Crisp, R. W.; Grimaldi, G.; Bergstein, H. A. C.; Du Fossé, I.; Van Der Stam, W.; Infante, I.; Houtepen, A. J. Finding and Fixing Traps in II-VI and III-V Colloidal Quantum Dots: The Importance of Z-Type Ligand Passivation. *J. Am. Chem. Soc.* **2018**, *140* (46), 15712–15723. <https://doi.org/10.1021/jacs.8b07783>.
- (36) Houtepen, A. J.; Hens, Z.; Owen, J. S.; Infante, I. On the Origin of Surface Traps in Colloidal II–VI Semiconductor Nanocrystals. *Chem. Mater.* **2017**, *29* (2), 752–761. <https://doi.org/10.1021/acs.chemmater.6b04648>.
- (37) Issac, A.; von Borczyskowski, C.; Cichos, F. Correlation between Photoluminescence Intermittency of CdSe Quantum Dots and Self-Trapped States in Dielectric Media. *Phys. Rev. B* **2005**, *71* (16), 161302. <https://doi.org/10.1103/PhysRevB.71.161302>.
- (38) Issac, A.; Krasselt, C.; Cichos, F.; von Borczyskowski, C. Influence of the Dielectric

References

- Environment on the Photoluminescence Intermittency of CdSe Quantum Dots. *ChemPhysChem* **2012**, *13* (13), 3223–3230. <https://doi.org/10.1002/cphc.201101040>.
- (39) Peng, X.; Schlamp, M. C.; Kadavanich, A. V.; Alivisatos, A. P. Epitaxial Growth of Highly Luminescent CdSe/CdS Core/Shell Nanocrystals with Photostability and Electronic Accessibility. *J. Am. Chem. Soc.* **1997**, *119* (30), 7019–7029. <https://doi.org/10.1021/ja970754m>.
- (40) Nan, W.; Niu, Y.; Qin, H.; Cui, F.; Yang, Y.; Lai, R.; Lin, W.; Peng, X. Crystal Structure Control of Zinc-Blende CdSe/CdS Core/Shell Nanocrystals: Synthesis and Structure-Dependent Optical Properties. *J. Am. Chem. Soc.* **2012**, *134* (48), 19685–19693. <https://doi.org/10.1021/ja306651x>.
- (41) Talapin, D. V.; Mekis, I.; Götzinger, S.; Kornowski, A.; Benson, O.; Weller, H. CdSe/CdS/ZnS and CdSe/ZnSe/ZnS Core-Shell-Shell Nanocrystals. *J. Phys. Chem. B* **2004**, *108* (49), 18826–18831. <https://doi.org/10.1021/jp046481g>.
- (42) Nann, T. Phase-Transfer of CdSe@ZnS Quantum Dots Using Amphiphilic Hyperbranched Polyethylenimine. *Chem. Commun.* **2005**, No. 13, 1735. <https://doi.org/10.1039/b414807j>.
- (43) Buckley, J. J.; Greaney, M. J.; Brutchey, R. L. Ligand Exchange of Colloidal CdSe Nanocrystals with Stibanates Derived from Sb₂S₃ Dissolved in a Thiol-Amine Mixture. *Chem. Mater.* **2014**, *26* (21), 6311–6317. <https://doi.org/10.1021/cm503324k>.
- (44) Chan, W. C. W. Quantum Dot Bioconjugates for Ultrasensitive Nonisotopic Detection. *Science* (80-.). **1998**, *281* (5385), 2016–2018. <https://doi.org/10.1126/science.281.5385.2016>.
- (45) Zaman, M. B.; Baral, T. N.; Zhang, J.; Whitfield, D.; Yu, K. Single-Domain Antibody Functionalized CdSe/ZnS Quantum Dots for Cellular Imaging of Cancer Cells. *J. Phys. Chem. C* **2009**, *113* (2), 496–499. <https://doi.org/10.1021/jp809159k>.
- (46) Katari, J. E. B.; Colvin, V. L.; Alivisatos, A. P. X-Ray Photoelectron Spectroscopy of CdSe Nanocrystals with Applications to Studies of the Nanocrystal Surface. *J. Phys. Chem.* **1994**, *98* (15), 4109–4117. <https://doi.org/10.1021/j100066a034>.
- (47) Grätzel, M. Dye-Sensitized Solar Cells. *J. Photochem. Photobiol. C Photochem. Rev.* **2003**, *4* (2), 145–153. [https://doi.org/10.1016/S1389-5567\(03\)00026-1](https://doi.org/10.1016/S1389-5567(03)00026-1).
- (48) Mathews, S. J.; Kumar, S. C.; Giribabu, L.; Rao, S. V. Nonlinear Optical and Optical

- Limiting Properties of Phthalocyanines in Solution and Thin Films of PMMA at 633 Nm Studied Using a Cw Laser. *Mater. Lett.* **2007**, *61* (22), 4426–4431. <https://doi.org/10.1016/j.matlet.2007.02.034>.
- (49) Stuchinskaya, T.; Moreno, M.; Cook, M. J.; Edwards, D. R.; Russell, D. A. Targeted Photodynamic Therapy of Breast Cancer Cells Using Antibody–Phthalocyanine–Gold Nanoparticle Conjugates. *Photochem. Photobiol. Sci.* **2011**, *10* (5), 822. <https://doi.org/10.1039/c1pp05014a>.
- (50) Sorokin, A. B. Phthalocyanine Metal Complexes in Catalysis. *Chem. Rev.* **2013**, *113* (10), 8152–8191. <https://doi.org/10.1021/cr4000072>.
- (51) Manbeck, G. F.; Fujita, E. A Review of Iron and Cobalt Porphyrins, Phthalocyanines and Related Complexes for Electrochemical and Photochemical Reduction of Carbon Dioxide. *J. Porphyr. Phthalocyanines* **2015**, *19* (01–03), 45–64. <https://doi.org/10.1142/S1088424615300013>.
- (52) MACK, J.; STILLMAN, M. J. 103 - Electronic Structures of Metal Phthalocyanine and Porphyrin Complexes from Analysis of the UV–Visible Absorption and Magnetic Circular Dichroism Spectra and Molecular Orbital Calculations. In *The Porphyrin Handbook*; Kadish, K. M., Smith, K. M., Guillard, R., Eds.; Academic Press: Amsterdam, 2003; pp 43–116. <https://doi.org/https://doi.org/10.1016/B978-0-08-092390-1.50008-4>.
- (53) Liao, M.-S.; Scheiner, S. Comparative Study of Metal-Porphyrins, -Porphyrazines, and -Phthalocyanines. *J. Comput. Chem.* **2002**, *23* (15), 1391–1403. <https://doi.org/10.1002/jcc.10142>.
- (54) Liao, M.-S.; Scheiner, S. Electronic Structure and Bonding in Metal Phthalocyanines, Metal=Fe, Co, Ni, Cu, Zn, Mg. *J. Chem. Phys.* **2001**, *114* (22), 9780–9791. <https://doi.org/10.1063/1.1367374>.
- (55) Ortí, E.; Brédas, J. L.; Clarisse, C. Electronic Structure of Phthalocyanines: Theoretical Investigation of the Optical Properties of Phthalocyanine Monomers, Dimers, and Crystals. *J. Chem. Phys.* **1990**, *92* (2), 1228–1235. <https://doi.org/10.1063/1.458131>.
- (56) Zhang, X.-F.; Li, X.; Niu, L.; Sun, L.; Liu, L. Charge Transfer Photophysics of Tetra(α -Amino) Zinc Phthalocyanine. *J. Fluoresc.* **2009**, *19* (6), 947–954. <https://doi.org/10.1007/s10895-009-0494-7>.
- (57) Kumar, K.; Liu, Q.; Hiller, J.; Schedel, C.; Maier, A.; Meixner, A.; Braun, K.; Lauth, J.;

References

- Scheele, M. Fast, Infrared-Active Optical Transistors Based on Dye-Sensitized CdSe Nanocrystals. *ACS Appl. Mater. Interfaces* **2019**, *11* (51), 48271–48280. <https://doi.org/10.1021/acsami.9b18236>.
- (58) Shinohara, H.; Tsaryova, O.; Schnurpfeil, G.; Wöhrle, D. Differently Substituted Phthalocyanines: Comparison of Calculated Energy Levels, Singlet Oxygen Quantum Yields, Photo-Oxidative Stabilities, Photocatalytic and Catalytic Activities. *J. Photochem. Photobiol. A Chem.* **2006**, *184* (1–2), 50–57. <https://doi.org/10.1016/j.jphotochem.2006.03.024>.
- (59) Słota, R.; Dyrda, G. UV Photostability of Metal Phthalocyanines in Organic Solvents. *Inorg. Chem.* **2003**, *42* (18), 5743–5750. <https://doi.org/10.1021/ic0260217>.
- (60) Vasiliev, R. B.; Vinogradov, V. S.; Dorofeev, S. G.; Kozyrev, S. P.; Kucherenko, I. V.; Novikova, N. N. IR-Active Vibrational Modes of CdTe and CdSe Colloidal Quantum Dots and CdTe/CdSe Core/Shell Nanoparticles and Coupling Effects. *Phys. Solid State* **2007**, *49* (3), 547–551. <https://doi.org/10.1134/S1063783407030304>.
- (61) Leatherdale, C. A.; Bawendi, M. G. Observation of Solvatochromism in CdSe Colloidal Quantum Dots. *Phys. Rev. B* **2001**, *63* (16), 165315. <https://doi.org/10.1103/PhysRevB.63.165315>.
- (62) Popovic, Z. D.; Sharp, J. H. Pulsed Photoconductivity Action Spectra of B-metalfree Phthalocyanine Thin Films. *J. Chem. Phys.* **1977**, *66* (11), 5076–5082. <https://doi.org/10.1063/1.433815>.
- (63) Anthopoulos, T. D.; Shafai, T. S. SCLC Measurements in Nickel Phthalocyanine Thin Films. *Phys. status solidi* **2000**, *181* (2), 569–574. [https://doi.org/10.1002/1521-396X\(200010\)181:2<569::AID-PSSA569>3.0.CO;2-Y](https://doi.org/10.1002/1521-396X(200010)181:2<569::AID-PSSA569>3.0.CO;2-Y).
- (64) Gould, R. D. Dependence of the Mobility and Trap Concentration in Evaporated Copper Phthalocyanine Thin Films on Background Pressure and Evaporation Rate. *J. Phys. D. Appl. Phys.* **1986**, *19* (9), 1785–1790. <https://doi.org/10.1088/0022-3727/19/9/023>.
- (65) Nalwa, H.; Sinha, J.; Vasudevan, P. Synthesis and Electrical Properties of Monomeric and Polymeric Iron-phthalocyanines. *Die Makromol. Chemie* **1981**, *182* (3), 811–816. <https://doi.org/10.1002/macp.1981.021820311>.
- (66) BIJWE, J.; PHOUGAT, N. Dielectric Properties of Iron Phthalocyanine Compounds. *J. Porphyr. Phthalocyanines* **1998**, *02* (03), 223–230. [https://doi.org/10.1002/\(SICI\)1099-](https://doi.org/10.1002/(SICI)1099-)

- 1409(199805/06)2:3<223::AID-JPP69>3.0.CO;2-A.
- (67) Aimai, N.; Gould, R. D.; Saleh, A. Space-Charge-Limited Conductivity in Evaporated α -Form Metal-Free Phthalocyanine Thin Films. *Vacuum* **1998**, *50* (1–2), 53–56. [https://doi.org/10.1016/S0042-207X\(98\)00014-1](https://doi.org/10.1016/S0042-207X(98)00014-1).
- (68) Casas Espínola, J. L.; Hernández Contreras, X. A. Effect of Dielectric Constant on Emission of CdSe Quantum Dots. *J. Mater. Sci. Mater. Electron.* **2017**, *28* (10), 7132–7138. <https://doi.org/10.1007/s10854-017-6539-9>.
- (69) Rabani, E.; Hetényi, B.; Berne, B. J.; Brus, L. E. Electronic Properties of CdSe Nanocrystals in the Absence and Presence of a Dielectric Medium. *J. Chem. Phys.* **1999**, *110* (11), 5355–5369. <https://doi.org/10.1063/1.478431>.
- (70) Talgorn, E.; Moysidou, E.; Abellon, R. D.; Savenije, T. J.; Goossens, A.; Houtepen, A. J.; Siebbeles, L. D. A. Highly Photoconductive CdSe Quantum-Dot Films: Influence of Capping Molecules and Film Preparation Procedure. *J. Phys. Chem. C* **2010**, *114* (8), 3441–3447. <https://doi.org/10.1021/jp9109546>.
- (71) Rabouw, F. T.; de Mello Donega, C. Excited-State Dynamics in Colloidal Semiconductor Nanocrystals. *Top. Curr. Chem.* **2016**, *374* (5), 58. <https://doi.org/10.1007/s41061-016-0060-0>.
- (72) Sorokin, A. B.; Kudrik, E. V. Phthalocyanine Metal Complexes: Versatile Catalysts for Selective Oxidation and Bleaching. *Catal. Today* **2011**, *159* (1), 37–46. <https://doi.org/10.1016/j.cattod.2010.06.020>.
- (73) Kim, W. J.; Kim, S. J.; Lee, K.-S.; Samoc, M.; Cartwright, A. N.; Prasad, P. N. Robust Microstructures Using UV Photopatternable Semiconductor Nanocrystals. *Nano Lett.* **2008**, *8* (10), 3262–3265. <https://doi.org/10.1021/nl8016219>.
- (74) Chen, O.; Riedemann, L.; Etoc, F.; Herrmann, H.; Coppey, M.; Barch, M.; Farrar, C. T.; Zhao, J.; Bruns, O. T.; Wei, H.; Guo, P.; Cui, J.; Jensen, R.; Chen, Y.; Harris, D. K.; Cordero, J. M.; Wang, Z.; Jasanoff, A.; Fukumura, D.; Reimer, R.; Dahan, M.; Jain, R. K.; Bawendi, M. G. Magneto-Fluorescent Core-Shell Supernanoparticles. *Nat. Commun.* **2014**, *5* (1), 5093. <https://doi.org/10.1038/ncomms6093>.
- (75) Wang, Y.; Fedin, I.; Zhang, H.; Talapin, D. V. Direct Optical Lithography of Functional Inorganic Nanomaterials. *Science* (80-.). **2017**, *357* (6349), 385–388. <https://doi.org/10.1126/science.aan2958>.

References

- (76) Park, J.-S.; Kyhm, J.; Kim, H. H.; Jeong, S.; Kang, J.; Lee, S.; Lee, K.-T.; Park, K.; Barange, N.; Han, J.; Song, J. D.; Choi, W. K.; Han, I. K. Alternative Patterning Process for Realization of Large-Area, Full-Color, Active Quantum Dot Display. *Nano Lett.* **2016**, *16* (11), 6946–6953. <https://doi.org/10.1021/acs.nanolett.6b03007>.
- (77) Tagliacruzchi, M.; Amin, V. A.; Schneebeli, S. T.; Stoddart, J. F.; Weiss, E. A. High-Contrast Photopatterning of Photoluminescence within Quantum Dot Films through Degradation of a Charge-Transfer Quencher. *Adv. Mater.* **2012**, *24* (27), 3617–3621. <https://doi.org/10.1002/adma.201201356>.
- (78) Wang, Y.; Tang, Z.; Correa-Duarte, M. A.; Pastoriza-Santos, I.; Giersig, M.; Kotov, N. A.; Liz-Marzán, L. M. Mechanism of Strong Luminescence Photoactivation of Citrate-Stabilized Water-Soluble Nanoparticles with CdSe Cores. *J. Phys. Chem. B* **2004**, *108* (40), 15461–15469. <https://doi.org/10.1021/jp048948t>.
- (79) Zucolotto, V.; Gattás-Asfura, K. M.; Tumolo, T.; Perinotto, A. C.; Antunes, P. A.; Constantino, C. J. L.; Baptista, M. S.; Leblanc, R. M.; Oliveira, O. N. Nanoscale Manipulation of CdSe Quantum Dots in Layer-by-Layer Films: Influence of the Host Polyelectrolyte on the Luminescent Properties. *Appl. Surf. Sci.* **2005**, *246* (4), 397–402. <https://doi.org/10.1016/j.apsusc.2004.11.044>.
- (80) Wang, X.; Zhang, J.; Nazzal, A.; Xiao, M. Photo-Oxidation-Enhanced Coupling in Densely Packed CdSe Quantum-Dot Films. *Appl. Phys. Lett.* **2003**, *83* (1), 162–164. <https://doi.org/10.1063/1.1590735>.
- (81) Asami, H.; Abe, Y.; Ohtsu, T.; Kamiya, I.; Hara, M. Surface State Analysis of Photobrightening in CdSe Nanocrystal Thin Films. *J. Phys. Chem. B* **2003**, *107* (46), 12566–12568. <https://doi.org/10.1021/jp035484a>.
- (82) Chen, J.; Chan, Y. H.; Yang, T.; Wark, S. E.; Son, D. H.; Batteas, J. D. Spatially Selective Optical Tuning of Quantum Dot Thin Film Luminescence. *J. Am. Chem. Soc.* **2009**, *131* (51), 18204–18205. <https://doi.org/10.1021/ja906837s>.
- (83) Pawley, J. B. *Handbook of Biological Confocal Microscopy*; Pawley, J. B., Ed.; Springer US: Boston, MA, 1995. <https://doi.org/10.1007/978-1-4757-5348-6>.
- (84) Gu, M. *Advanced Optical Imaging Theory*; Springer Series in Optical Sciences; Springer Berlin Heidelberg: Berlin, Heidelberg, 2000; Vol. 75. <https://doi.org/10.1007/978-3-540-48471-4>.

- (85) Abbe, E. Beiträge Zur Theorie Des Mikroskops Und Der Mikroskopischen Wahrnehmung. *Arch. für Mikroskopische Anat.* **1873**, *9* (1), 413–468. <https://doi.org/10.1007/BF02956173>.
- (86) Rayleigh. XV. On the Theory of Optical Images, with Special Reference to the Microscope. *London, Edinburgh, Dublin Philos. Mag. J. Sci.* **1896**, *42* (255), 167–195. <https://doi.org/10.1080/14786449608620902>.
- (87) Hames, D.; Hooper, N. Bioimaging. In *Instant Notes Biochemistry*; Taylor & Francis, 2006; Vol. 33, pp 18–23. <https://doi.org/10.4324/9780203967621-4>.
- (88) Rayleigh. XXXI. Investigations in Optics, with Special Reference to the Spectroscope. *London, Edinburgh, Dublin Philos. Mag. J. Sci.* **1879**, *8* (49), 261–274. <https://doi.org/10.1080/14786447908639684>.
- (89) Minsky, M. US3013467a, M. Minsky Microscopy Apparatus, 1957.
- (90) Yu, W. W.; Qu, L.; Guo, W.; Peng, X. Experimental Determination of the Extinction Coefficient of CdTe, CdSe, and CdS Nanocrystals. *Chem. Mater.* **2003**, *15* (14), 2854–2860. <https://doi.org/10.1021/cm034081k>.
- (91) Wackenhut, F.; Virgilio Failla, A.; Züchner, T.; Steiner, M.; Meixner, A. J. Three-Dimensional Photoluminescence Mapping and Emission Anisotropy of Single Gold Nanorods. *Appl. Phys. Lett.* **2012**, *100* (26), 263102. <https://doi.org/10.1063/1.4729152>.
- (92) Wackenhut, F.; Failla, A. V.; Meixner, A. J. Multicolor Microscopy and Spectroscopy Reveals the Physics of the One-Photon Luminescence in Gold Nanorods. *J. Phys. Chem. C* **2013**, *117* (34), 17870–17877. <https://doi.org/10.1021/jp407353r>.
- (93) Märker, B.; Hiller, J.; Wackenhut, F.; Braun, K.; Meixner, A.; Scheele, M. Simultaneous Positive and Negative Optical Patterning with Dye-Sensitized CdSe Quantum Dots. *J. Chem. Phys.* **2019**, *151* (14), 141102. <https://doi.org/10.1063/1.5124232>.
- (94) Jung, S. H.; Ha, C.-S. Syntheses and Characterization of Polyimide Containing Metal Phthalocyanine for Organic Electroluminescent Devices. *High Perform. Polym.* **2006**, *18* (5), 679–696. <https://doi.org/10.1177/0954008306068230>.
- (95) Alzeer, J.; Roth, P. J. C.; Luedtke, N. W. An Efficient Two-Step Synthesis of Metal-Free Phthalocyanines Using a Zn(II) Template. *Chem. Commun.* **2009**, No. 15, 1970. <https://doi.org/10.1039/b822985f>.

References

- (96) Knauf, R. R.; Lennox, J. C.; Dempsey, J. L. Quantifying Ligand Exchange Reactions at CdSe Nanocrystal Surfaces. *Chem. Mater.* **2016**, *28* (13), 4762–4770. <https://doi.org/10.1021/acs.chemmater.6b01827>.
- (97) Dayal, S.; Królicki, R.; Lou, Y.; Qiu, X.; Berlin, J. C.; Kenney, M. E.; Burda, C. Femtosecond Time-Resolved Energy Transfer from CdSe Nanoparticles to Phthalocyanines. *Appl. Phys. B* **2006**, *84* (1–2), 309–315. <https://doi.org/10.1007/s00340-006-2293-z>.
- (98) Adegoke, O.; Nyokong, T. Conjugation of Mono-Substituted Phthalocyanine Derivatives to CdSe@ZnS Quantum Dots and Their Applications as Fluorescent-Based Sensors. *Synth. Met.* **2014**, *188*, 35–45. <https://doi.org/10.1016/j.synthmet.2013.11.016>.
- (99) Nyk, M.; Palewska, K.; Kepinski, L.; Wilk, K. A.; Strek, W.; Samoc, M. Fluorescence Resonance Energy Transfer in a Non-Conjugated System of CdSe Quantum Dots/Zinc-Phthalocyanine. *J. Lumin.* **2010**, *130* (12), 2487–2490. <https://doi.org/10.1016/j.jlumin.2010.08.017>.
- (100) Szostak, J.; Jarosz, G.; Signerski, R. Photovoltaic Properties of Cadmium Selenide–Titanyl Phthalocyanine Planar Heterojunction Devices. *Chem. Phys.* **2015**, *456*, 57–60. <https://doi.org/10.1016/j.chemphys.2015.04.010>.
- (101) Saha, S. K.; Guchhait, A.; Pal, A. J. Organic/Inorganic Hybrid Pn -Junction between Copper Phthalocyanine and CdSe Quantum Dot Layers as Solar Cells. *J. Appl. Phys.* **2012**, *112* (4), 044507. <https://doi.org/10.1063/1.4747835>.
- (102) André, A.; Zherebetsky, D.; Hanifi, D.; He, B.; Samadi Khoshkhoo, M.; Jankowski, M.; Chassé, T.; Wang, L.-W.; Schreiber, F.; Salleo, A.; Liu, Y.; Scheele, M. Toward Conductive Mesocrystalline Assemblies: PbS Nanocrystals Cross-Linked with Tetrathiafulvalene Dicarboxylate. *Chem. Mater.* **2015**, *27* (23), 8105–8115. <https://doi.org/10.1021/acs.chemmater.5b03821>.
- (103) André, A.; Theurer, C.; Lauth, J.; Maiti, S.; Hodas, M.; Samadi Khoshkhoo, M.; Kinge, S.; Meixner, A. J.; Schreiber, F.; Siebbeles, L. D. A.; Braun, K.; Scheele, M. Structure, Transport and Photoconductance of PbS Quantum Dot Monolayers Functionalized with a Copper Phthalocyanine Derivative. *Chem. Commun.* **2017**, *53* (10), 1700–1703. <https://doi.org/10.1039/C6CC07878H>.
- (104) Talgorn, E.; Abellon, R. D.; Kooyman, P. J.; Piris, J.; Savenije, T. J.; Goossens, A.; Houtepen, A. J.; Siebbeles, L. D. A. Supercrystals of CdSe Quantum Dots with High

- Charge Mobility and Efficient Electron Transfer to TiO₂. *ACS Nano* **2010**, *4* (3), 1723–1731. <https://doi.org/10.1021/nn901709a>.
- (105) Yoon, S. J.; Guo, Z.; dos Santos Claro, P. C.; Shevchenko, E. V.; Huang, L. Direct Imaging of Long-Range Exciton Transport in Quantum Dot Superlattices by Ultrafast Microscopy. *ACS Nano* **2016**, *10* (7), 7208–7215. <https://doi.org/10.1021/acsnano.6b03700>.
- (106) Bethell, D.; Brust, M.; Schiffrin, D. J.; Kiely, C. From Monolayers to Nanostructured Materials: An Organic Chemist's View of Self-Assembly. *J. Electroanal. Chem.* **1996**, *409* (1–2), 137–143. [https://doi.org/10.1016/0022-0728\(96\)04533-0](https://doi.org/10.1016/0022-0728(96)04533-0).
- (107) Wang, G. X.; Park, M. S.; Liu, H. K.; Wexler, D.; Chen, J. Synthesis and Characterization of One-Dimensional CdSe Nanostructures. *Appl. Phys. Lett.* **2006**, *88* (19), 193115. <https://doi.org/10.1063/1.2202725>.
- (108) Yükselici, M. H.; Aşıkoğlu Bozkurt, A.; Ömür, B. C. A Detailed Examination of the Growth of CdSe Thin Films through Structural and Optical Characterization. *Mater. Res. Bull.* **2013**, *48* (7), 2442–2449. <https://doi.org/10.1016/j.materresbull.2013.02.068>.
- (109) Sivanesan, A.; John, S. A. Amino Group Position Dependent Orientation of Self-Assembled Monomolecular Films of Tetraaminophthalocyanatocobalt(II) on Au Surfaces. *Langmuir* **2008**, *24* (5), 2186–2190. <https://doi.org/10.1021/la702863a>.
- (110) Murray, C.; Dozova, N.; McCaffrey, J. G.; FitzGerald, S.; Shafizadeh, N.; Crépin, C. Infra-Red and Raman Spectroscopy of Free-Base and Zinc Phthalocyanines Isolated in Matrices. *Phys. Chem. Chem. Phys.* **2010**, *12* (35), 10406. <https://doi.org/10.1039/c0cp00055h>.
- (111) Lokesh, K. S.; Adriaens, A. Synthesis and Characterization of Tetra-Substituted Palladium Phthalocyanine Complexes. *Dye. Pigment.* **2013**, *96* (1), 269–277. <https://doi.org/10.1016/j.dyepig.2012.08.018>.
- (112) Kale, R. B.; Sartale, S. D.; Chougule, B. K.; Lokhande, C. D. Growth and Characterization of Nanocrystalline CdSe Thin Films Deposited by the Successive Ionic Layer Adsorption and Reaction Method. *Semicond. Sci. Technol.* **2004**, *19* (8), 980–986. <https://doi.org/10.1088/0268-1242/19/8/006>.
- (113) Asami, H.; Abe, Y.; Ohtsu, T.; Kamiya, I.; Hara, M. Surface State Analysis of Photobrightening in CdSe Nanocrystal Thin Films. *J. Phys. Chem. B* **2003**, *107* (46), 12566–12568. <https://doi.org/10.1021/jp035484a>.

References

- (114) Cordero, S. R.; Carson, P. J.; Estabrook, R. A.; Strouse, G. F.; Buratto, S. K. Photo-Activated Luminescence of CdSe Quantum Dot Monolayers. *J. Phys. Chem. B* **2000**, *104* (51), 12137–12142. <https://doi.org/10.1021/jp001771s>.
- (115) Jasieniak, J.; Califano, M.; Watkins, S. E. Size-Dependent Valence and Conduction Band-Edge Energies of Semiconductor Nanocrystals. *ACS Nano* **2011**, *5* (7), 5888–5902. <https://doi.org/10.1021/nn201681s>.
- (116) Kim, L.; Anikeeva, P. O.; Coe-Sullivan, S. A.; Steckel, J. S.; Bawendi, M. G.; Bulović, V. Contact Printing of Quantum Dot Light-Emitting Devices. *Nano Lett.* **2008**, *8* (12), 4513–4517. <https://doi.org/10.1021/nl8025218>.
- (117) Lin, Q.; Yun, H. J.; Liu, W.; Song, H.-J.; Makarov, N. S.; Isaienko, O.; Nakotte, T.; Chen, G.; Luo, H.; Klimov, V. I.; Pietryga, J. M. Phase-Transfer Ligand Exchange of Lead Chalcogenide Quantum Dots for Direct Deposition of Thick, Highly Conductive Films. *J. Am. Chem. Soc.* **2017**, *139* (19), 6644–6653. <https://doi.org/10.1021/jacs.7b01327>.
- (118) Nanda, K. .; Sarangi, S. .; Sahu, S. . Measurement of Surface Roughness by Atomic Force Microscopy and Rutherford Backscattering Spectrometry of CdS Nanocrystalline Films. *Appl. Surf. Sci.* **1998**, *133* (4), 293–297. [https://doi.org/10.1016/S0169-4332\(98\)00212-8](https://doi.org/10.1016/S0169-4332(98)00212-8).
- (119) Inamdar, S. N.; Ingole, P. P.; Haram, S. K. Determination of Band Structure Parameters and the Quasi-Particle Gap of CdSe Quantum Dots by Cyclic Voltammetry. *ChemPhysChem* **2008**, *9* (17), 2574–2579. <https://doi.org/10.1002/cphc.200800482>.
- (120) Tagliazucchi, M.; Amin, V. A.; Schneebeli, S. T.; Stoddart, J. F.; Weiss, E. A. High-Contrast Photopatterning of Photoluminescence within Quantum Dot Films through Degradation of a Charge-Transfer Quencher. *Adv. Mater.* **2012**, *24* (27), 3617–3621. <https://doi.org/10.1002/adma.201201356>.
- (121) Hines, D. A.; Becker, M. A.; Kamat, P. V. Photoinduced Surface Oxidation and Its Effect on the Exciton Dynamics of CdSe Quantum Dots. *J. Phys. Chem. C* **2012**, *116* (24), 13452–13457. <https://doi.org/10.1021/jp303659g>.
- (122) Ipe, B. I.; Lehnig, M.; Niemeyer, C. M. On the Generation of Free Radical Species from Quantum Dots. *Small* **2005**, *1* (7), 706–709. <https://doi.org/10.1002/smll.200500105>.
- (123) Li, Y.; Zhang, W.; Li, K.; Yao, Y.; Niu, J.; Chen, Y. Oxidative Dissolution of Polymer-Coated CdSe/ZnS Quantum Dots under UV Irradiation: Mechanisms and Kinetics. *Environ.*

- Pollut.* **2012**, *164*, 259–266. <https://doi.org/10.1016/j.envpol.2012.01.047>.
- (124) Jones, M.; Nedeljkovic, J.; Ellingson, R. J.; Nozik, A. J.; Rumbles, G. Photoenhancement of Luminescence in Colloidal CdSe Quantum Dot Solutions. *J. Phys. Chem. B* **2003**, *107* (41), 11346–11352. <https://doi.org/10.1021/jp035598m>.
- (125) Ostler, R. B.; Scully, A. D.; Taylor, A. G.; Gould, I. R.; Smith, T. A.; Waite, A.; Phillips, D. The Effect of PH on the Photophysics and Photochemistry of Di-Sulphonated Aluminum Phthalocyanine. *Photochem. Photobiol.* **2000**, *71* (4), 397. [https://doi.org/10.1562/0031-8655\(2000\)071<0397:TEOPOT>2.0.CO;2](https://doi.org/10.1562/0031-8655(2000)071<0397:TEOPOT>2.0.CO;2).
- (126) Kuznetsova, N. A.; Gretsova, N. S.; Derkacheva, V. M.; Mikhalenko, S. A.; Solov'eva, L. I.; Yuzhakova, O. A.; Kaliya, O. L.; Luk'yanets, E. A. Generation of Singlet Oxygen with Anionic Aluminum Phthalocyanines in Water. *Russ. J. Gen. Chem.* **2002**, *72* (2), 300–306. <https://doi.org/10.1023/A:1015402524813>.
- (127) Černý, J.; Karásková, M.; Rakušan, J.; Nešpůrek, S. Reactive Oxygen Species Produced by Irradiation of Some Phthalocyanine Derivatives. *J. Photochem. Photobiol. A Chem.* **2010**, *210* (1), 82–88. <https://doi.org/10.1016/j.jphotochem.2009.11.016>.